AAU Energy Technology
Department of Energy Engineering

Hierarchical control strategies for Parallel connected Inverters in AC Microgrids

Master Thesis

Hierarchical control strategies for Parallel-connected Inverters in AC Microgrids

Master Thesis
October 1, 2021

By
RAJIV KUMAR KARN

Cover photo: Rajiv Kumar Karn, 2020
Published by: AAU, Department of Energy Engineering, Fredrik Bajers Vej 7K, 9220 Aalborg East Denmark
www.en.aau.dk/

Approval

This thesis has been prepared over six months at the Section for Indoor Climate, Department of Energy Engineering, at the Aalborg University, Denmark, AAU, in partial fulfilment for the degree Master of Science in Engineering, MSc Eng.

RAJIV KUMAR KARN -

....

Signature

....

Date

Abstract

With the increase of concerns over global warming renewable energy sources (RESs) has been the center stage of academia, industry, national and international policy makers. In power systems, with the increasing integration of these distributed energy resources (DERs) like solar and wind, microgrid (MG) concept has been a favorite topic in recent times. Microgrids (MGs) are small-scale electricity networks that integrate distributed electricity generation with consumers/prosumers and potentially with storage systems. MG is typically equipped with power converters like inverters as interfaces and has become one of the most promising active distribution networks. It is normally controlled to provide the required flexible operation (like islanded operation) and to maintain the specified power quality and energy output. With regard to multi-power inverters in parallel, several decentralized control methods have been proposed, such as the power droop control method. Moreover, power droop control-based hierarchical control architecture is proposed, including primary, secondary, and tertiary control levels to achieve power sharing control, synchronization control, power flow management, and economic optimization. In this thesis, centralized and distributed power droop controller-based secondary controllers are developed for AC Microgrids to restore voltage magnitude and frequency deviations considering communication delays. Parameters for inner voltage and current loops, virtual impedance, and power droop coefficients are designed. Harmonic suppression method is used to reduce voltage total harmonic distortion for a three-phase voltage-controlled inverter with a non-linear load. The proposed control approaches are validated by using Matlab/Simulink or dSPACE 1006-based hardware in the loop simulation platform.

Preface

The report titled, 'Hierarchical control strategies for Parallel-connected Inverters in AC Microgrids' has been written by Rajiv Kumar Karn of Group PED4-1051 of 10th semester, at the Department of Energy Technology, Aalborg University, for completion of 4th semester master thesis.

I would like to thank my supervisors Dr. Yajuan Guan and Prof. Juan C. Vasquez for their untiring support and continuous motivation throughout the project duration. I would also like to express my gratitude to Prof. Josep M. Guerrero and Dr. Saeed Golestan (Department of Energy Technology, AAU) for providing their expertise in this topic.

Wolfram Mathematica, MATLAB/Simulink softwares, and dSAPCE 1006 hardware in the loop platform were used in this project for carrying out various simulations and results. The report was written using LaTeX in Overleaf.

Aalborg University, October 1, 2021

Rajiv Karn
<rkarn19@student.aau.dk>

Acknowledgements

[Dr. Yajuan Guan], **[Asst. Professor]**, [Energy Technology, AAU]

[Dr. Juan C. Vasquez], **[Professor]**, [Energy Technology, AAU]

[Dr. Josep M. Guerrero], **[Professor]**, [Energy Technology, AAU]

[Dr. Saeed Golestan], **[Asst. Professor]**, [Energy Technology, AAU]

Science is a wonderful thing
if one does not have to earn one's living at it.
Albert Einstein

Contents

1 Introduction

Electric Power is an indicator of progress of any country. Thomas Edison's developed Pearl Street Station to power entire system by direct current and electrify customers by incandescent light bulb [1]. Since this pioneering step, humankind has set lots of central power plant which unfortunately has become a most acceptable mode of electricity generation and most of these were fired by polluting sources such as coal and gas. But few decades earlier facing pressure from environmental pollution, global warming, climate change, depleting conventional fuel etc, the trend is slowly moving away from central polluting power generation towards distributed power generation. Also, a major accident Fukushima Daiichi Nuclear Power Plant, wildfire in Australia and California and Hurricanes affected both generation source and transmission cable. These incident showed that in order to supply continuous power with high resiliency, distributed energy generation should be used. These led to development of a new power system technology called Microgrid (MG). MG can be defined as a collection of various distributed energy resources (renewable and non-renewable), energy storage systems and loads to solve energy demand.

One of the main aspect of a microgrid is that it can connect and disconnect with the main grid for an extended amount of time. So it can run on fully island mode, thus saving cost and increasing the resiliency of the system. Incorporating renewable sources like fuel cell, solar, wind or both decrease the greenhouse gas emission and lowers the total energy costs of the transmission and distribution system. The application of DG units requires stable power generation, storage and sharing of load. Since solar and wind sources have intermittent nature and when active power generation varies maintaining voltage and frequency stable becomes the major challenge for the microgrid. Microgrid hierarchical control strategies provides many solutions to power quality improvement, voltage and frequency deviation restoration, power sharing control, synchronization control, power flow management, and economic optimization.

1.1 Problem Formulation

Microgrid is a promising solution to include renewable energy resources, energy storage systems and loads, and provide uninterrupted power supply. Proper control strategies, control structures and control parameters need to be well developed and designed for microgrids to have a stable and efficient operation. The developed control approaches and structures need to stabilize bus voltage and frequency, share the active and reactive power among the paralleled distributed generators, meet the power quality requirements when supply non-linear loads, remove voltage magnitude and frequency deviations and maintain stable operation with communication delays.

1.2 Scope and Objective

With the increase of global concerns over environmental pollution, climate change and CO_2, there is tremendous pressure to power the world by perpetual and green source like wind and solar. To achieve this, distributed energy resources (DERs) should be integrated into main grid, the concept of Microgrid came few decades earlier. Hierarchical control strategy for microgrids has bee proposed to achieve stable, efficient and optimal operation. Hierarchical control structure is divided into three layers, namely primary, secondary and tertiary.

The thesis aims at achieving the following main goals:

1. To develop a power quality improvement method for a three-phase voltage-controlled inverter with non-linear loads;
2. To develop a voltage/frequency deviation restoration method for parallel-connected three-phase inverters based on MG hierarchical control structure;
3. To compare the control performance of the centralized and distributed secondary control methods with various communication delays
4. To test the performance of the proposed controllers.

1.3 Methodology

In order to fulfill the objectives of the project, the methodology is arranged as follows-

1. Review the literature and to understand the state of art of Microgrid operation and its hierarchical control structure
2. Parameters design for inner voltage and current loops
3. Parameters design for primary control - power droop controller
4. Matlab/Simulink model development and test for the power droop controlled parallel inverters
5. Develop the centralized and distributed secondary controllers considering communication delay
6. Perform harmonic suppression controller for a voltage controlled inverter
7. Validation of the proposed algorithms in the Hardware in the loop simulation tests

1.4 Limitation

The main limitations of the project are as follows-

- For centralized and distributed secondary control, the data package drop-out affection are not considered or compared.
- The developed control methods, for instance the centralized and distributed secondary control, and harmonic suppression control are not validated on experimental setup.
- Energy management system at the tertiary layer could be included with the developed primary and secondary controllers.

1.5 Contents of report

The thesis report is divided into eight chapters which are illustrated below:

1. **Introduction**: In this first chapter, a basic background regarding the emergence and purpose of microgrids are explained in brief and motivation behind the research topic is briefly discussed. This chapter also includes the problem formulation, the scope and objectives of the thesis, the methodology used and the main limitations in this research thesis work.
2. **State of Art**: This chapter deals with the importance of microgrid in the present context. The theory behind Hierarchical control structure for Microgrids is explained

in brief. Also, the relevant theory behind the main aspects of the study in this project like Phase Locked Loop (PLL) and Second Order Generalized Integrator (SOGI) are also discussed.

3. **Parameter design for inner loop controllers** : This chapter deals with Inner loop control or Zero level control. Block diagram explanation nested loop for voltage and current loops is designed. Also, the parameters like proportional and resonant terms for voltage and current loops are designed and validated by different approaches.
4. **Power droop-controlled inverters** : The fourth chapter deals with primary control. In this chapter droop method is explained in details with its origin and drawbacks.
5. **Centralized and Decentralized Secondary control** In this chapter, secondary layer of Hierarchical control is explained in detail like how it mitigates the drawback of droop based method. Moreover two approaches of secondary control: centralized and distributed are explained in details and compared with each other in different test cases.
6. **Harmonic mitigation solution for a microgrid with a non-linear load** In this chapter, a brief introduction of harmonics and THD is explained. Likewise harmonic compensation methods in both DQ and $\alpha\beta$ reference frames are explained and comparison between two compensation frames is presented with simulation results
7. **Hardware-in-the-loop simulation** In this seventh chapter, the experimental set-up is explained in brief. One of the microgrid model developed in simulink platform is tested in dSPACE 1006 platform and the simulation results are shown.
8. **Conclusion and Future Work**: This chapter contains a summary of all the chapters described in this thesis. It also discusses the shortcomings and possible future works that can be done.

2 State of Art

2.1 Microgrid

Microgrids are small-scale electricity networks that incorporate distributed electricity generation with consumers/prosumers [2]. Generally, it also has storage systems associated with it. The typical microgrids is shown in figure 2.1. One of the main aspect of a microgrid is that it can connect and disconnect with the main grid and work in islanded mode. This results in increasing resiliency of the system. Since, microgrids can integrate renewable sources like solar, wind or both, it reduces the greenhouse gas emission and lowers the total energy costs of the transmission and distribution system.

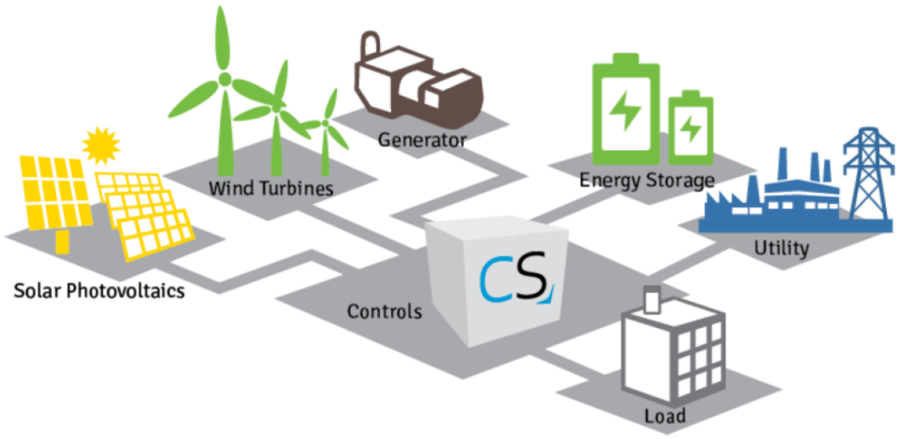

Figure 2.1: Schematic diagram a typical microgrid [3]

2.2 Hierarchical control levels of a Microgrid

Micrograds is designed to work in grid-connected mode, islanded mode and flexible mode (operate in both grid connected and islanded). Each mode is different and the associated operational characteristics are also different. For example, the larger capacity of main grid dominates frequency in grid connected mode whereas in islanded mode, frequency pose a significant challenge in regular operation [4]. Hierarchical control strategies are able to meet operational challenges and can control different grid variables like frequency and voltage. Hierarchical control is usually divided into three layers- Primary, Secondary and Tertiary. Each control layer has different functions and provides supervisory control over lower-level control [5], which ensures command as well as reference signal are passed from one level to another for robust performance. So response speed or bandwidth must decrease with an increase in the control level. The schematic diagram of a hierarchical control structure of a microgrid is shown in figure 2.2. The three layers of hierarchical control are explained below-

2.2.1 Primary Layer

The primary level is often divided into inner current and voltage loops (also referred as zero layer) and droop control. The power droop approach is used to to adjust the amplitude and frequency of the output voltage without any communication. It generates the reference for zero layer to regulate voltage and current for a stable operation. Virtual impedance loop is also used to emulate line impedance.

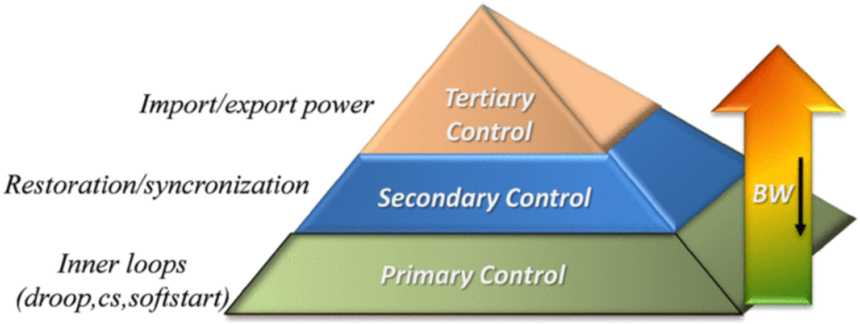

Figure 2.2: Schematic diagram of a hierarchical control levels of a Microgrid [5]

2.2.2 Secondary Layer

Secondary layer compensates the frequency and amplitude deviations that are introduced by primary control loop. Whenever there is change in load, it ensures the frequency and voltage deviations are regulated toward zero by low bandwidth communication. It is also used to synchronize the microgrid with the main grid before it is connected to the utility. It is further divided into centralized and distributed Secondary control which are explained in Chapter 5.

2.2.3 Tertiary Layer

This layer controls the energy flow in the best economical way. Energy management system also falls in this level. So it deals with power flow in grid connected mode and ensures optimal operation.

2.3 Current Status of Research on Parallel Inverter Control Technology

The control strategies for parallel inverters are the fundamantal of microgrid control. Every inverter should proportionally share the common loads. But due to inherent differences in each inverter, impedance mismatch, etc. some of the inverter will be loaded more than other. Due to rapid development in control technologies, it is able to arrest these differences.

Parallel operation of the parallel inverters can be divided based on active load-sharing technologies and on droop based method [6]. Droop based method, adjust the output voltage amplitude and frequency based on active and reactive power of the inverter. It is discussed in Chapter 4 in detail. Likewise, in active load-sharing technologies, centralized and master slave control are discussed in this thesis. One of major difference between active load-sharing and droop based method is that in active load sharing, intercommunication link is needed whereas in droop method, it does not need communication link.

2.3.1 Centralized Control

The centralized control is shown in figure 2.3. The current reference in each module i^* is found by dividing the total current i_L by total number of modules, which is given by equation 2.1[6].

$$i_j^* = \frac{i_L}{N}, \qquad \text{for} \qquad j = 1, \ldots, N. \tag{2.1}$$

In this method, the current reference value is subtracted by the current of each module

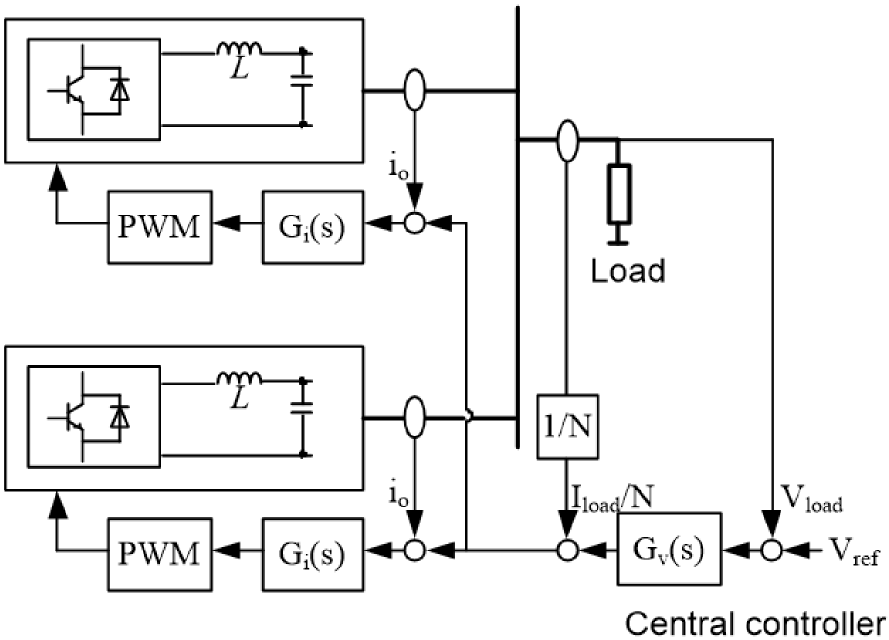

Figure 2.3: Schematic diagram of a Centralized Controller for parallel UPS system

and error Δ_j is processed through control loop. This method is commonly used when multiple inverters are connected in parallel. However, this method must use a central control board to measure the total load current, so it is not very suitable for large-scale distributed systems.

2.3.2 Master Slave Control

In the master slave control method, master module as shown in figure 2.4 controls the load voltage and command the reference current (i_S) for rest of the modules (also known as slaves) which is expressed in equation 2.2.

$$i_S^* = i_M, \qquad \text{for} \qquad S = 2, \dots, N. \tag{2.2}$$

From the figure 2.4, it can be seen that the master acts as a voltage source inverter and on the other hand slave works as a current source inverter. However, if master module fails, other modules can replace the master and function properly as required.

2.4 Phase Locked Loop and Space Vector theory

Space Vector theory is a useful tool for modeling three phase systems. The origin of space vector theory comes from rotating mmf in electrical machines. For example, when voltage is passed through stator of the Induction motor or Synchronous motor which is spatial displaced by $120°$, then rotating mmf is produced in space. So, space vector is a mathematical representation which is useful for visualizing or representing the effect of three phase variable in space.

Due to addition of increasing number of distributed energy in the grid, it will led to innovative way in which we analyze and design modern power systems. For this, accurate way of estimating power quality parameters like frequency, current and voltage phasors is very important. And this call for the Clarke and Park transforms for designed stable grids operation.

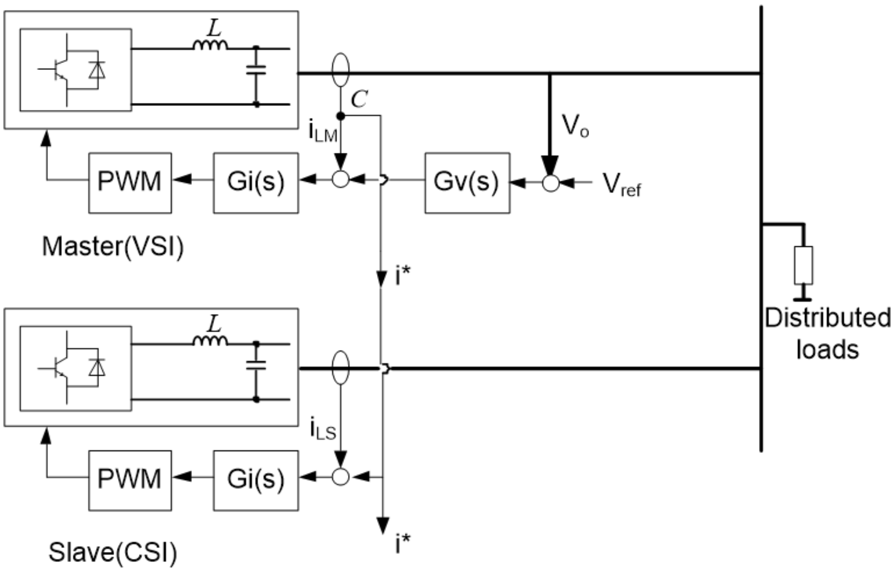

Figure 2.4: Schematic diagram of a Master Slave control

2.4.1 Clarke Transformation

The Clarke transform is also also known as the αβ transform, was first formulated by was introduced by Edith Clarke in 1943 who was first female professor of Electrical Engineering in the USA [7].It is a mathematical transformation which simplify the time-domain components of a three-phase system in an (abc) reference frame to a stationary components in (α-β-0) reference frame. The zero component for the balanced system is equal to zero. The Clarke transformation is mathematically represented by Eq. 2.3 in a matrix form.

$$\begin{bmatrix}\alpha\\ \beta\\ 0\end{bmatrix} = \frac{2}{3}\begin{bmatrix}1 & -\frac{1}{2} & -\frac{1}{2}\\ 0 & \frac{\sqrt{3}}{2} & -\frac{\sqrt{3}}{2}\\ \frac{1}{2} & \frac{1}{2} & \frac{1}{2}\end{bmatrix}\begin{bmatrix}a\\ b\\ c\end{bmatrix} \tag{2.3}$$

Here, a, b, and c are the components (may be current or voltage) of the three-phase system in the abc reference frame and (α-β-0) are the components for the stationary reference frame.

2.4.2 Park Transformation

It is very similar to Clarke transformation. The Park Transformation converts the time-domain components of a three-phase system in an abc reference frame to time-invariant direct, quadrature, and zero components in a rotating reference frame. The Park transformation is mathematically represented by Eq. 2.4 in a matrix form.

$$\begin{bmatrix}q\\ d\\ 0\end{bmatrix} = \frac{2}{3}\begin{bmatrix}\cos\theta & \sin(\theta) & 0\\ -\sin\theta & \cos(\theta)) & 0\\ 0 & 0 & 1\end{bmatrix}\begin{bmatrix}\alpha\\ \beta\\ 0\end{bmatrix} \tag{2.4}$$

Fig. 2.5 shows stator winding magnetic axis in abc frame and the rotating reference frame with rotational speed of ω. While, θ is the angle between a-axis and q-axis in $qd0$ reference frame or it can be between a-axis and d-axis in $dq0$ reference frame.

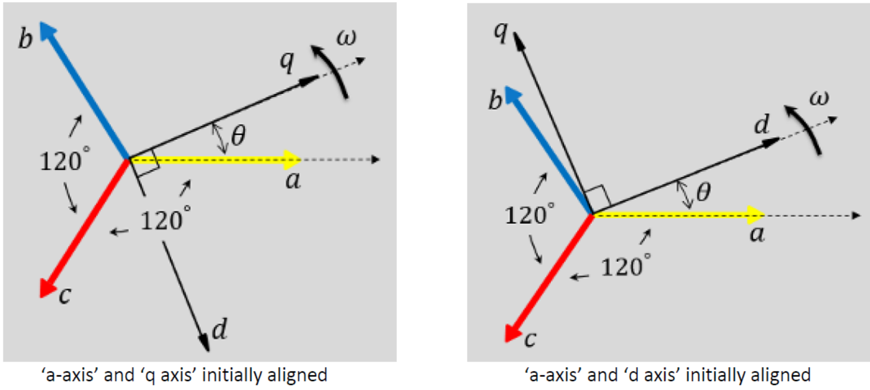

Figure 2.5: 'qdo'(left) & 'dqo'(right) reference frame[8]

2.5 Introduction to PLL

As the name suggests, it is the closed loop control system which maintains the same phase between the input and the output signal. Since its inception, it is used widely in the electronics application from computing to communication.

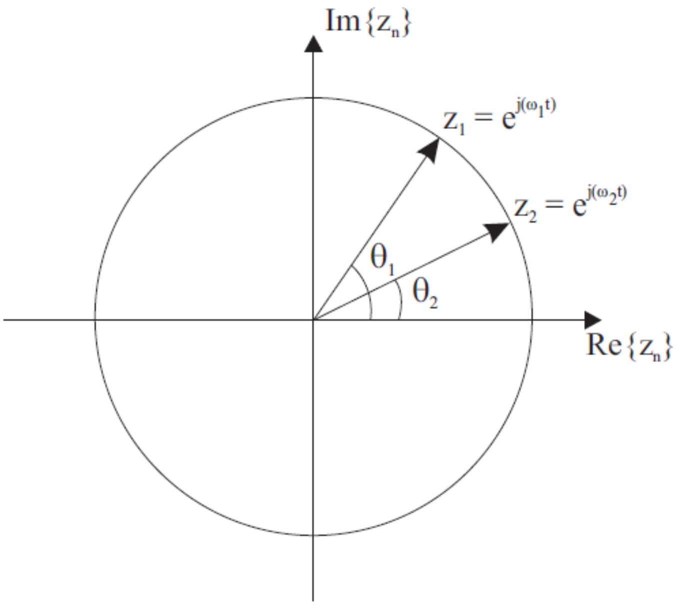

Figure 2.6: Complex Representation of two signal Z1 and Z2 [9]

In figure 2.6, there are two vectors namely Z1 and Z2 rotating with angular speed $\omega 1$ and $\omega 2$ respectively in complex plane. Since phase is a function of time, it is represented in equation 2.5

$$\theta_n(t) = \int_{-\infty}^{t} \omega_n(t)\, dt \tag{2.5}$$

To make the vector Z2 track or follow Z1, it should adjust its phase so that distance between two vectors is minimum or zero. This is known as phase error, represented θe. When the phase error between two system is constant or zero, it is said to be in locked state. It is done by increasing or decreasing the phase of the angular frequency.

2.6 Building Block of PLL

Phase locked loops are popularly used in grid connected power converter to synchronize the grid voltage. An ideal PLL can provide the quick and accurate information of synchronization. PLL is most widely using synchronization technique for time-varying signal

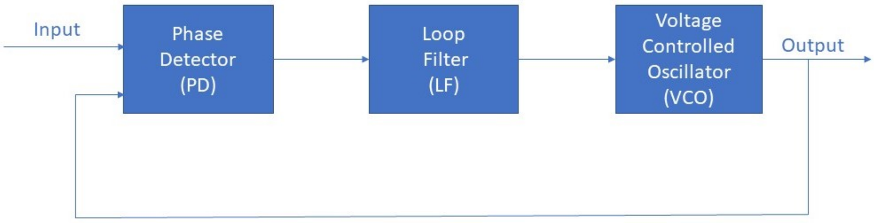

Figure 2.7: Basic Block Diagram of Phase Locked Loop

The fundamental structure of a PLL is shown in figure 2.7. PLL consists of three basic blocks which has three fundamental blocks namely-

1. **Phase Detector (PD)**: It compares the phase of the PLL's output and input signals, and then generates an error signal which is proportional to the difference of the phases.
2. **Loop Filter**: The error signal produced by PD is passed through loop filter. It removes the high frequency component from the signal Filters the output of the phase detector, as the phase detector might introduce unwanted components into the error signal. The filter output is send to the voltage controllable oscillator.
3. **Voltage Controlled Oscillator**: Based on the output from Loop filter, it either increases or decreases the oscillator frequency untill the VCO's frequency locks to the input frequency. Mathematically, it can be written as-
$freq(out) = freq(inp)$ and phase difference(ϕ)=0 or const

2.7 Synchronous Reference Frame PLL (SRF PLL)

With the high penetration of renewable energy sources such as wind power and solar, power generation systems are connected to the grid by the means of power electronics-based switches that not only control the power delivered to the network, but also contribute to the grid stability and supporting the grid parameters like voltage/frequency under both normal and grid faults conditions [10]. The power electronics based devices doesn't have high inertia mass as compared to conventional generator like steam. So, the most important issues in the grid is the synchronization of the grid voltage at the point of common coupling (PCC) with the grid-connected converters. In the advent of any grid faults grid-connected switches should be properly synchronized to keeping the generation running without ant fluctuation. Hence, the designing all the parameters of PLL is particularly challenging in the weak grid.

Phase-locked loops (PLL) have traditionally been used for many decades in synchronizing the control system of power converters with the grid voltage. In Figure 2.8, the layout of a control structure for a three-phase power converter connected to the grid is shown. In the figure 2.8, the grid synchronization block is responsible for estimating the magnitude frequency and phase angle of the grid voltage. These values is fed to the current controller block and last block will vary if the power converter is acting as an active filter, a STATCOM, or a power processor belonging to a power generation plant [10].

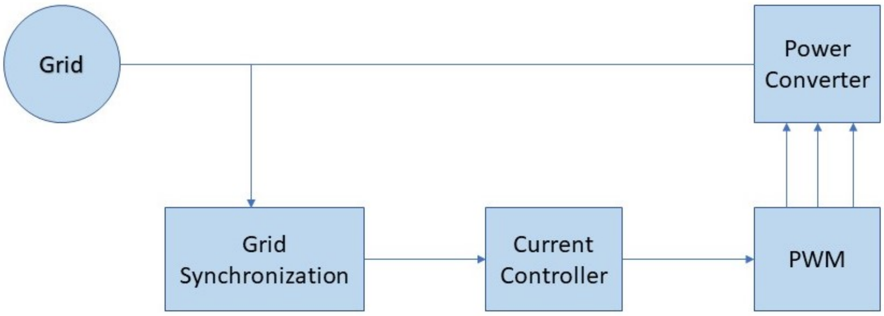

Figure 2.8: Grid synchronization diagram for the control of a grid-connected three-phase power converter

There are many types of PLL but due to limit of the scope of the project following two types of PLL is extensively used in simulation and discussed in detail:

1. **Synchronous Reference Frame PLL (SRF PLL)**:
2. **Second Order Generalized Integrator (SOGI)**:

2.8 Analysis of SRF PLL

Let the input signal contains three phase voltages separated by $120°$ from each other. In SRF PLL, the three phase input signals is passed through Clarke transformation and then Park's transformation. The q axis output is passed through low pass filter i.e. PI controller. The resultant signal which contains frequency component is passed through integrator or VCO to obtain the phase angle.

$$\begin{aligned} v_a(t) &= V\cos(\theta_{grid}) \\ v_b(t) &= V\cos\left(\theta_{grid} - \frac{2\pi}{3}\right) \\ v_c(t) &= V\cos\left(\theta_{grid} + \frac{2\pi}{3}\right) \end{aligned} \tag{2.6}$$

Here V and θ_{grid} are the voltage amplitude and phase angle of the three-phase signals, respectively whereas $\hat{V}$ and $\hat{\theta}$ are the amplitude and phase angle estimated by the SRF-PLL respectively. After applying Clarke's transformations, we get equation 2.7-

$$\begin{bmatrix} v_\alpha \\ v_\beta \end{bmatrix} = \frac{2}{3}\begin{bmatrix} 1 & -\frac{1}{2} & -\frac{1}{2} \\ 0 & \frac{\sqrt{3}}{2} & -\frac{\sqrt{3}}{2} \end{bmatrix}\begin{bmatrix} v_a \\ v_b \\ v_c \end{bmatrix} \tag{2.7}$$

From Park transformation, we get:

$$\begin{bmatrix} v_d \\ v_q \end{bmatrix} = \begin{bmatrix} cos\hat{\theta} & -sin\hat{\theta} \\ sin\hat{\theta} & cos\hat{\theta} \end{bmatrix} \begin{bmatrix} v_\alpha \\ v_\beta \end{bmatrix} \tag{2.8}$$

Putting the value of v_a, v_b and v_c from equation 2.6 to equation 2.7 and on solving equation 2.8, equations 2.9 and equation 2.10 are obtained:

$$v_{\mathrm{d}} = Vcos(\theta_{grid} - \hat{\theta}) \approx V \tag{2.9}$$

$$v_{\mathrm{q}} = Vsin(\theta_{grid} - \hat{\theta}) \approx (\theta_{grid} - \hat{\theta}) \tag{2.10}$$

It can be seen from equation 2.10, the signal v_q contains the phase error information and from equation 2.9, signal v_d evaluates the amplitude of the three-phase voltage vector.

Also, for grid synchronization the $\hat{\theta}$ must be equal to θ_{grid}. But, if there is a small error in (θ_{grid}-$\hat{\theta}$) then by designing proper algorithm of Proportional integral, it can be nearly zero or error is made very small.

2.9 SOGI

The second order generalized integrator (SOGI) phase locked loop is a well known method for filtering and synchronization in the power electronics application. Since SOGI has natural resonant characteristic, it makes itself work as a Voltage Controlled Oscillator (VCO). SOGI is applicable to both single-phase and three-phase system, and has excellent performance in reduction of low frequency harmonics [11]. The block diagram of SOGI is shown in figure 2.9. It is a simple method to estimate the phase, frequency, and amplitude of the signal.

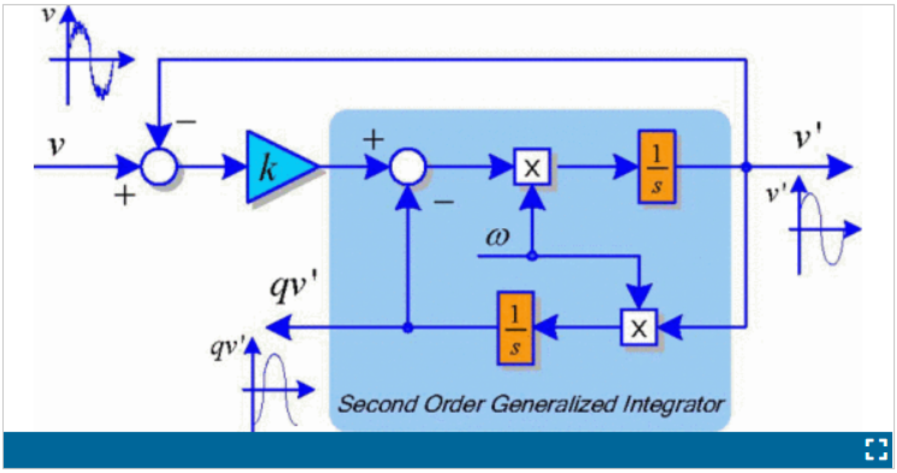

Figure 2.9: General Representation of the Second Order Generalized Integrator [12]

Figure 2.9 shows the graphical representation of the Second Order Generalized Integrator. The same is made in simulink which is shown in figure A.1 and MATLAB code shown can be found in appendix B.1. Upon modelling two output signals i.e. two sine waves (v' and qv') with a phase shift of $90°$ can be validated from figure 2.10. Moreover, the signal component v' has the same phase and magnitude as the fundamental of the input signal (v) can be validated from same modelling in figure 2.10 and figure 2.9.

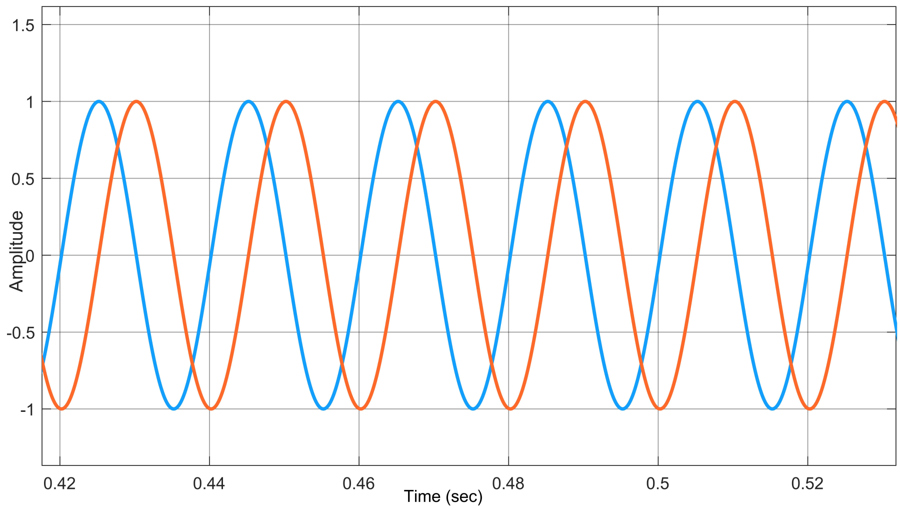

Figure 2.10: Two orthogonal system with phase shift of $90°$

The transfer functions of the SOGI, can be represented by equation 2.11.

$$GI = \frac{\omega s}{s^2 + \omega^2} \tag{2.11}$$

The closed-loop transfer functions of in-phase and in-quadrature axis of SOGI $(GV = \frac{v'}{v})$ and $GV_1 = (\frac{qv'}{v})$ respectively can be defined from figure 2.9 by equation 2.12 and equation 2.13.

$$GV(s) = \frac{v'}{v}(s) = \frac{k\omega s}{s^2 + k\omega s + \omega^2} \tag{2.12}$$

$$GV_1(s) = \frac{qv'}{v}(s) = \frac{k\omega^2}{s^2 + k\omega s + \omega^2} \tag{2.13}$$

The Bode plots of equation 2.12 and equation 2.13 are shown in Fig. 2.11a and 2.11b respectively. Moreover, it can be seen that the transfer functions defined by 2.12 and 2.13, behave like a band-pass filter (BPF) and a low-pass filter (LPF) respectively and the frequency of the input grid voltage can be locked by the SOGI-PLL.
It can also be seen that the tuning frequency (ω) affects the resonance frequency of the SOGI and the gain (k) determines the bandwidth of both in-phase and in-quadrature component [13] which can be seen from figure 2.11. Hence, a proper trade-off is required between good dynamics and harmonics rejection capability when choosing the value of gain (k) and resonance frequency.

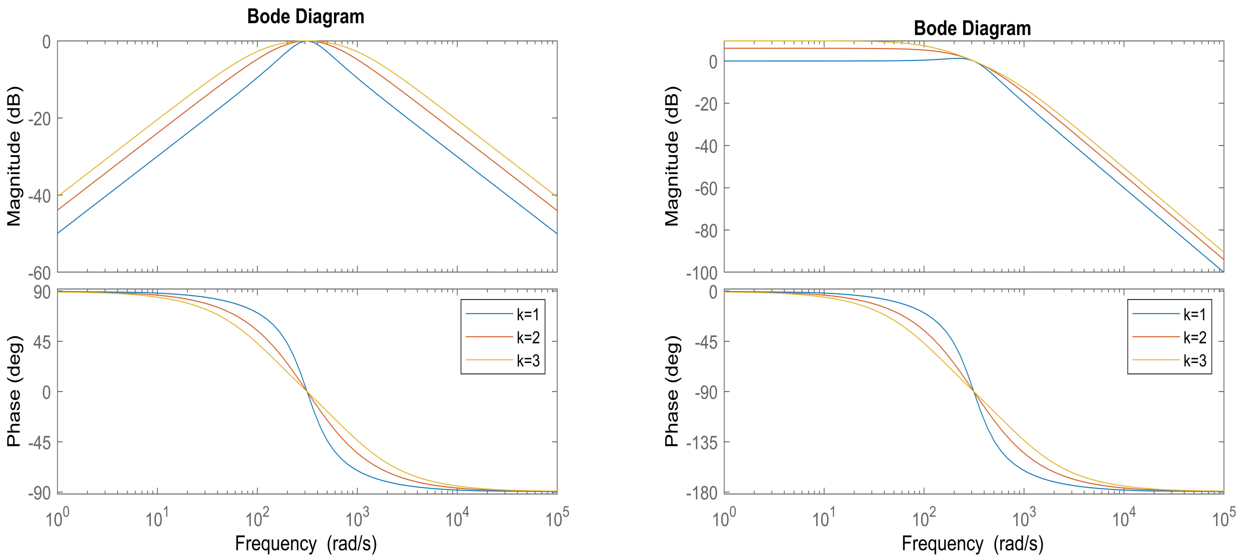

(a) Bode plot of transfer function of GV (b) Bode plot of transfer function of GV_1

Figure 2.11: Bode plot of in-phase and in-quadrature function with different value of k

2.10 Summary

In this chapter, microgrid introduction and its importance is discussed. Likewise all the three hierarchical control strategies for microgrids are presented. Clarke and Park transformation methods with equations are formulated. Synchronous Reference frame PLL governing equations are shown together with second order generalized integrator (SOGI) block simulink model and bode plots containing magnitude and phase are included.

3 Parameter design for inner loop controllers

3.1 Background

Due to global warming and climate change, conventional central electricity generation sources like coal and fossil fuel are slowly put off and distributed energy sources (DERs) such as wind, fuel cell and solar are encouraged in almost every part of the world. But, clean sources such as wind and solar do not generate constant voltage or frequency. Hence, there is a role of Inverter. Inverter can be defined as a power electronic circuitry which basically converts DC signal into AC signal. Voltage Source Inverter (VSI) acts as an interface between DERs and the main grid.
The main components can be explained in brief as follows-

1. **DC Source**: There should be a DC source which produces DC voltage or current such as Solar Photo-voltaic, battery, fuel cell etc.

2. **Power Electronic Switches**: Switches such as Thristors, MOSFET's, IGBT's can be turned on and off very fast and this operation help to convert DC into ACor vice versa. VSI can be three phase or single phase. For three phase inverter, switches are typically arranged in bridge configuration consisting of three legs having two switches each which is shown in figure 3.1.

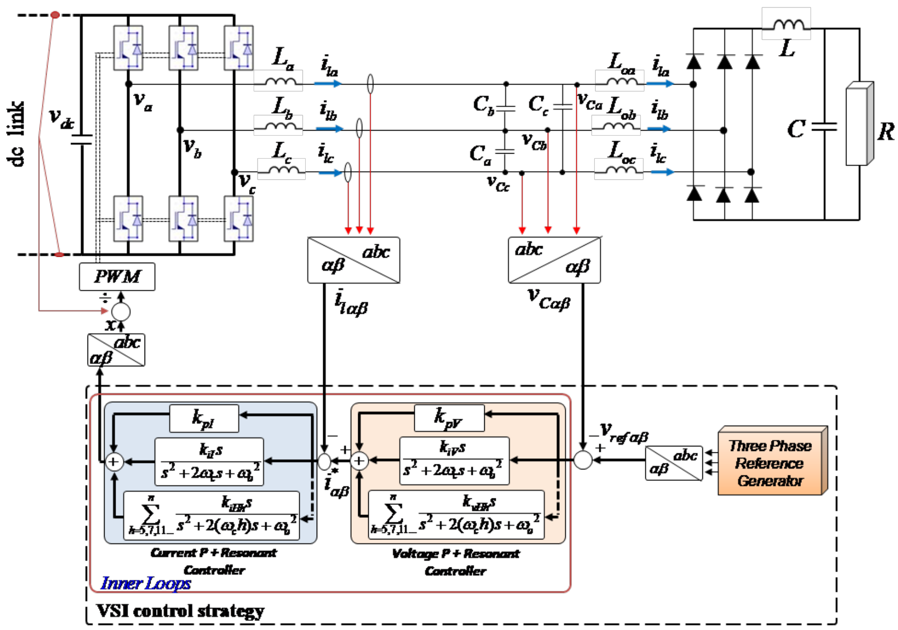

Figure 3.1: Block Diagram of VSI [14]

3. **Passive Filter**: Due to high switching frequency behavior of the switches, there is generation of harmonics. So, it is recommended to attenuate the harmonics by suitable filter as per standard set by the local grid code. There are four main types of filters generally used for VSI design, which are mentioned below-

    - L Filter

- LC Filter
- LCL Filter
- LCL Filter with damping resistor

In the model of the VSI used in thesis LC filter is considered. However, LCL (inductive-capacitive-inductive) circuit is used as it offers many advantages. The LCL-filters give benefits in terms of costs and dynamic performance since smaller inductors can be used as compared to L-filters only in order to achieve the necessary damping of the switching harmonics [15]. But, this type of filter is complex and needs to consider many factors, such as the total impedance of the filter, current ripple through inductors, resonance phenomenon, reactive power absorbed by filter capacitors, etc [15].

4. **Voltage and current sensors**: It is also an important component as current and voltage need to be measured and continuously be compared to implement closed loop and for designing controller. In the figure 3.1, it is denoted by oval side boxes.

5. **Controller**: It is also an important parameter for considering design of VSI. Voltage loop stabilize the voltage output and frequency. While current loop improve anti-disturbance capability and provide fast dynamic response

6. **Pulse Width Modulator**: It is necessary to generate gating pulses for the power electronics switches.

3.2 Synchronous reference frame and Stationary reference frame control

3.2.1 Synchronous Reference Frame Control

Synchronous reference frame control is also called ”dq” control, is used to transform the sinusoidal waveforms into a reference frame that rotates synchronously with a given angular frequency (abc→dq) by Park Transformation explained in sub- section 2.4.2 . The main aim of this transformation is to change the control variables to dc which makes filtering and controlling easier. The dq control structure is done with proportional–integral (PI) controllers and in matrix form (or Laplace form) it can be represented as equation 3.1.

$$\left[G_{\text{PI}}^{(dq)}(s)\right] = \begin{bmatrix} K_p + \frac{K_I}{s} & 0 \\ 0 & K_p + \frac{K_I}{s} \end{bmatrix} \tag{3.1}$$

Here, K_P and K_I is the proportional gain and the integral gain of the controller respectively and d coordinate represents the direct component while q coordinate represents the quadrature component. The PI current controller is easy to implement and hence is preferred for many control applications. In dq reference frame, the sinusoidal signals become DC variables, therefore PI controllers are enough for removing steady state errors. Moreover, it is poor at eliminating the low order harmonics [16].

3.2.2 Stationary Reference Frame Control

It transforms the grid currents and voltage waveform into stationary reference frame (i.e.abc→ $\alpha\beta$) and shown in equation 3.2.

$$\left[G_{\text{PR}}(s)\right] = \begin{bmatrix} K_P + \frac{K_I s}{s^2+\omega^2} & 0 \\ 0 & K_p + \frac{K_I s}{s^2+\omega^2} \end{bmatrix} \tag{3.2}$$

Here, K_P and K_I are the proportional gain and the resonant gain of the controller respectively. PR controller is a combination of both proportional term and a resonant term. It offers a very high gain around resonance and hence able to eliminate the steady-state error between the control signal and the sinusoidal reference signal. The width of the frequency band around the resonance frequency depends on the resonant time constant K_I. A lower K_I gives to a very narrow band, whereas a higher K_I offers a wider band [10].

The transfer function of a PR controller $G_{PR}(s)$ in Laplace domain is represented by:

$$G_{PR}(s) = K_P + K_I \frac{s}{s^2 + \omega_0^2} \tag{3.3}$$

where, K_P is the proportional gain
K_I is the resonant gain of the controller
ω_0 is the resonant frequency
Equation 3.3 represents an ideal PR controller which can give stability problems because of the infinite gain at resonance. So to avoid these problems, the PR controller is made non-ideal by introducing damping [17] as shown in equation 3.4

$$G_{PR}(s) = K_P + K_I \frac{2 \cdot \omega_c \cdot s}{s^2 + 2 \cdot \omega_c \cdot s + \omega_0^2} \tag{3.4}$$

Where, ω_c is the cut-off frequency.

3.3 Inner Loop Design

Voltage Source Inverter consisting of a three-phase pulsewidth modulation (PWM) ,LC filter, dc link voltage, Voltage and Current Control Loop are shown in schematic diagram 3.2. In order to analyze the closed-loop dynamics of the system, the deduction of block diagram is shown in figure 3.3. Mason's theorem is applied for block diagram and the transfer function obtained is shown in equation 3.5.

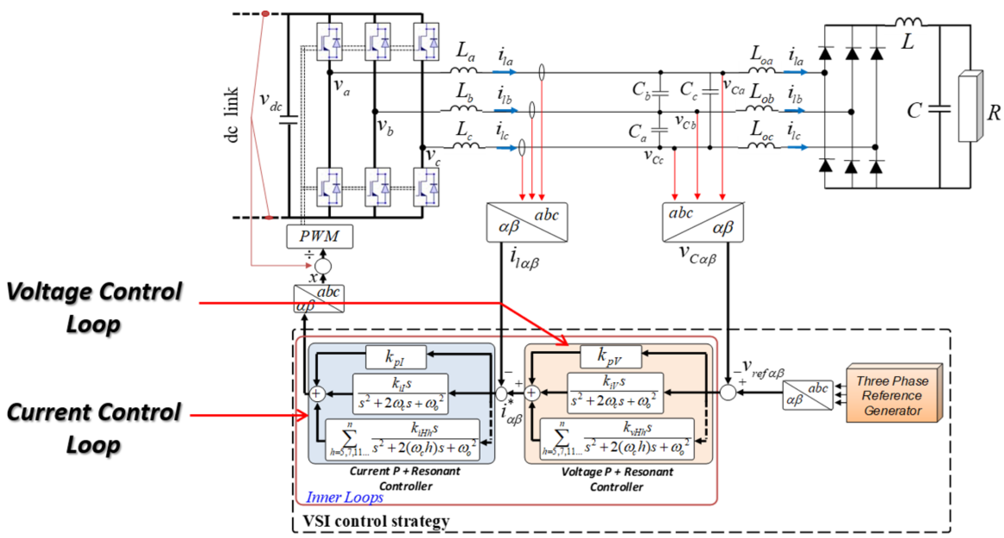

Figure 3.2: Diagram showing Current and Voltage Control Loop [14]

3.4 Block Diagram Reduction

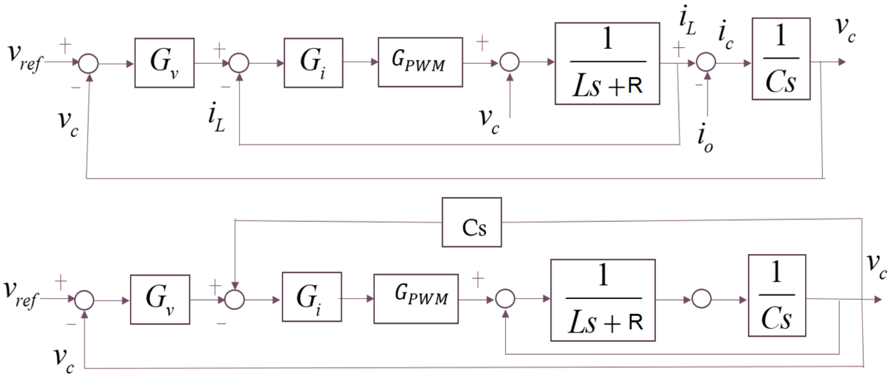

Figure 3.3: Diagram showing Every Block of VSI

$$v_c(s) = \frac{G_v(s)G_i(s)G_{PWM}}{LCs^2 + RCs + (Cs + G_v(s))G_i(s)G_{PWM} + 1} v_{ref} - \frac{Ls + R + G_i(s)G}{LCs^2 + RCs + (Cs + G_v(s))G_i(s)G_{PWM} + 1} i_0 \tag{3.5}$$

Here, v_{ref} is the voltage reference and i_0 is the output current. Similarly, v_c is the capacitor voltage, L being the inductor filter and C is the filter capacitor. The equation 3.5 shows that the output voltage depends on both the reference voltage (first term of equation 3.5) and the output current (second term of the same equation 3.5). The second term is also called output impedance.

While obtaining equation for current loop in steady state,outer loops are neglected. So, from figure 3.3, the transfer function for inner current loop and outer voltage loop are given by equation 3.6 and 3.7.

$$G_{inner} = \frac{i_L}{i_{ref}} = \frac{G_i(s)G_{PWM}}{Ls + R + G_i(s)G_{PWM}} \tag{3.6}$$

$$G_{outer} = \frac{v_c}{v_{ref}} = \frac{G_v(s)G_i(s)G_{PWM}}{LCs^2 + RCs + (Cs + G_v(s))G_i(s)G_{PWM} + 1} \tag{3.7}$$

The proposed controller is based on the stationary reference frame which includes voltage and current control loops. Though the control loops include proportional + resonant (PR) terms tuned at the fundamental frequency, 5th, 7th, and 11th harmonics, but for discussion in this chapter harmonics components are neglected.

$$G_i(s) = k_{pI} + \frac{k_{iI}s}{s^2 + \omega_0^2} + \sum_{h=5,7,11} \frac{k_{hI}s}{s^2 + (\omega_0 h)^2} \tag{3.8}$$

The function of the current controller $G_i(s)$ is to match the output I_L to the reference current i_{ref} as closely as possible and minimizing any error.

$$G_v(s) = k_{pV} + \frac{k_{iV}s}{s^2 + \omega_0^2} + \sum_{h=5,7,11} \frac{k_{hV}s}{s^2 + (\omega_0 h)^2} \tag{3.9}$$

Here, k_{pI} and k_{pV} are the proportional term coefficients for current and voltage respectively. Whereas, k_{iI} and k_{iV} are the resonant term coefficients for current and voltage respectively. Also, k_{hI} and k_{hV} are the resonant coefficient terms for the harmonics. Likewise, G_{PWM} is the transfer function corresponding to the delay (T_s) caused by computation devices and also to the PWM signal (T_s). Ts as the sampling period and equation for G_{PWM} is shown in 3.10.

$$G_{PWM}(s) = \frac{1}{1 + 1.5T_s s} \tag{3.10}$$

3.5 Simulation Results and Discussion

In the nested control loop, the inner current loop is designed the fastest with higher bandwidth while the outer is designed relatively slower with lower bandwidth. Using, this approach, current loop is fastest and we can ignore the resonant term for easy calculation. Since we are dealing with $\alpha\beta$ frame as shown in figure 3.2, we use PR controller. Ignoring both harmonics component and resonant term, the equation 3.8 becomes-

$$G_i(s) = k_{pI} \tag{3.11}$$

Putting value of current controller in equation 3.6, equation 3.12 is obtained below-

$$G_{inner} = \frac{k_{pI} \cdot G_{PWM}}{Ls + R + k_{pI} \cdot G_{PWM}} \tag{3.12}$$

The table 5.1 shows the value of different parameters used in simulation-

Table 3.1: System parameter value for the simulation

Parameter	**Notation**	**Value**
Inductors	L	1.8mH
Capacitors	C	27μF
Resistance	R	0.2Ω
Resonance frequency	ω_0	$314 = (2 \times \pi \times 50)$
Cut off frequency	ω_c	$0.314 = (0.001 \times 2 \times \pi \times 50)$
Switching Frequency	f_{swich}	10 kHz

3.5.1 Solving by Bandwidth Approach

Current loop

Bandwidth refers to how fast the system can track agiven input before the performance starts to degrade. In control application, it is the frequency of input before system response drops 3dB from DC gain. Taking the magnitude of equation 3.12, the equation 3.13 is obtained as follows-

$$|G_{inner}| = |\frac{k_{pI} \cdot G_{PWM}}{Ls + R + k_{pI} \cdot G_{PWM}}| \tag{3.13}$$

But, the value of G_{inner} is as follows in equation 3.14-

$$|G_{inner}| = 10^{-0.15} = 0.707945784 \approx \frac{1}{\sqrt{2}} \tag{3.14}$$

Solving equation 3.13 (with bandwidth of 2kHz) with the value obtained from equation 3.14 in Wolfram Mathematica software (which is shown in appendix A.2), the value of k_{pI} is found to be 0.0330837.The bode plot for current loop is shown in figure 3.4. The same plot can be validated by step function. In the validation, k_{pI} value is varied from 0.01 to 0.05 and the result obtained is shown in figure 3.5. From the same step figure, it can be seen, k_{pI} value around 0.03 is trade-off between settling time, rise time, and overshoot.

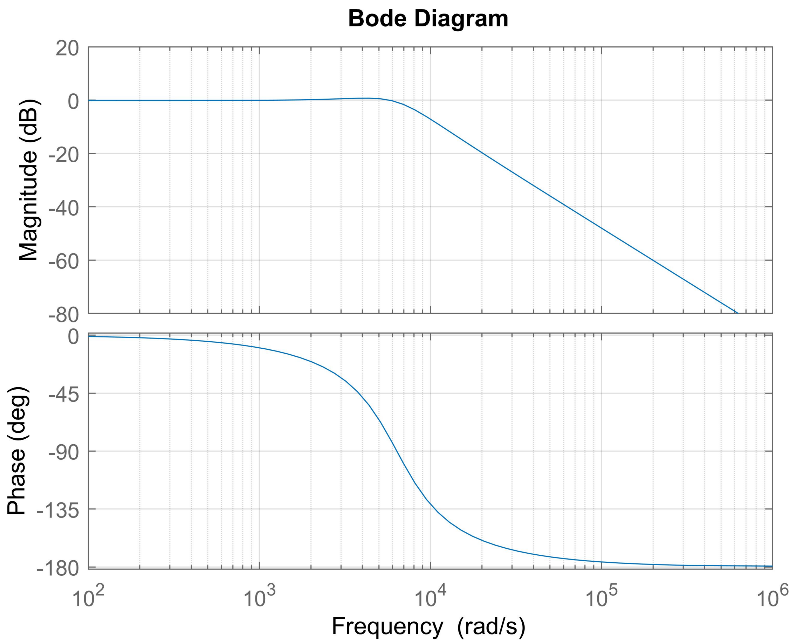

Figure 3.4: Bode plot of the Current loop

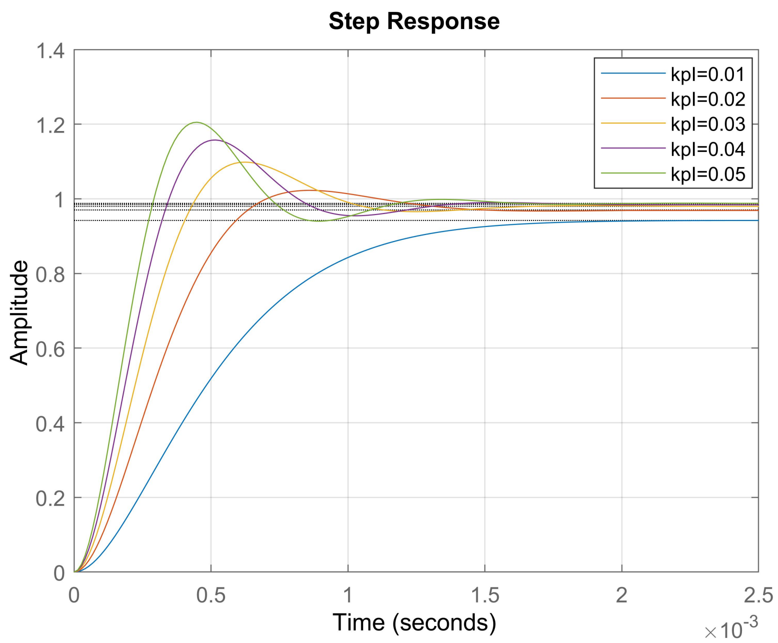

Figure 3.5: Step Response

Voltage loop

Outer voltage is also found by the same bandwidth approach as discussed in the current-loop. As the outer loop is slower, usually for the design purpose, the bandwidth of the outer loop is one fourth or one fifth of the bandwidth of the inner loop in order to avoid interaction. In this design, 500Hz is considered which is one fifth of the 2kHz (Inner loop frequency). Taking the magnitude of equation 3.9, the equation 3.15 is obtained as follows-

$$|G_v(s)| = |k_{pV} + \frac{k_{iV}s}{s^2 + \omega_0^2} + \sum_{h=5,7,11} \frac{k_{hV}s}{s^2 + (\omega_0 h)^2}| \tag{3.15}$$

Harmonics component is ignored and for finding k_{pV}, the resonant part k_{iV} is assumed to be zero. In this way proportional part of a controller is found. Then integral part is found and for this frequency considered is resonance i.e. 50 Hz. Wolfram Matimatica is used for solving k_{pV} and k_{iV} and the value obtained is 0.0430695 and 9.67622 respectively. The solution is attached in Appendix. The bode plot obtained is shown in figure 3.6

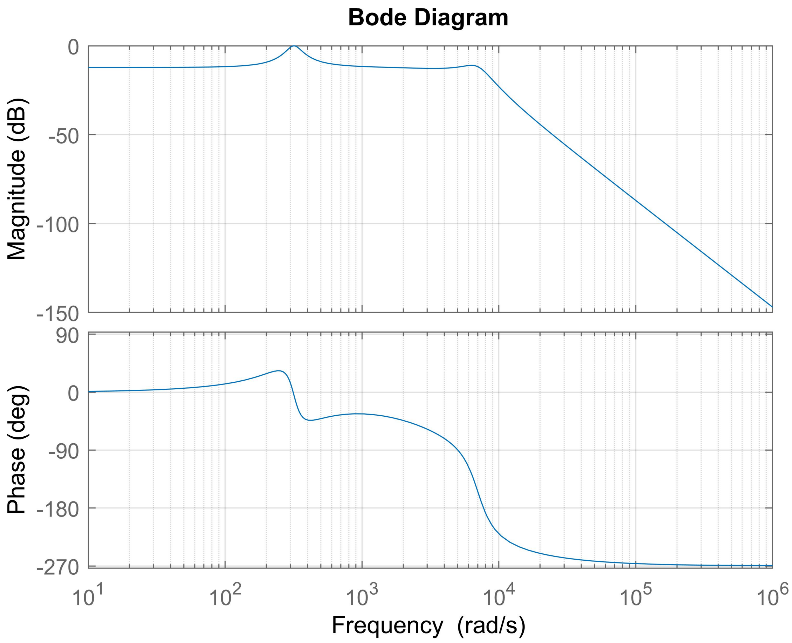

Figure 3.6: Bode plot of voltage loop

3.6 Summary

The control parameters at the zero level which contains current and voltage loops are designed in this chapter. To avoid interaction, the cut-off frequency of the outer voltage loop is designed as one-fourth of the inner current loop. The PR controller parameters for current and voltage loops are identified by the bandwidth approach and are validated by the bode diagram. The designed controller parameters are listed in table 3.2.

Table 3.2: Values of different parameters

Parameter	**Symbol**	**Value**
Proportional term for current loop controller	k_{pI}	0.0330837
Proportional term for voltage loop controller	k_{pV}	0.0430695
Resonant term for voltage	k_{iV}	9.67622

4 Power droop control for parallel inverters

4.1 Introduction to Droop Control

In conventional gas and coal-fired generator, the frequency of the generated voltage is stabilized by the rotational inertia of the gas or steam generator. In such power generation system, the rate of change of frequency (ROCOF) is inversely proportional to the rotor inertia constant of the system [18]. The ROCOF is the time derivative of the power system frequency (df/dt) [19] or rate of change of frequency. In conventional synchronous generation, ROCOF was of minor significance as inertia of these large generators significantly curtails the load disturbances and limit the scope of ROCOF in these cases. However, due to climate change and to curb global warming, there is high number of solar, wind, battery, fuel cell replacing conventional power generation. Moreover, these distributed energy resources have very small inertia or no inertia at all. And in these cases, the concept of ROCOF is of prime importance.

For a stable operation of a grid system and to stop blackouts, the control of the real power and the reactive power is very significant. Real power (P) depends predominantly on the power angle and reactive power (Q) depends predominantly on the voltage amplitude which is proved in subsequent section of the report. For maintaining these conditions when there is change in load, droop control is very handy as this method ensure loads are taken by the inverter in a predetermined manner or predetermined set-point without use of any communication. This method uses the frequency and voltage droop characteristics when the load changes without any wire communication. Hence, every DG unit is able to operate independently and form the basics of modular concept. Being, wireless control, it offers many advantages. Firstly, as droop control method does not require high speed communication, it is very economical. Secondly, in this control methodology, only local measurement is used, so it can be used in remote places where DG is spread over a long distance.

4.2 Theoretical Framework

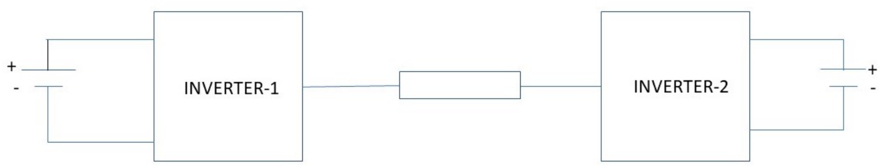

Figure 4.1: Schematic diagram of two inverterS

Figure 4.1 shows the power schematic diagram of two parallel inverter connected to the common load or point of common coupling (PCC). Let $E_i\angle\phi_i$ is the voltage of 'i' number of inverter and ϕ_i is the phase angle difference between E_i and V (voltage at the common node). $Z\angle\theta$ is the equivalent impedance between the inverter and the common bus impedance, which considers the inverter output impedance and the line impedance of the connection wires.

Assuming a single inverter unit connected to a common bus through a transmission line with impedance $Z = R+jX$ as shown in figure 4.2 . X and R are reactance and resistance value of feeder impedance respectively. θ represents the impedance angle. The apparent power S delivering to the bus from the inverter is given in equation 4.1.

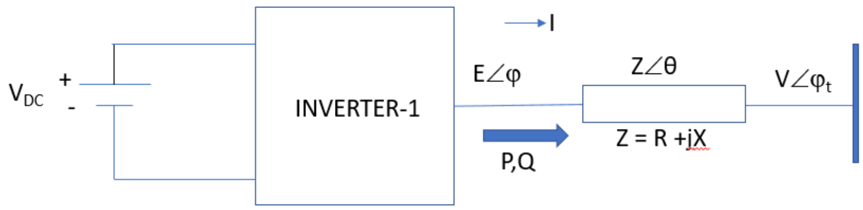

Figure 4.2: Schematic diagram of a single inverter connected to the common bus

$$S = P + jQ \tag{4.1}$$

Here, P and Q are active and reactive powers output from the inverter to the bus respectively, and I is the current flowing through the transmission line from the inverter to the common bus, which is given by 4.2:

$$I = \frac{E\angle\phi - V\angle\phi_t}{Z\angle\theta} \tag{4.2}$$

$$I = \frac{E}{Z}\angle\phi - \theta - \frac{V}{Z}\angle\phi_t - \theta \tag{4.3}$$

Apparent power, S (volt-amperes), also known by the complex power is found by multiplying E by the conjugate of I or vice versa as shown in equation 4.4.

$$S = P + jQ = \mathbf{E} \times \mathbf{I}^* = E\angle\phi\left[\frac{E}{Z}\angle\theta - \phi - \frac{V}{Z}\angle\theta - \phi_t\right] = \frac{E^2}{Z}\angle\phi - \frac{E \times V}{Z}\angle\theta + \phi - \phi_t \tag{4.4}$$

Thus the active and reactive power can be expressed as in equation 4.5 and 4.6.

$$P = \frac{E^2}{Z}\cos\theta - \frac{E \times V}{Z}\cos(\theta + \phi - \phi_t) \tag{4.5}$$

$$Q = \frac{E^2}{Z}\sin\theta - \frac{E \times V}{Z}\sin(\theta + \phi - \phi_t) \tag{4.6}$$

For medium and high voltage transmission lines usually have small resistance compared to inductance (shown in table 4.1), i.e. $Z\angle\theta = X\angle 90^0$, which means impedance angle, $\theta = 90^0$. So, the active and reactive powers drawn to the bus can be expressed in equation 4.7 and 4.8.

Table 4.1: Line Impedances Values [20]

Type of transmission line	$R(\Omega/km)$	$X(\Omega/km)$	R/X (p.u.)
Low Voltage Line	0.642	0.083	7.7
Medium Voltage Line	0.161	0.190	0.85
High Voltage Line	0.06	0.191	0.31

$$P = \frac{E \times V}{Z} \sin(\phi - \phi_t) \tag{4.7}$$

$$Q = \frac{E^2}{Z} - \frac{E \times V}{Z} \cos(\phi - \phi_t) \tag{4.8}$$

From equation 4.7 and equation 4.8, it can be seen there are two variables angle 'ϕ' and output voltage amplitude 'E' that can affect both active and reactive power. Taking partial fraction of 4.7 and equation 4.8, we get equation 4.9, 4.10, 4.11 and 4.12.

$$\frac{\partial P}{\partial \phi} = \frac{E \times V}{Z} \cos(\phi - \phi_t) \tag{4.9}$$

$$\frac{\partial P}{\partial E} = \frac{V}{Z} \sin(\phi - \phi_t) \tag{4.10}$$

$$\frac{\partial Q}{\partial \phi} = \frac{E \times V}{Z} \sin(\phi - \phi_t) \tag{4.11}$$

$$\frac{\partial Q}{\partial E} = \frac{2E}{Z} - \frac{V}{Z} \cos(\phi - \phi_t) \tag{4.12}$$

When ϕ is very close to ϕ_t, equations 4.9, 4.10, 4.11 and 4.12 can be simplified to equations 4.13, 4.14, 4.15 and 4.16.

$$\frac{\partial P}{\partial \phi} \approx \frac{E \times V}{Z} \tag{4.13}$$

$$\frac{\partial P}{\partial E} \approx 0 \tag{4.14}$$

$$\frac{\partial Q}{\partial \phi} \approx 0 \tag{4.15}$$

$$\frac{\partial Q}{\partial E} \approx \frac{2E}{Z} - \frac{V}{Z} \tag{4.16}$$

Therefore, active power output is mainly dominated by angular frequency, while reactive power output is mainly dominated by voltage magnitude when the line impedance is inductance dominated.

The droop control is a widely used method and based on the above equations 4.13 and 4.16, the following two conclusion can be made as-

1) Active power (P) mainly depends on angle ϕ, which is changing by frequency ω.
2) Reactive power (Q) depends on inverter voltage amplitude E.
This is the fundamental basics for the conventional droop characteristic, which can be represented as equation 4.17 and 4.18 with output frequency ω and voltage E of an inverter:

$$\omega = \omega^* - mP \tag{4.17}$$

$$E = E^* - nQ \tag{4.18}$$

Here, ω^* and E^* are the output angular frequency at no load condition and m and n are the droop coefficients for the frequency and amplitude, respectively.

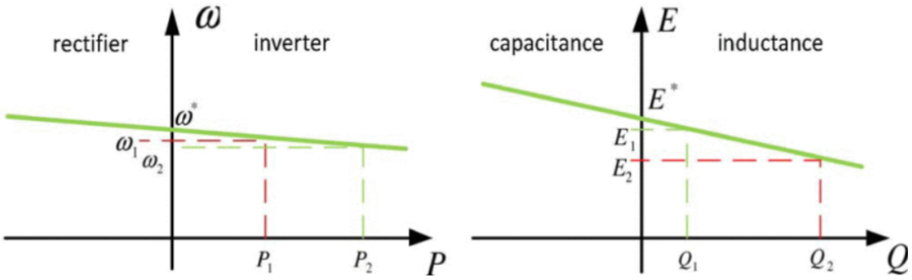

Figure 4.3: Droop characteristics of $P - \omega$ and Q-E [21]

The Droop characteristics of $P - \omega$ and Q-E are shown in figure 4.3. So to implement this droop characteristics in VSI, the outer droop block is developed [21] which is shown in figure 4.4 and shown in equation 4.19 and 4.20

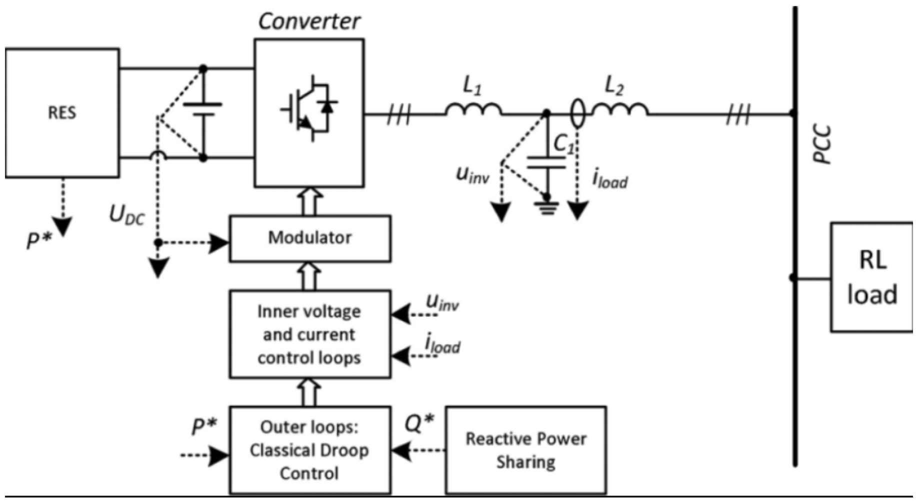

Figure 4.4: Block diagram showing outer droop control of an islanded MG [21]

$$\omega = \omega^* - G_p(s) \cdot (P - P^*) \tag{4.19}$$

$$E = E^* - G_q(s) \cdot (Q - Q^*) \tag{4.20}$$

In classical droop control, G_p and G_q are proportional droop coefficients and is given by equation 4.21 and 4.22 and schematic diagram is shown in figure 4.5.

$$G_p(s) = m = \frac{\Delta\omega_{\text{max}}}{P_{\text{max}}} \tag{4.21}$$

$$G_q(s) = n = \frac{\Delta E_{\text{max}}}{Q_{\text{max}}} \tag{4.22}$$

Here,
m = active power coefficient
n = reactive power coefficient
$\Delta\omega_{max}$ = maximum allowed frequency deviation (droop)
ΔE_{max} = maximum allowed voltage amplitude deviation (droop)
P_{max} = maximum allowed active power
Q_{max} = maximum allowed reactive power

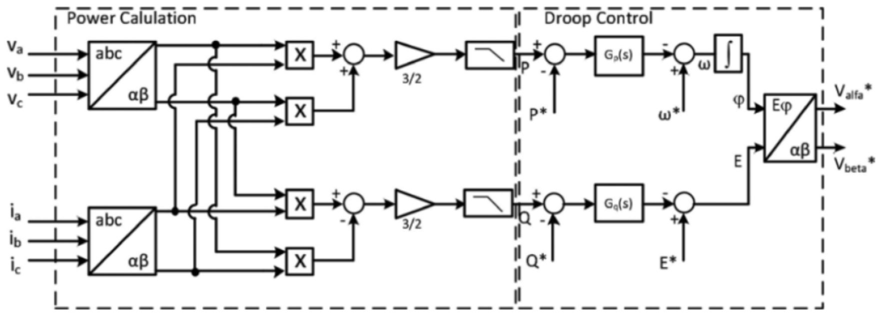

Figure 4.5: Schematic Diagram of classical droop control [21]

4.3 Power droop controller design

Due to growing number of distributed energy resources in the main grid, two or more VSI are connected in parallel. Droop based control scheme regulate the frequency and voltage amplitude and send the reference to the inner current and outer voltage control loop as shown in figure 4.4. It emulates the controller behaviour of the synchronous generator and decreases the frequency when the active power increases [22]. The droop control used is shown in figure 4.6 and droop functions used is illustrated below in equation 4.23 and 4.24.

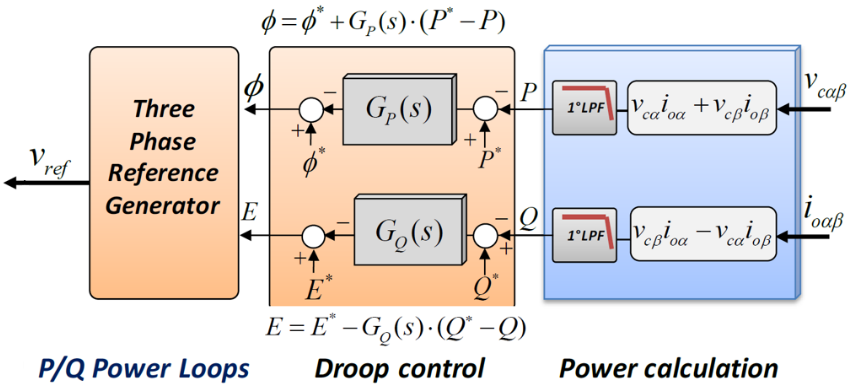

Figure 4.6: Control Scheme of droop control [22]

$$\phi = \phi^* - G_P(s) \cdot (P - P^*) \tag{4.23}$$

$$E = E^* - G_Q(s) \cdot (Q - Q^*) \tag{4.24}$$

Here, ϕ is the phase of voltage reference V_{ref} as shown in figure 4.6 that is fed to inner loop. Since, angle ϕ is found by integrating electrical frequency which is shown in equation 4.25. P^* and Q^* are the active and reactive power references respectively and is normally set to zero in standalone mode as power outputs are decided by the loads. G_P and G_Q are the transfer function of the controller which is defined by equation 4.26 and 4.27 respectively.

$$\phi^* = \omega^* \int dt = \omega^* t \tag{4.25}$$

$$G_P(s) = \frac{k_{iP} + s \cdot k_{pP}}{s} \tag{4.26}$$

$$G_Q(s) = \frac{k_{iQ} + s \cdot k_{pQ}}{s} \tag{4.27}$$

Where, k_{iP} and k_{pQ} are static droop coefficient [22] and its value can be found from equation 4.21 and 4.22. Whereas k_{pP} and k_{iQ} are known as transient droop term or considered virtual inertia of the system [22].

4.4 Designing the Controller

4.4.1 Design of the virtual impedance

We assume the inverter exports 2 kW to the grid, with a maximum angle of 1 degree between the inverter and the grid (E=230 V, V=230 V) to calculate the value of output impedance. The design of the proper controller is shown in figure 4.7.

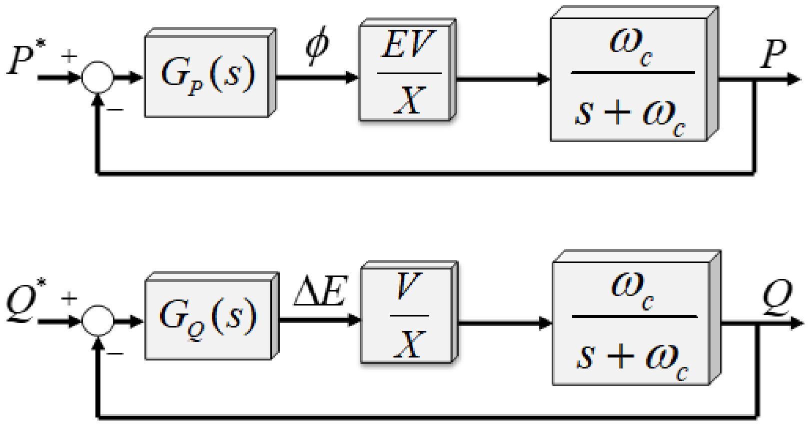

Figure 4.7: Block Diagram of the droop control [22]

$$P = \frac{E \times V \times \sin\phi}{X} \tag{4.28}$$

$$X = 2 \times pi \times f \times L \tag{4.29}$$

The inverter and bus voltage is assumed to be 230V, with the inverter exports 2 kW to the grid and using equation 4.28 and 4.29, the inductance or virtual inductance was found to be 1.47 mH.

4.4.2 Designing k_{iP} and k_{pQ}

The same initial condition of virtual impedance is considered. The purpose of low-pass filter is to filter the measured output power to obtain average power outputs. The frequency of low-pass filter considered in the simulation is 5 Hz. For calculating k_{iP}, it is assumed that a nominal power of 2 kW causes a 0.16 Hz of frequency deviation. For calculating k_{pQ}, it is assumed that a 50 VAr of reactive power deviation results in an error of 2 percent of the amplitude.

Using equation 4.21 and 4.22, the value of 'm' and 'n' are found to be 5.0265e-04 and 0.0920 respectively which in turn are the values of k_{iP} and k_{pQ} respectively.

4.4.3 Designing k_{pP} and k_{iQ}

After finding the values of k_{iP} and k_{pQ}, the values of k_{pP} and k_{iQ} are found by phase margin ($30^0 - 75^0$) and are validated by root-locus method.
The value of k_{pP} is varied from 0.000001 to 0.00005 and at a interval of 0.00001. For design purpose, it is assumed that the phase margin should fall between $30^0 - 75^0$. When the transfer function shown in figure 4.7 is implemented in MATLAB, the value of k_{pP} with above mentioned phase margin is found to be 2.1000e-05. In this case, the phase margin is 75.2781 and overshoot is around 7 percent, step response is fast and settling time is low. The step response and root-locus for different values of k_{pP} are shown in figure 4.8 and 4.9. From the rootlocus in figure 4.9, it can be seen the value chosen has damping around 0.74, which is represented by '*' sign. Hence, the controller has optimum value for which there is increased damping and decreased oscillation. Also, it has sufficient stability margin considering uncertainty in the modelling of physical system.

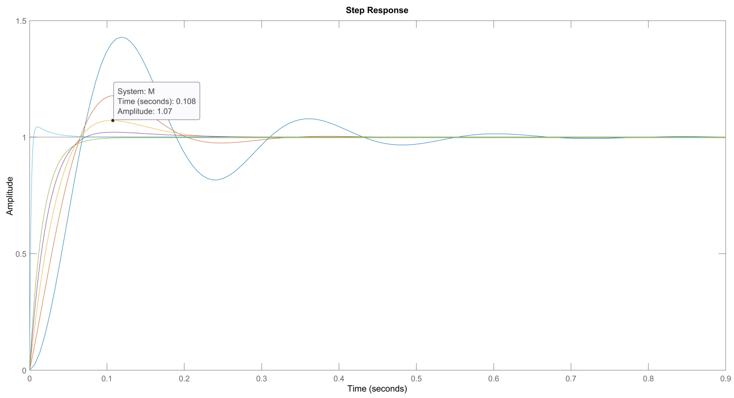

Figure 4.8: Step Response for controller design

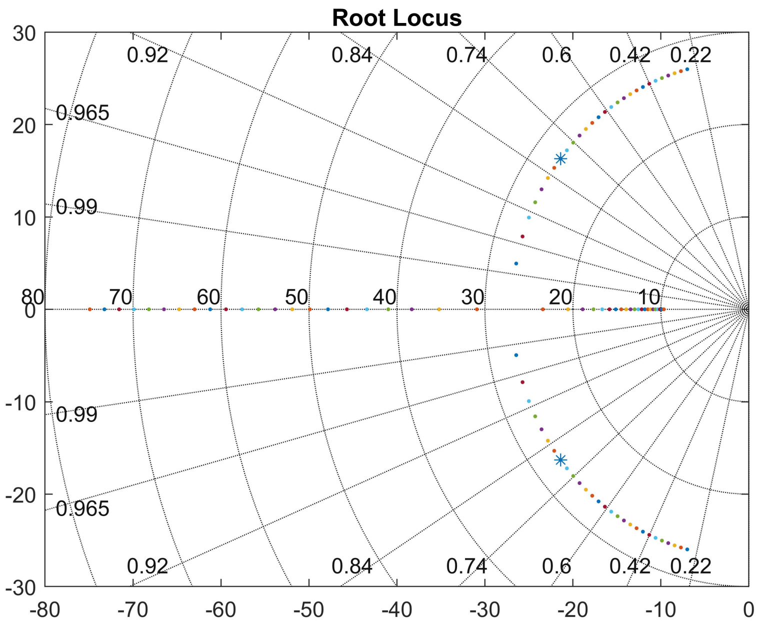

Figure 4.9: Root locus for controller design

The value of k_{iQ} is varied from 0.01 to 5. For design purpose k_{iQ} is supposed to fall between $30^0 - 75^0$. After seeing the results in step function and root locus, k_{iQ} with value 0.5 is chosen as the phase margin at this point is 67.0156 and overshoot is around 16 percent and step response is fast and settling time is low. The step response and root-locus for different values of k_{iQ} are shown in figure 4.10 and 4.11. From the rootlocus figure 4.11, it can be seen the damping coefficient is around 0.74. This is around critically damped frequency. Hence, as discussed earlier in finding k_{pP}, the designed controller has optimum value and it has sufficient stability margin considering uncertainty in the modelling of physical system.

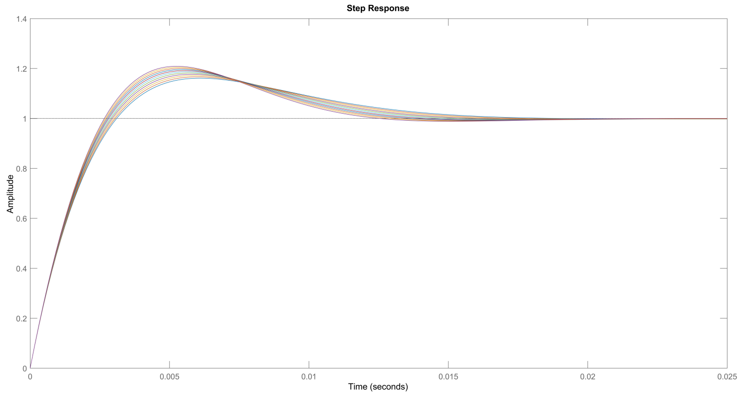

Figure 4.10: Step Response for controller design

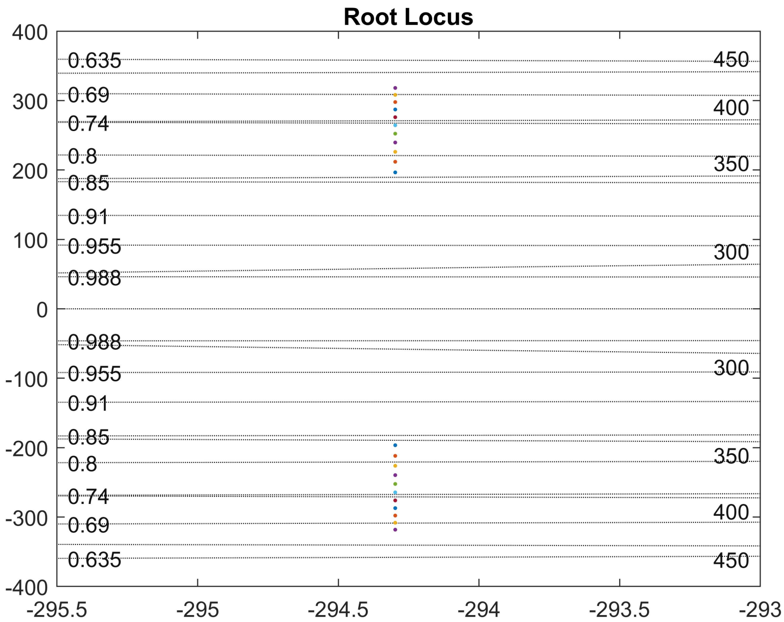

Figure 4.11: Root locus for controller design

4.5 Summary

In this chapter, droop-based method is used in primary control to simulate physical behaviour of the system. Droop equations for inverter is derived and proved mathematically that active power output is mainly dominated by angular frequency, while reactive power output is mainly dominated by voltage magnitude when the line impedance is inductance dominated. The droop control is applied to achieve the active and reactive power sharing without using communication channels. The designed droop coefficients are listed in table 4.2.

Table 4.2: Values of different parameters

Parameter	Symbol	Value
virtual inductance	L	1.47 mH
static droop coefficient	k_{iP}	5.0265e-04
static droop coefficient	k_{pQ}	0.0920
transient droop term	k_{pP}	2.1000e-05
transient droop term	k_{iQ}	0.5

5 Centralized and Decentralized Secondary Control

5.1 Introduction

Multilayer hierarchical control has become widely used as an operation solution for both AC and DC microgrids. Hierarchical control commonly consists of three control layers namely primary, secondary, and tertiary. Each layer has different time constant, speed of operation, and bandwidth for control.

The primary control maintains the stability of voltage and frequency, and achieves the active and reactive power sharing without using communication channels by droop control method. Though primary control, maintains frequency and voltage amplitude within preset value, but the droop in observed in both frequency and voltage which is shown in figure 4.3. Basically, primary layer by using the droop based method, emulates the behavior of the synchronous generators but causes frequency and voltage steady-state deviations. So, in order to restore their value, Secondary control compares the measured voltage magnitude and frequency with reference values and regulate the deviations toward zero after any variation in power generation and load.
1) Inverter connected to another inverter
2) Inverter connected to the main utility

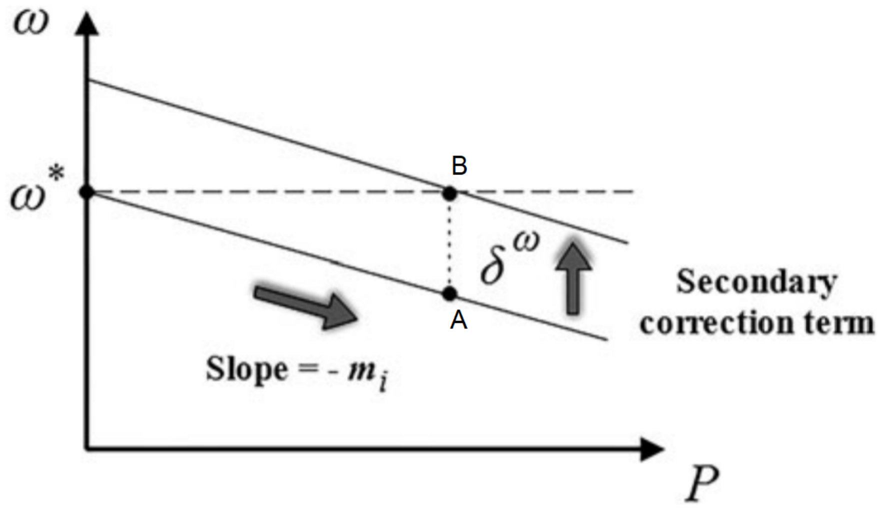

Figure 5.1: Schematic diagram of Primary and secondary control actions [4]

5.1.1 Mathematical Expression

Secondary layer compensate the steady-state errors or deviations produced by the primary layer. It corrects frequency and voltage deviations by adding an extra term in the main control equations [4] as expressed in equation 5.1 and 5.2. In figure 5.1, it can be seen when the active power demand increases, there is a droop in angular frequency , and it drops from point B to point A. By implementing secondary controller, the frequency is shifted back from point A to point B by adding term δ_i^ω. The same phenomenon is observed when increase in reactive power brings deviation or droop in output voltage amplitude in inductive dominated grid.

$$\omega_i = \omega^* - m_i P_i + \delta_i^\omega \tag{5.1}$$

$$V_i = V^* - n_i Q_i + \delta_i^V \tag{5.2}$$

Here,
ω_i = Angular frequency at a given load,
ω_i = Angular frequency at the reference,
V_i = amplitude of the converter output voltage,
V^* = amplitude of the converter output voltage at the reference,
m_i = droop coefficient for active power,
n_i = droop coefficient for reactive power,
P_i = output active power,
Q_i = output reactive power,
i = represented for converter i,
δ_i^V = secondary control term for voltage amplitude,
δ_i^ω = secondary control term for frequency

5.1.2 Synchronisation Loop

It is very important to synchronize all the voltage source inverters with each other before the parallel connection. It can be done in secondary controller. The synchronization process is done by using the $\alpha\beta$ components of the common bus voltage cross multiply with the $\alpha\beta$ components of a inverter voltage outputs. If the cross product of two vectors is the zero vector, then either one or both of the inputs is the zero vector, (a = 0 or b = 0) or else they are parallel or anti-parallel so that the sine of the angle between them is zero (θ = 0 or θ = 180 and sinθ = 0). The output variable of the voltage angular frequency/phase synchronization loop is added to the rotation angular frequency of the PR voltage controller of the inner voltage control loop.

a $\times$ **b** $= 0$
θ = $0°$ or $180°$

5.2 Centralized Secondary Control

As discussed in previous chapters, primary control uses local measurement to apply its control algorithm. Moreover, it lacks the inter-communications with parallel connected DG units. So in order to achieve global control in MG, all DG sets should be brought into one centralized control platform, for which secondary control is very useful. As shown in figure 5.3 , the remote sensing block collects the required parameter compares with the reference values in the Microgrid Centralized Controller (MGCC) by means of a low-bandwidth communication system. The controller compensates the error by sending the output signal to each DG sets through primary control. The main advantage from this centralized controller is that unidirectional signal are send from each secondary control to each DG units which makes the communication channel less busy. But the main drawback is that failure to a secondary controller will stop the entire secondary control action.

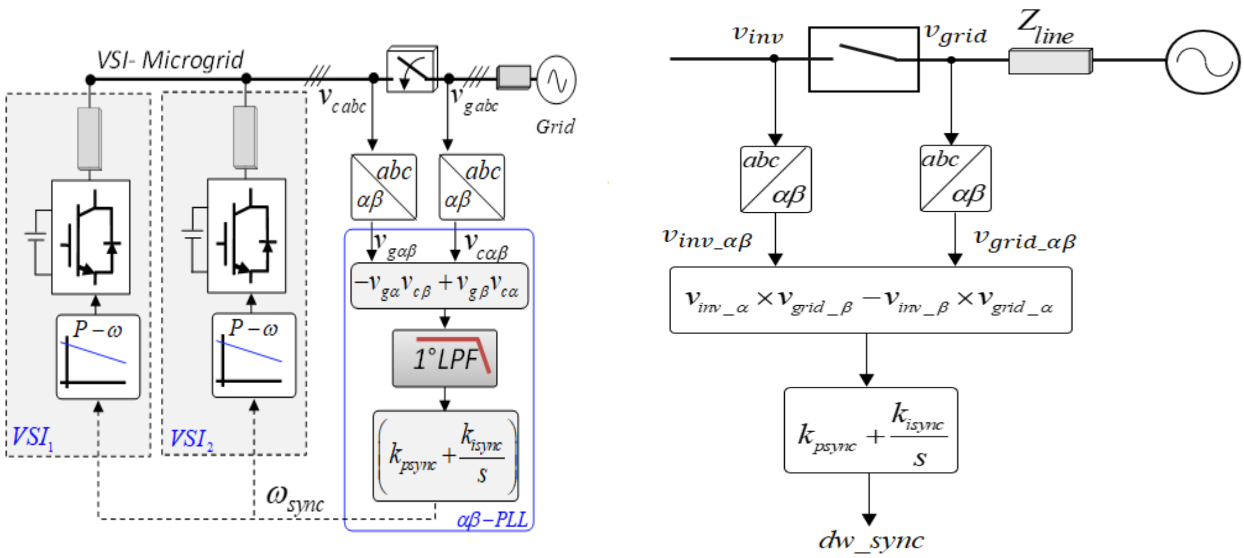

Figure 5.2: Block Diagram of Synchronization Loop [22]

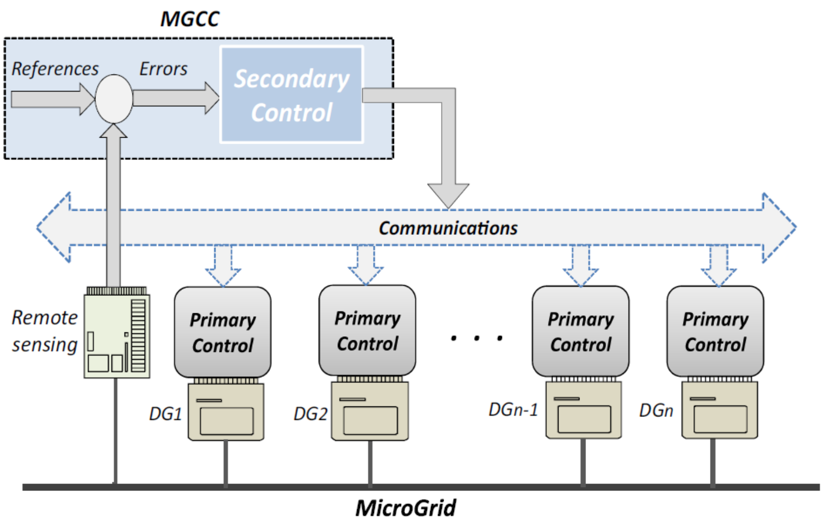

Figure 5.3: Schematic diagram of Centralized Secondary Control [23]

5.2.1 Frequency Restoration

Conventionally, large power plant used secondary controller for frequency restoration. Now the same concept is used in microgrid to integrate many distributed energy resources. It brings the grid frequency deviation within the allowable prescribed limit, for e.g. ±0.2 Hz in synchronous grid of Continental Europe and ±0.1 Hz in Nordel (North of Europe) [22]. It is known as Load Frequency Control (LFC) in Europe or Automatic Generation Control (AGC) in USA [23]. This central controller uses slow PI controller to regulate frequency deviations in the entire microgrid and the output of the controller is sent to the DG sets to compensate for the frequency variations. In figure 5.4, it can be seen f_{MG} is detected and compared with the reference value f^*_{MG} and the error is generated. The error is compensated by PI controller and the required command signal is sent to all DG units to restore the output frequency.

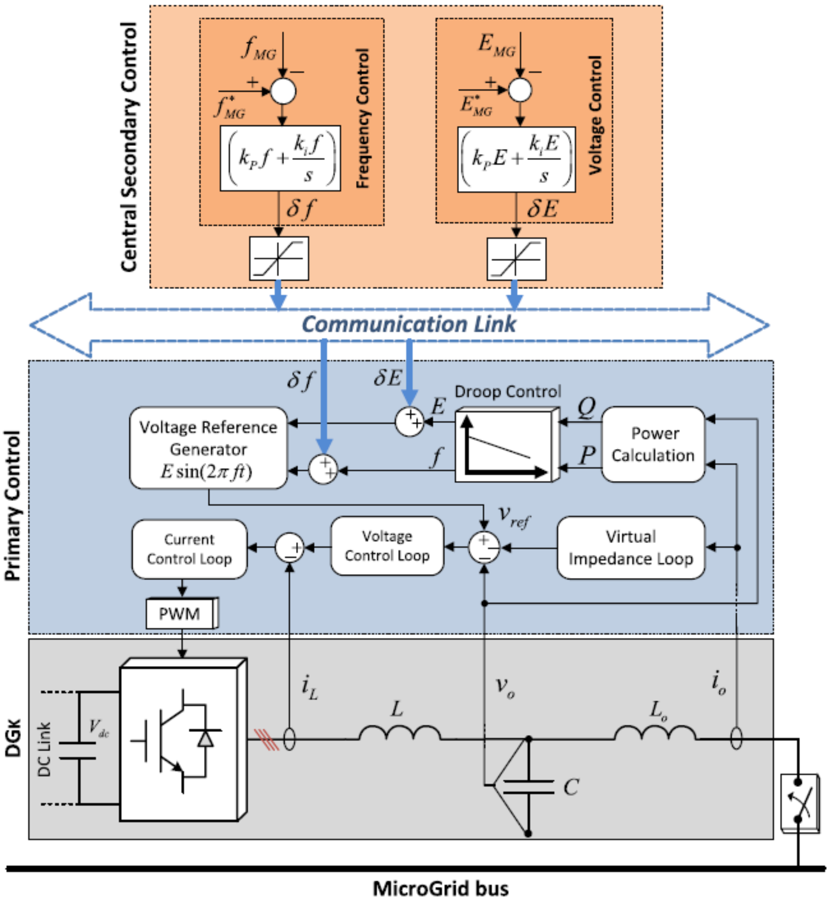

Figure 5.4: Schematic diagram of Centralized Secondary Control in a Microgrid [23]

Mathematically, it can be expressed in equation 5.3 where k_{pf} and k_{if} are the proportional and integral parameters respectively for the secondary PI control. The signal δf is the error signal sent to DG units after comparing frequency signal f_{MG} with reference signal f^*_{MG}.

$$\delta \mathrm{f} = k_{pf}\,(f^*_{\mathrm{MG}} - f_{\mathrm{MG}}) + k_{if} \int (f^*_{\mathrm{MG}} - f_{\mathrm{MG}})\,dt \tag{5.3}$$

5.2.2 Voltage Restoration

The voltage restoration can also be done in the similar process as explained in frequency restoration in the subsection 5.2.1. When the voltage magnitude is deviated from the prescribed rms value, then the error signal is generated which applies on the PI control. The controller compensates the voltage by passing the information to each DG which is shown in figure 5.4. Mathematically, voltage control loop can be expressed in equation 5.4. Here, k_{pE} and k_{iF} are the controller proportional and integral parameters and the error signal δE is generated by comparing voltage amplitude signal E_{MG} with reference signal E^*_{MG}.

$$\delta \mathrm{E} = k_{pE}\,(E^*_{\mathrm{MG}} - E_{\mathrm{MG}}) + k_{iE} \int (E^*_{\mathrm{MG}} - E_{\mathrm{MG}})\,dt \tag{5.4}$$

5.3 Distributed Secondary Control

The main demerit with centralized controller is that a single fault or failure in the secondary controller can collapse the whole system. So to address these imperfection of the centralized controller, the distributed control function came into existence. In this distributed controller, primary and secondary controller acts together as a local controller which is depicted in figure 5.5. In the same figure, it can be seen secondary control lies between communication system and the primary control. In distributed system, secondary control of each DG unit collects the required measurements like frequency, voltage amplitude and reactive power from other DG unit through common communication links, sum them and average is taken. Then the appropriate control signal is sent to the primary level to compensate the deviations.

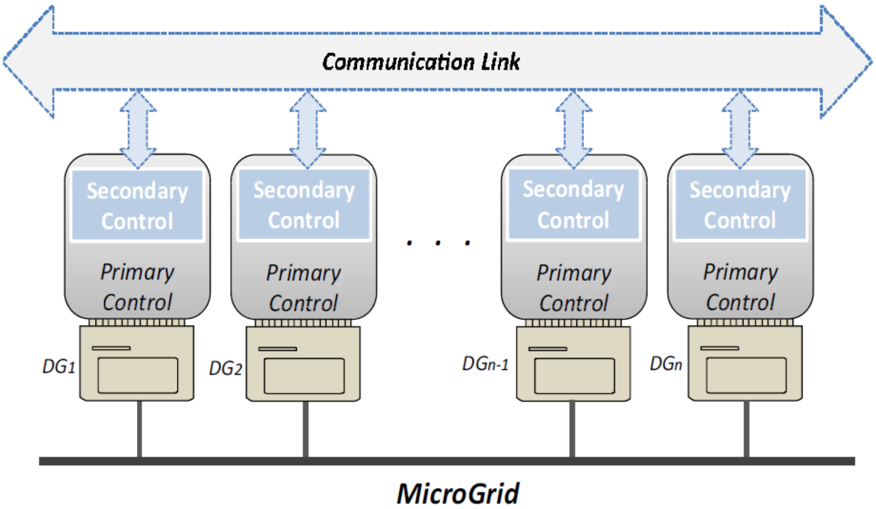

Figure 5.5: Schematic diagram of Centralized Secondary Control in a Microgrid [23]

5.3.1 Frequency Restoration

Contrary to the frequency restoration in the centralized control explained in sub-section 5.2.1, here each DG units takes the frequency measurement and the same signal is sent to other DG units too. Finally, the received frequency sample is averaged and then sent to primary level to compensate and remove the steady-state error. Mathematically, it can be expressed in equation 5.5 and 5.6 [23].

$$\delta \mathrm{f}_{\mathrm{DG_k}} = k_{pf}\left(f^*_{\mathrm{MG}} - \bar{f}_{\mathrm{DG_k}}\right) + k_{if}\int\left(f^*_{\mathrm{MG}} - \bar{f}_{\mathrm{DG_k}}\right)dt \tag{5.5}$$

$$\bar{f}_{\mathrm{DG_k}} = \frac{\sum_{\mathrm{i=1}}^{\mathrm{N}} \mathrm{f}_{\mathrm{DG_i}}}{\mathrm{N}} \tag{5.6}$$

Here,
k_{pf} = proportional term for the secondary PI control
k_{if} = Integral term for the secondary PI control
f_{MG} = frequency reference for the microgrid
$\bar{f}_{\mathrm{DG_k}}$ = average of frequency for all DG units
i = 1,2,3....N
k = 1,2,3....n
n = number of DG units

δf_{DG_k} = the error signal generated by the secondary controller of each DG_k unit in every sample of time
N = Number of packages i.e. frequency measurements done in the communication system

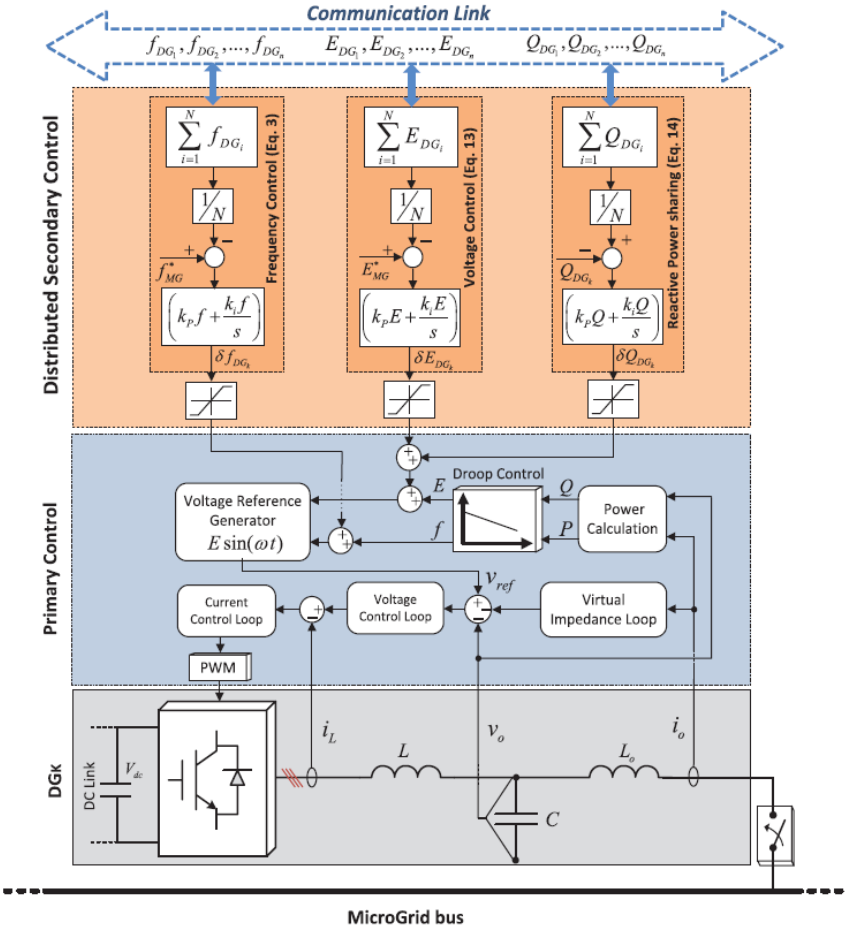

Figure 5.6: Schematic diagram of the Distributed Secondary control for in a Microgrid [23]

5.3.2 Voltage Restoration

The voltage restoration is done in the similar process as explained in frequency restoration in distributed controller in subsection 5.3.1. When there is deviation in voltage magnitude, each DG units takes the voltage amplitude measurement and averages and then sent to primary level to compensate and remove the steady-state error. It can be expressed in equation 5.7 and 5.8.

$$\delta \mathrm{E}_{\mathrm{DG_k}} = k_{pE}\left(E^*_{\mathrm{MG}} - \bar{E}_{\mathrm{DG_k}}\right) + k_{iE}\int\left(E^*_{\mathrm{MG}} - \bar{E}_{\mathrm{DG_k}}\right)dt \tag{5.7}$$

$$\bar{E}_{\mathrm{DG_k}} = \frac{\sum_{\mathrm{i=1}}^{\mathrm{N}} \mathrm{E}_{\mathrm{DG_i}}}{\mathrm{N}} \tag{5.8}$$

Here, $\delta \mathrm{E}_{\mathrm{DG_k}}$ is the restoration voltage of any DG unit. DG_k is generated by distributed controller when voltage amplitude E_{MG} is compared with $\bar{E}_{\mathrm{DG_k}}$. And k_{pE} and k_{iE} are controller parameter.

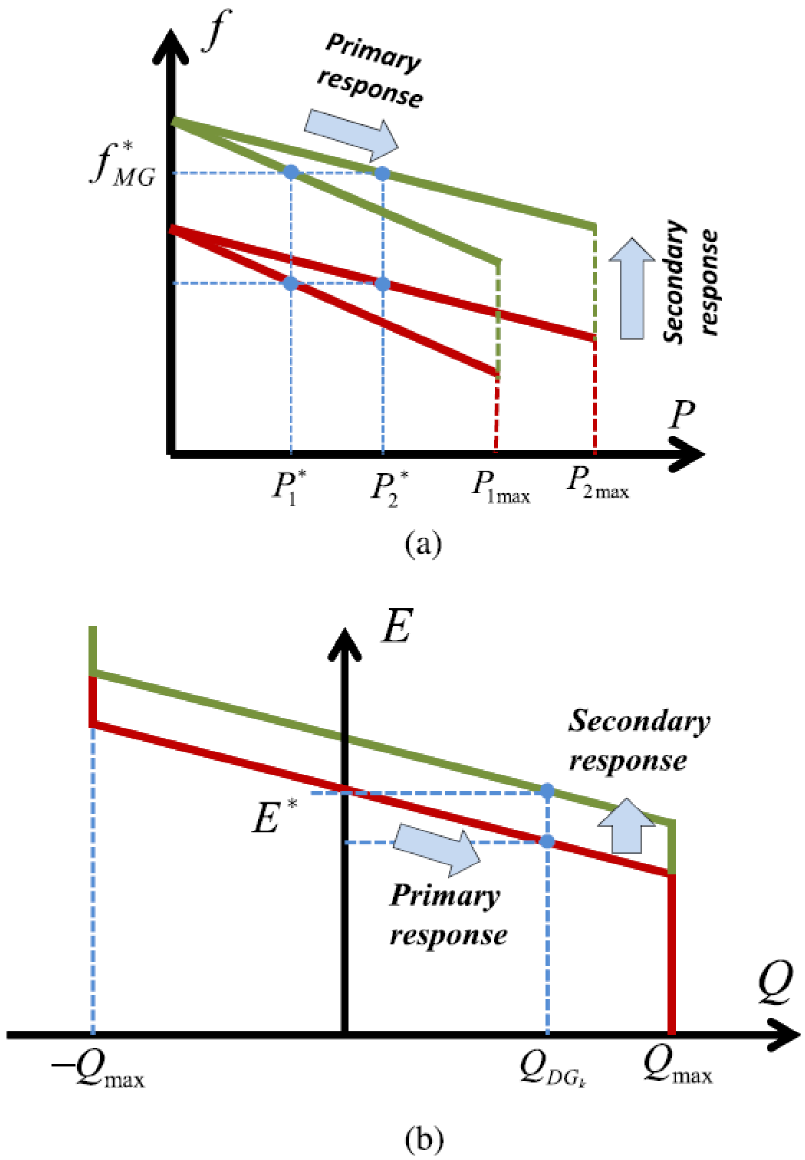

Figure 5.7: Schematic diagram of Secondary control response versus primary control response: (a) frequency restoration; (b) voltage amplitude restoration. [23]

After primary control, there are still droops in both frequency and voltage amplitude which are shown by red line in figure 5.7. After application of distributed controller, both frequency and voltage amplitude deviations have been removed and moved to reference levels.

5.4 Simulation model description

A Microgrid consists of two islanded inverters in islanded operation mode in Simulink platform. Figure 5.8 shows the microgrid model. Green color block which lies on left side of the figure 5.8, shows the parameter that are set for the simulation. The deviation in the voltage for inverter 1 is from 0 V to 10 V which means rms (root mean square) voltage is varied from 230+10 Vrms to 230–10 Vrms. The same voltage setting is done for inverter 2. And by default it is 230V. The phase, frequency and voltage magnitude synchronization loops are developed to ensure the synchronization between two inverter voltage outputs before parallel connection. As explained in secondary control, there are communication channel present in this controller which bring communication delay into play and this delayed can be varied from 0 to 1 second. Likewise, time for load disturbance is set between 10 to 15 second in which load disturbance will cause frequency and voltage amplitude to vary which in turn led to change in active and reactive power. Active is varied from 2000W to 3000W and reactive power to vary from 500 VAR to 1000 VAR in load disturbance time. At last different mode of centralized and distributed connection can be changed with time for connecting to secondary control too. The parameters which can be changed during the experiment is shown in appendix figureA.4

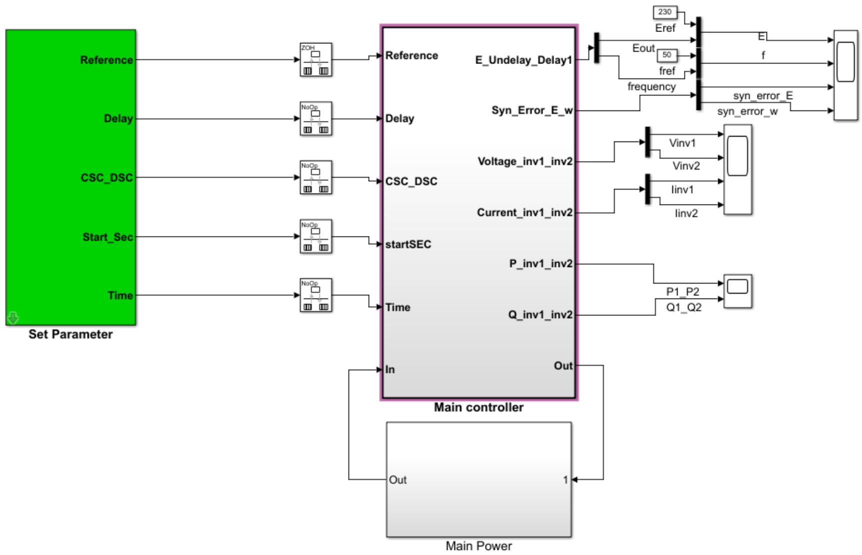

Figure 5.8: Schematic diagram of the secondary control method in Microgrid Model

Similarly, the controller block of secondary is shown in appendix A.5. Here, two yellow block in the lower portion shows the control of inverter 1 and 2. Grey block shows the synchronization block which is shown in appendix figure A.6. The block diagram for frequency and voltage synchronization for parallel connected two inverters is shown in appendix figures A.7 and A.8. Similarly, appendix figure A.8 shows two inverters in parallel forming grid in appendix figure A.9.

Likewise, figures 5.9 and 5.10 show distributed and centralized secondary control respectively. It can be seen clearly from figure 5.9 that communication delay is before secondary block in distributed control. Distributed secondary block gives compensating signal to primary controller (droop) which finally transfer signal to inner voltage and current block (also called zero level control) can also be visualized from figure 5.9. In centralized controller, communication delay is after central secondary control which is depicted in figure 5.10. Block diagram of centralized and distributed controller is shown in appendix figure A.10 and A.11. In both centralized and distributed controller, SOGI (Second Order Generalized Integrator, which is explained in section 2.9) is used to obtain angular frequency and voltage magnitude. Then both voltage amplitude and frequency error signals are send to respective PI controllers to remove deviations. The table 5.1 shows different parameters with value and symbol used in secondary control.

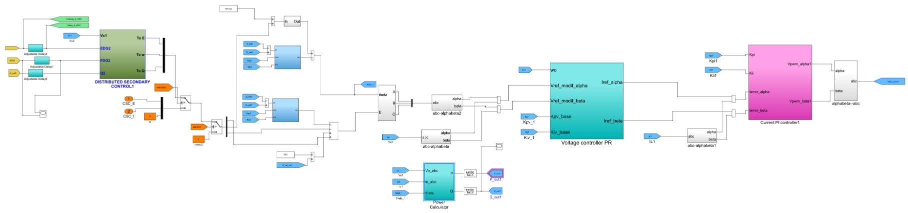

Figure 5.9: Schematic diagram of the Distributed secondary control

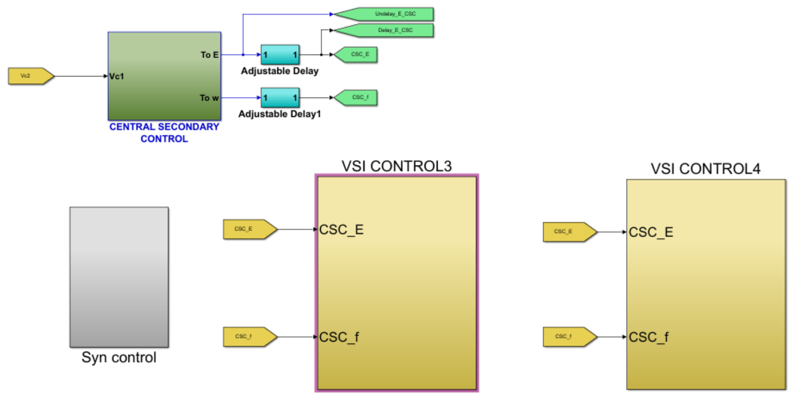

Figure 5.10: Schematic diagram of the Centralized secondary control

Table 5.1: System parameter value for the Secondary control simulation

Parameter	Notation	Value
Filter Inductance	L	1.8mH
Load Inductance	L	1.8mH
Capacitance	C	27μF
Resistance	R	0.2Ω
Frequency reference	f_{ref}	50 Hz
Switching Frequency	f_{swich}	10 kHz
Proportional term for frequency (secondary)	k_{pf}	0.1
Integral term for frequency (secondary)	k_{if}	10
Proportional term for Voltage Amplitude (secondary)	k_{pE}	0.002
Integral term for Voltage Amplitude (secondary)	k_{IE}	2

5.5 Simulation results of centralized secondary control

5.5.1 Case 1

After forming the block in the simulink, four different scenarios is created to check the application of centralized control and results shown alongside. In case 1st there is no deviation in both inverter voltage reference i.e. both are fixed at 230V . Synchronization time is fixed between 0.5 to 3 second in which two parallel inverter can synchronize with each other and time for connecting is 3 second. Since, inverter starting is in a sequential manner, so there are some transient at the start. And hence secondary control is started at 0.5 second. Time for load disturbance is between 10 to 15 second. On running the following observation is seen as shown in figure 5.18c.

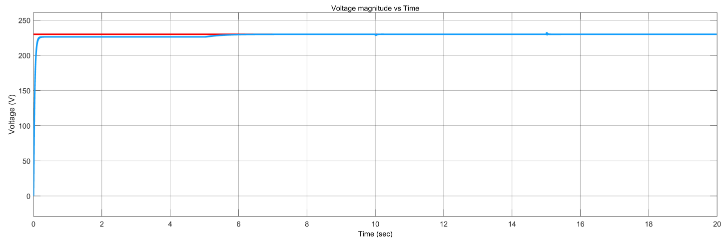

(a) Voltage vs Time

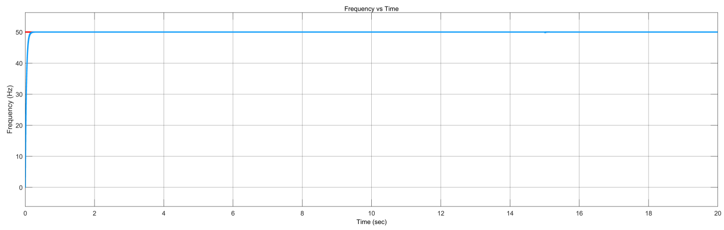

(b) Frequency vs Time

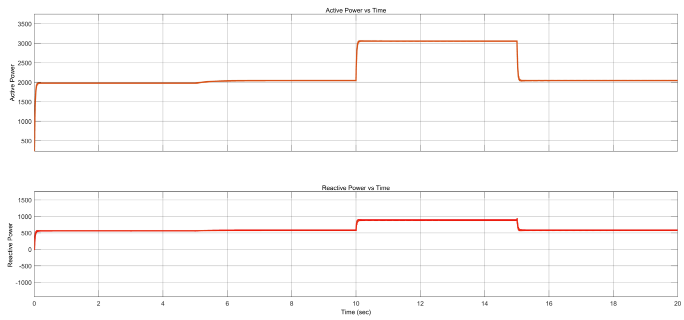

(c) Active and Reactive Power vs Time

Figure 5.11: Centralized Secondary Control

From figure 5.11a it can be seen as soon as secondary control executes around 0.5 second, voltage magnitude of inverter 2 catches up with voltage magnitude of inverter 1. Small frequency and voltage magnitude drops can be found due to the active and reactive power outputs and line impedance. In reactive power curve, the power is always greater than 500 VAR due to addition of filter in the circuit which always consumes a bit of VAR. When load is added between 10-15 second, there is increase in 2000 W of active and 500 VAR of reactive power which is shared by both inverter equally leading to 1000W and 250 VAR increase in each inverter in between 10-15 second.

5.5.2 Case 2

In this case voltage is varied by 10 V in rms value and synchronization time is done between 0.5 to 3 second. Secondary control is started at 25 second but simulation time is 20 second which means secondary control is not implemented at all. Time for load disturbance is between 25 to 35 second which does not execute between simulation.

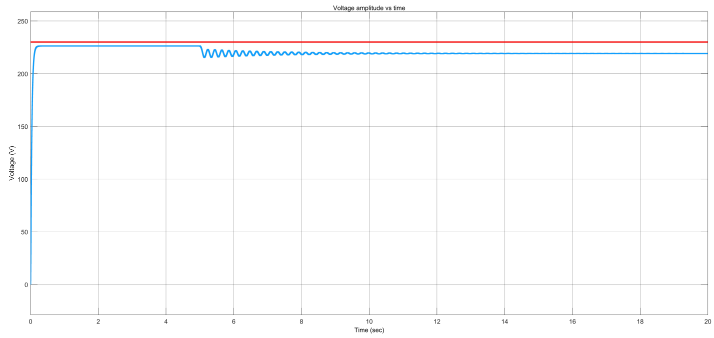

(a) Voltage vs Time

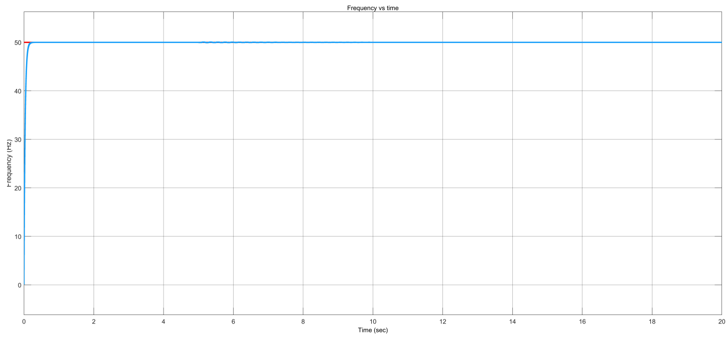

(b) Frequency vs Time

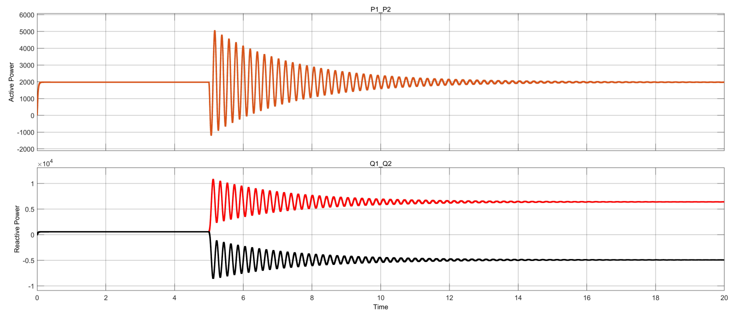

(c) Active and Reactive Power vs Time

Figure 5.12: Centralized Secondary Control

As there is voltage variation and secondary control is not implemented, there is oscillations in voltage curve as primary droop control alone cannot dampen all the oscillations. This can be considered a case of weak grid. Voltage oscillation variation also result in oscillation in active and reactive power of both inverters.

5.5.3 Case 3

In this case voltage is varied by 10 V in rms value and synchronization time is done between 0.5 to 3 second. Secondary control is started at 10 second. Time for load disturbance is between 25 to 35 second which does not execute as simulation time is only 20 second.

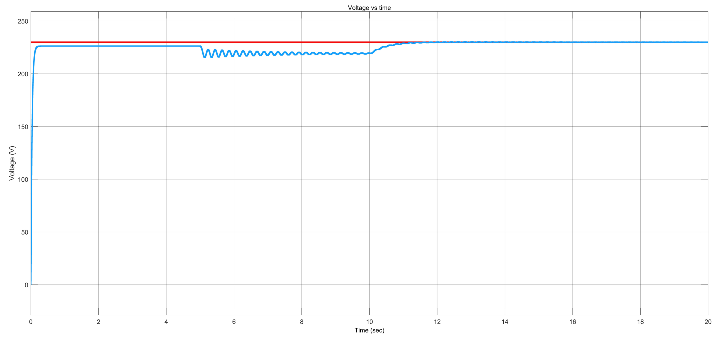

(a) Voltage vs Time

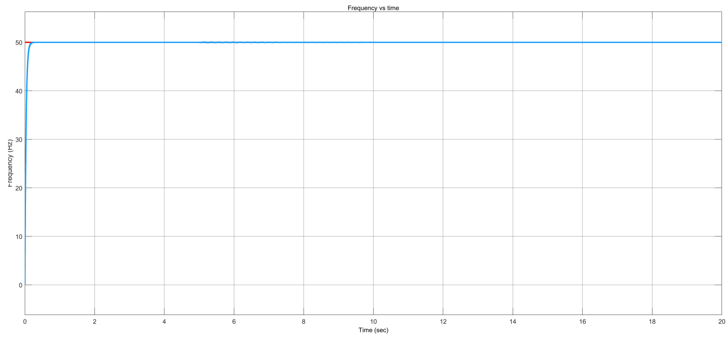

(b) Frequency vs Time

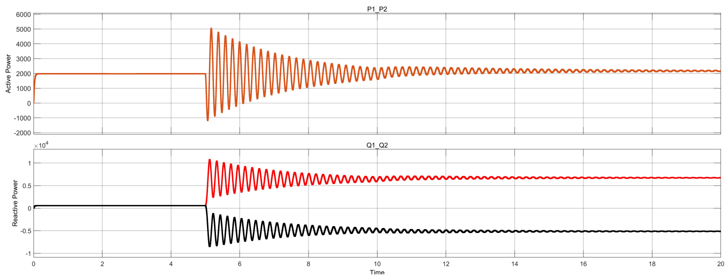

(c) Active and Reactive Power vs Time

Figure 5.13: Centralized Secondary Control

Contrary to previous case, in this test secondary control is applied after 10 second and this can be seen in voltage curve, where voltage magnitude has less deviation. However, oscillations are still observed in active and reactive power cannot be shared between the two inverters due the voltage magnitude deviations.

5.5.4 Case 4

In case 1st there is no deviation in both inverter voltage i.e. both are fixed at 230V . Synchronization time is fixed between 0.5 to 3 second in which two parallel inverter can synchronize with each other and time for connecting is 3 second. Secondary control is started at 5 second. Time for load disturbance is between 10 to 15 second and communication delay of 1 second is considered.

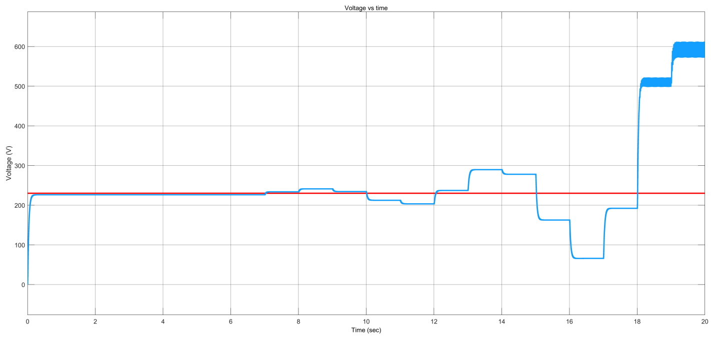

(a) Voltage vs Time

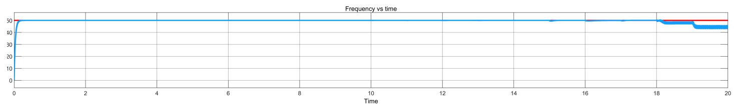

(b) Frequency vs Time

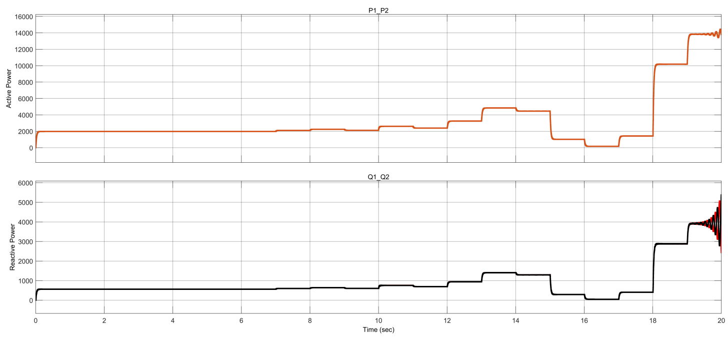

(c) Active and Reactive Power vs Time

Figure 5.14: Centralized Secondary Control

It can be observed from Fig. 5.14, when the communication delay increases to 1s, the centralized secondary control cannot maintain stable operation.

5.6 Simulation results of distributed secondary control

5.6.1 Case 1

Four different scenarios are created to check the application of distributed control and results shown alongside. In this case there is no deviation in both inverter voltage i.e. both are fixed at 230V . Synchronization time is fixed between 0.5 to 3 second in which two parallel inverter can synchronize with each other and time for connecting is 3 second. Ssecondary control is started at 5 second. Time for load disturbance is between 10 to 15 second. On running the following observation is seen as shown in figure 5.18c.

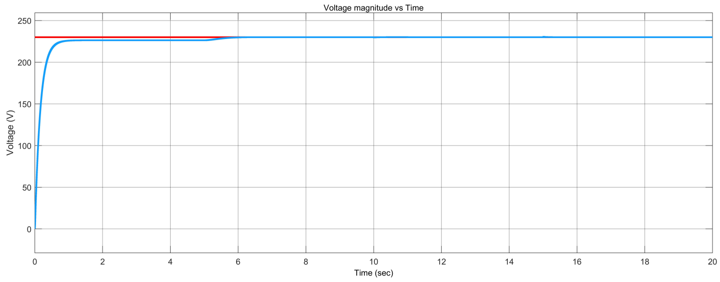

(a) Voltage vs Time

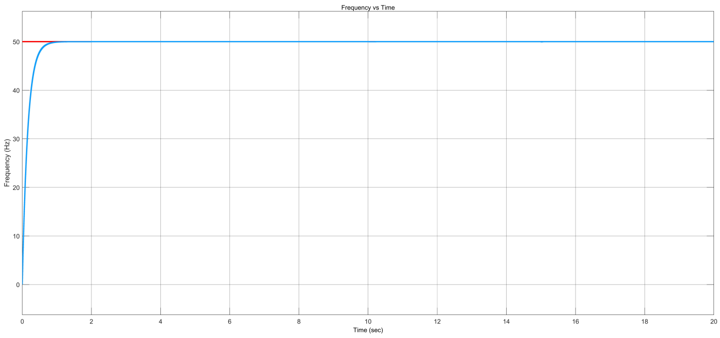

(b) Frequency vs Time

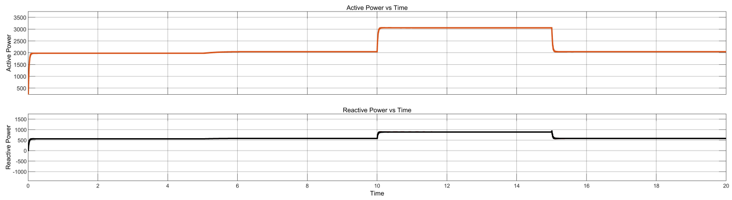

(c) Active and Reactive Power vs Time

Figure 5.15: Distributed Secondary Control

As observed from Fig. 5.15, similar simulation results can be obtained as the centralized secondary control. Stable parallel operation and power sharing can be obtained. Small voltage magnitude deviations can be identified due to the power flow and line impedance.

5.6.2 Case 2

In this case voltage is varied by 10 V in rms value and synchronization time is done between 0.5 to 3 second. Secondary control is started at 25 second but simulation time is 20 second which means secondary control is not implemented at all. Time for load disturbance is between 25 to 35 second which does not execute between simulation.

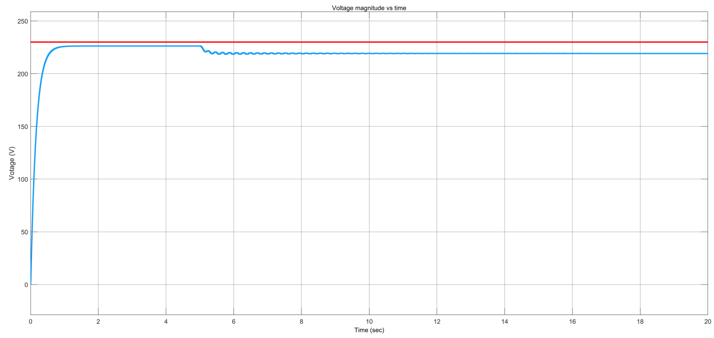

(a) Voltage vs Time

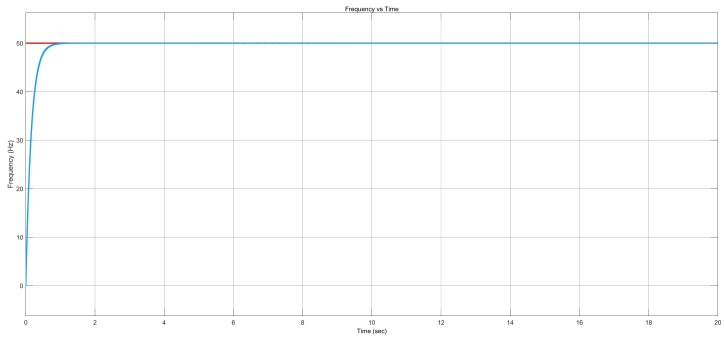

(b) Frequency vs Time

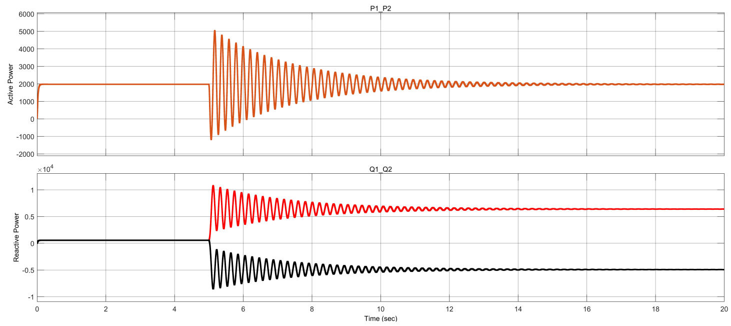

(c) Active and Reactive Power vs Time

Figure 5.16: Distributed Secondary Control

As secondary control is not implemented in this case, there is continuous deviations in voltage magnitude with the reference and the same results in power curve too

5.6.3 Case 3

In this case voltage is varied by 10 V in rms value and synchronization time is done between 0.5 to 3 second. Secondary control is started at 10 second. Time for load disturbance is between 25 to 35 second which does not execute as simulation time is only 20 second.

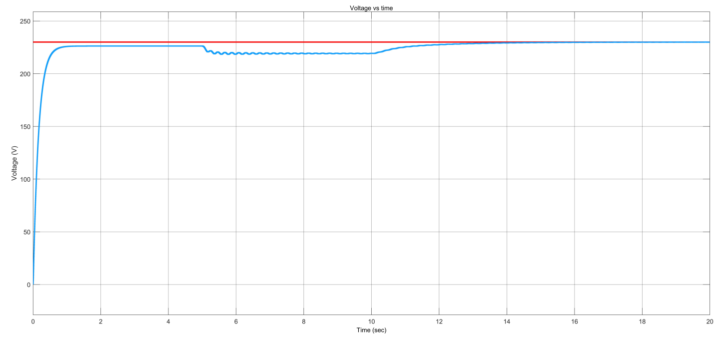

(a) Voltage vs Time

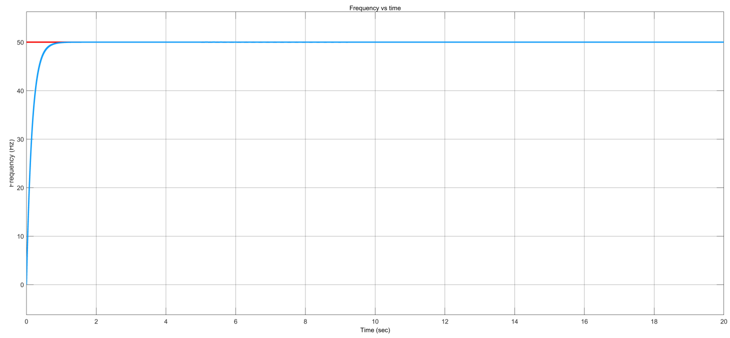

(b) Frequency vs Time

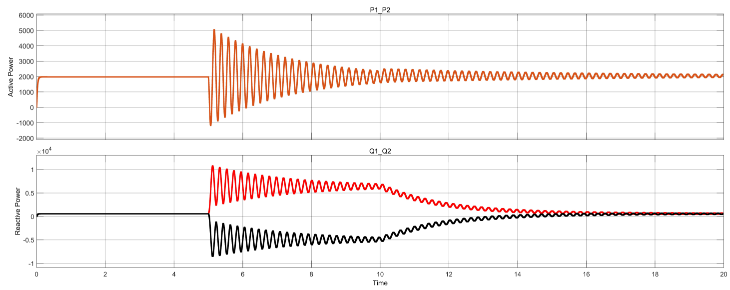

(c) Active and Reactive Power vs Time

Figure 5.17: Distributed Secondary Control

As observed before secondary is implemented, there are oscillations but compared to centralized, oscillations is less. There are oscillations observed in power curves, but after the secondary control enables, the oscillations are mitigated and reactive power is shared again between the two inverters.

5.6.4 Case 4

In case 1st there is no deviation in both inverter voltage i.e. both are fixed at 230V . Synchronization time is fixed between 0.5 to 3 second and time for connecting is 3 second. Secondary control is started at 5 second. Time for load disturbance is between 10 to 15 second and communication delay of 1 second is considered.

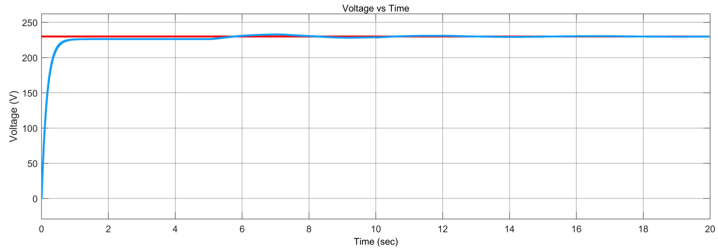

(a) Voltage vs Time

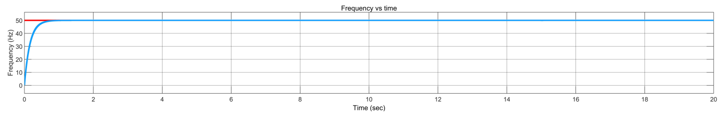

(b) Frequency vs Time

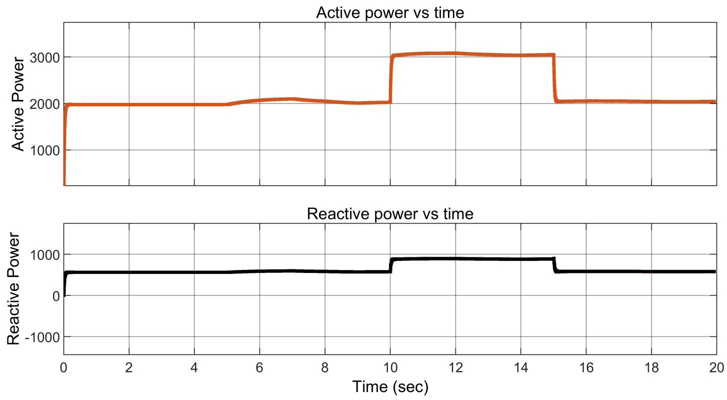

(c) Active and Reactive Power vs Time

Figure 5.18: Distributed Secondary Control

Comparing the results with centralized system in the same given case, distributed system gives smooth result in voltage, frequency and power curve. There is no oscillations observed in voltage or power curve. So when there is communication delay distributed control performs better than centralized one.

5.7 Summary

In this chapter, secondary control is used for frequency and amplitude restoration by low bandwidth communication channels. Two different secondary controllers (centralized and distributed) are explained and their differences are shown in schematic way. Comparative simulation tests are performed with different scenarios, for instance with/without voltage reference deviations, with/without secondary controllers, with centralized or distributed secondary controllers, and with different communication delays. As shown from the simulation results, the distributed secondary control performed better than the centralized manner in most of the cases.

6 Harmonic mitigation solution for a microgrid with non-linear load

6.1 Introduction

When a sinusoidal voltage is applied in a non-linear load, then the resulting current is no longer sinusoidal. This current causes voltage distortion at the load terminals and this phenomena is called harmonics. Due to increase in distributed energy resources, power electronics dominated devices are on rise in power system. Though, it helps in integrating renewable energy resources in the main grid, but simultaneously it bring in harmonic distortion in the power grid. Semicondoctors switches like rectifiers also causes harmonics in the system. Harmonics pose a serious problem to the grid, grid components and the appliances connected to it. Harmonic currents causes overheating which causes temperature rise, voltage stress, power loss and reduces overall plant life [24].

6.2 Total Harmonic Distortion

Due to the rapid increase in power electronics based power system, harmonics is almost everywhere in power distribution system. So, it is very important to measure the harmonics level in current or voltage sinusoidal waveform. Generally, there are two definitions of harmonics, first type is when harmonic content is compared to its fundamental and for second definition, harmonic content is compared to rms value [25]. For the purpose of the thesis work, we use when it is compared to its fundamental and is expressed by equation 6.1 [26].

$$\text{THD}_t = \frac{\sqrt{\sum\limits_{h=2}^{H} I_h^2}}{I_1} \times 100 \tag{6.1}$$

where,
I_h is the rms of the harmonic components h
I_1 is the rms value of fundamental component

6.3 Harmonics Compensation

6.3.1 Harmonics Compensation by PI Controller

Generally, Proportional integral (PI) controllers are used in synchronous (dq) reference frame and can be used for harmonic compensation. The main demerit in this method is that harmonic compensator should be used for both positive and negative sequence and this increases control complexity.

6.3.2 Harmonics Compensation by PR Controller

Proportional resonance (PR) controller has major advantages as it provides gain only on selected frequency (resonant frequency) and for rest part of frequency there is attenuation. In this controller, compensation is attained by cascading several generalized integrators tuned to resonate at the specified frequency [10]. The harmonic compensator transfer function designed to compensate the fifth, seventh and eleventh harmonics is expressed in equation 6.2:

$$G_h(s) = \sum_{h=5,7,11} K_{ih} \frac{s}{s^2 + (\omega \cdot h)^2} \tag{6.2}$$

As shown in figure 6.1, just by adding more resonant controllers in parallel, this method can be used to compensate harmonics. Unlike, PI controller, in this controller, harmonic compensator works on both positive and negative sequences of the selected harmonics.

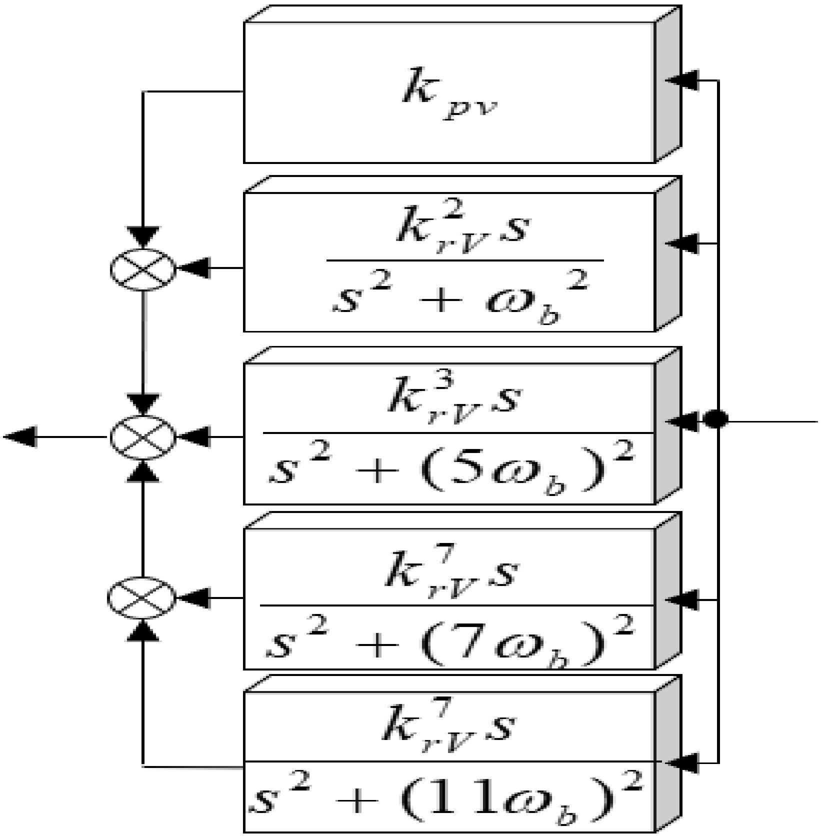

Figure 6.1: Schematic diagram of the PR harmonic compensate controllers

6.4 Simulation Model Description

6.4.1 Simulation Model Description for DQ reference frame

A non-linear load is connected to the inverter as shown in appendix figure A.12. The different value for inductance, resistance and capacitance are shown in table 6.1. The schematic diagram of harmonic interface model developed in simulink is shown in figure 6.2.

Table 6.1: Simulation controller parameters for Grid

Parameter	Symbol	Value
Filter Inductance	L	1.8 mH
Resistance	R	0.1Ω
Capacitance	C	9μF

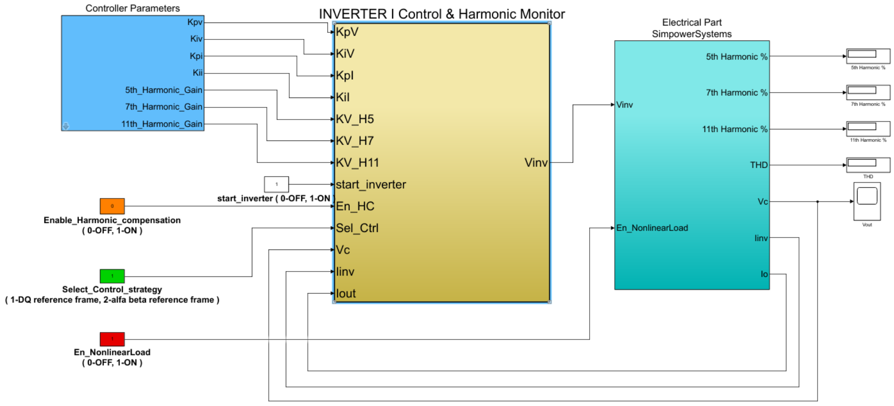

Figure 6.2: Layout of the simulation model

The measured capacitor voltage, line current and output current from inverter outputs is taken to the controller block which is represented in light yellow color at the middle of the figure 6.2.

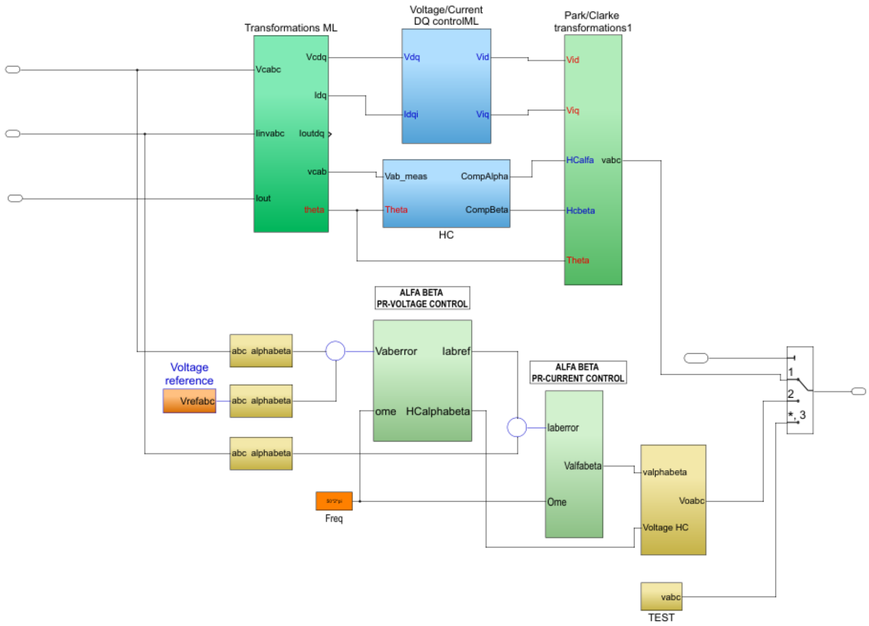

Figure 6.3: Layout of controller block

In transformation block, capacitor voltage in abc reference frame is converted to $\alpha\beta$ reference frame by Clark transformation which is explained in 2.4.1. Then, voltage in $\alpha\beta$ is converted into dq reference frame by Park transformation which is explained in 2.4.2. Likewise, inductance current is also transformed to $\alpha\beta$ and then to dq reference frame. As observed in Fig. 6.4, the measurements are all transferred to the dq reference frame with fundamental rotation frequency.

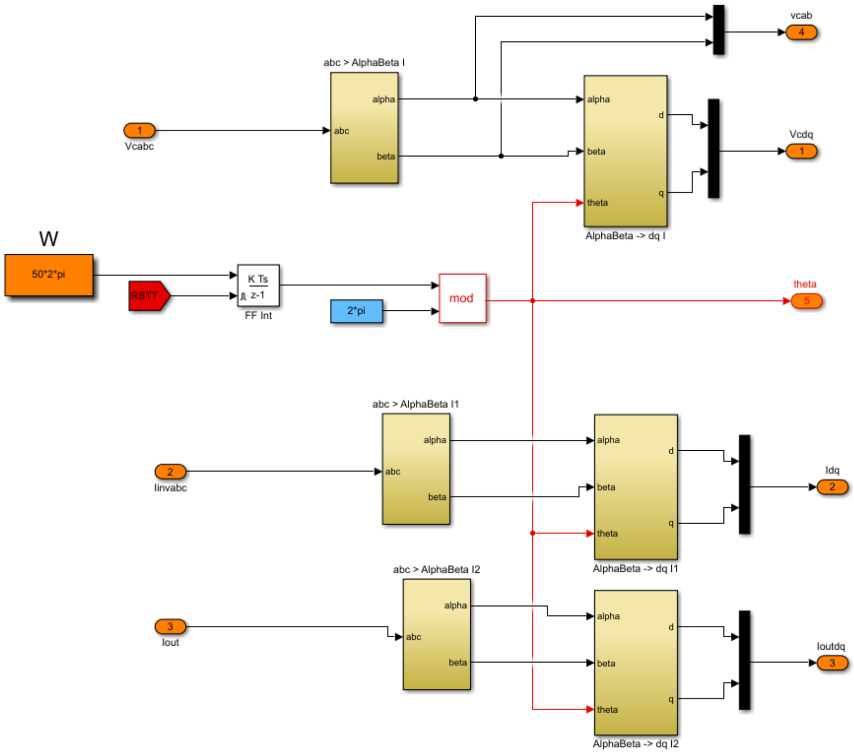

Figure 6.4: Layout of transformation block

The voltage obtained from transformation block in dq frame is compared with reference and error is generated which is fed to PI controller which is shown in 6.5. Cross-coupling in d and q co-ordinates are used in both voltage and current block. The proportional and integral term for Voltage and Current block is shown in table 6.2. Positive sequence harmonics, e.g. 7th, 13th, rotate in the same direction as the fundamental frequency and negative sequence harmonics, e.g. 5th, 11th, rotate against the fundamental frequency. For each harmonic value, fundamental frequency is multiplied with the given harmonic order and then fed for transformation from $\alpha\beta$ to dq frame as shown in 6.6. Then the compensator value for 5th, 7th and 11th value is obtained in $\alpha\beta$ frame. This compensator value will be added to the output from current block and changed from dq frame to $\alpha\beta$ frame and then changed to suitable PWM signal in abc frame.

Table 6.2: Parameters value for Voltage and Current block

Parameter	**Symbol**	**Value**
Proportional term for Voltage	k_{pV}	0.01
Integral term for Voltage	k_{iV}	50
Proportional term for Current	k_{pI}	10
Integral term for Current	k_{iI}	200
Compensation gain for 5^{th} Harmonic	KV_{H5}	30.0
Compensation gain for 7^{th} Harmonic	KV_{H7}	30.0
Compensation gain for 11^{th} Harmonic	KV_{H11}	100.0

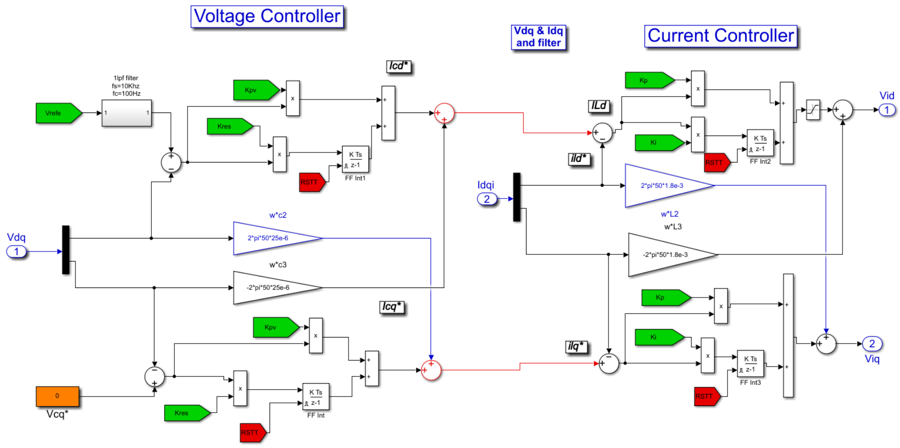

Figure 6.5: Layout of Voltage and Current Control Loops

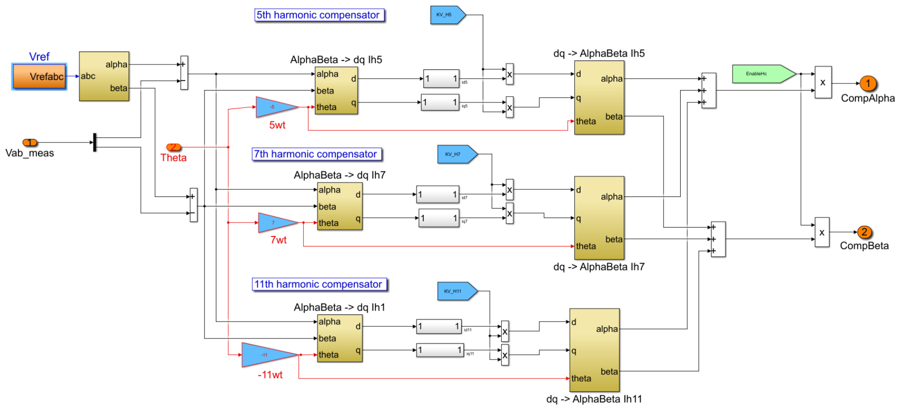

Figure 6.6: Layout of Harmonic Compensator block in dq frame

6.4.2 Simulation Model Description for $\alpha\beta$ reference frame

The measured capacitor voltage and inductance current are transformed from abc to $\alpha\beta$ frame. The voltage on $\alpha\beta$ frame is compared with the reference voltage and the error is generated, which is sent to PR Voltage control block as shown in figure 6.3.

The upper part of figure 6.5 shows the PR voltage controller at fundamental frequency and the lower part shows the compensation part with different harmonic compensators (5th, 7th and 11th).

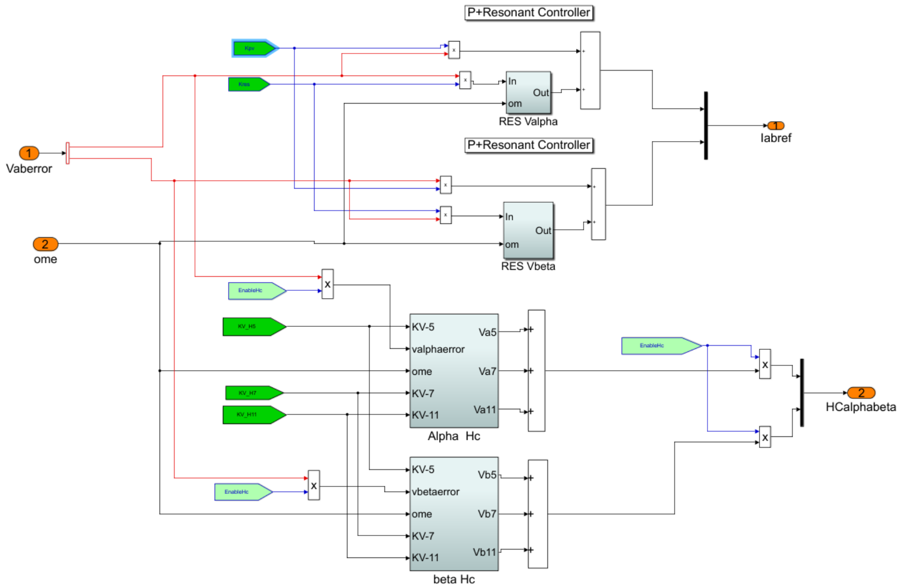

Figure 6.7: Layout of PR Voltage control block

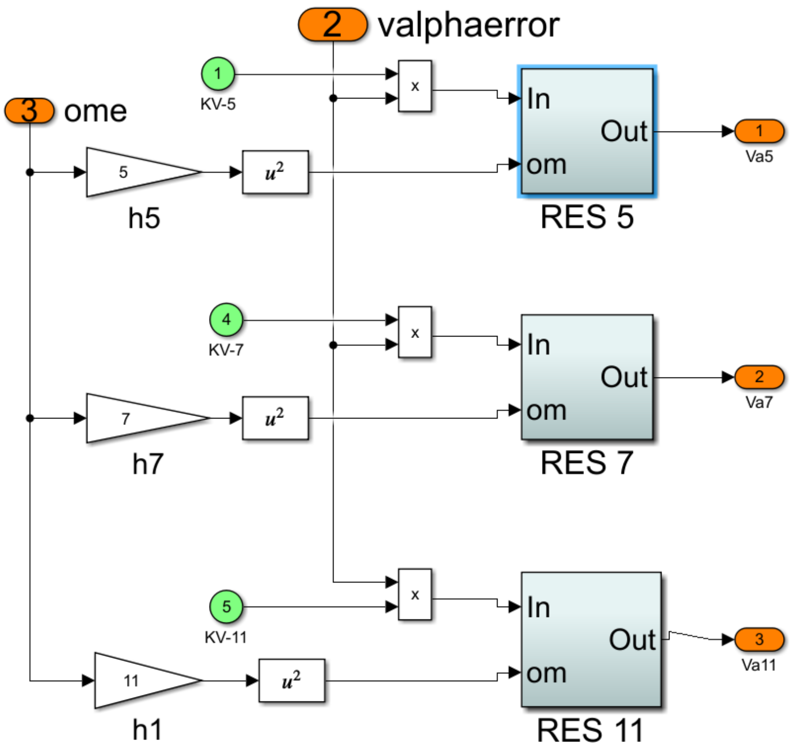

Figure 6.8: Layout of Compensator block

The fundamental frequency, voltage error and compensator gain for different harmonic are sent to $\alpha\beta$ PR compensator block as shown in figure 6.8. Since, PR is used in stationary frame, so there is no rotation and fundamental part of frequency can be directly multiplied with different harmonic orders.

6.5 Simulation Results

6.5.1 In DQ reference frame

The simulation results with the voltage harmonic suppression controllers in dq reference frame are shown in Fig. 6.9. Also 5^{th}, 7^{th}, 11^{th} and THD are shown in table 6.3.

Table 6.3: Voltage harmonics in the DQ reference frame

Type of Harmonic	Value
5^{th}	0.004168
7^{th}	0.004474
11^{th}	0.003382
THD	1.52

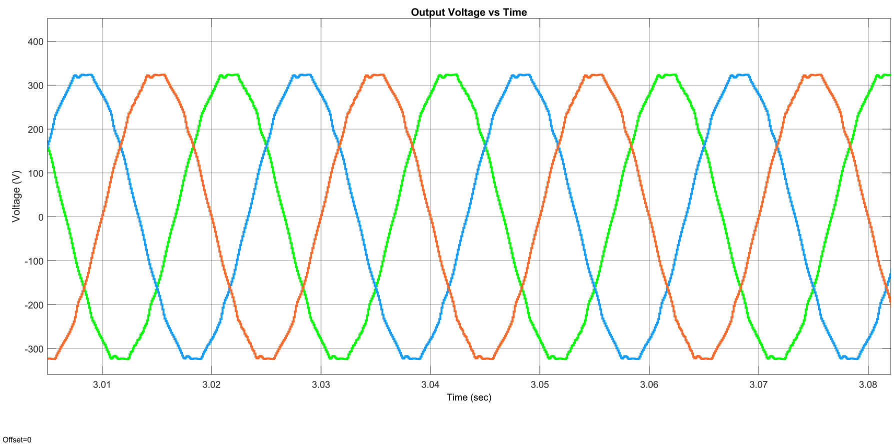

Figure 6.9: Output voltage waveform in dq reference frame

6.5.2 In $\alpha\beta$ reference frame

The simulation results with the voltage harmonic suppression controllers in $\alpha\beta$ reference frame are shown in Fig. 6.10. 5^{th}, 7^{th}, 11^{th} voltage harmonics and THD are shown in table 6.4 and The output voltage waveform in the same $\alpha\beta$ frame is shown in figure 6.10.

Table 6.4: Harmonic value in the $\alpha\beta$ reference frame

Type of Harmonic	Value
5^{th}	0.4222
7^{th}	0.8477
11^{th}	0.4292
THD	1.536

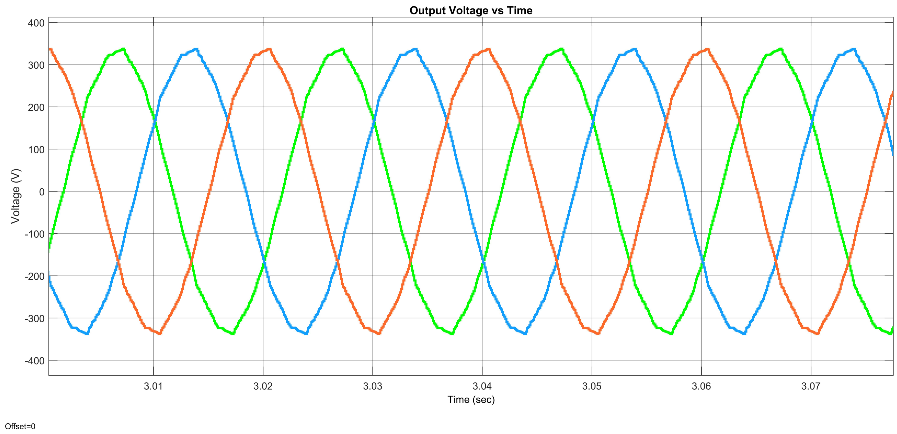

Figure 6.10: Output voltage waveform in $\alpha\beta$ reference frame

On close examining table no. 6.3 and 6.3, it can be seen the individual 5^{th}, 7^{th} and 11^{th} harmonic value is greater in dq reference frame as compared to $\alpha\beta$ reference frame. But, total harmonic distortion is almost in both frame.

6.6 Summary

This chapter deals with harmonic compensation by Proportional integral (PI) controllers and Proportional resonance (PR) controllers in dq and $\alpha\beta$ reference frames respectively. With PI controllers, harmonic compensators are used for both positive and negative sequences. With PR controllers, the compensation is attained by cascading several generalized resonators tuned to resonate at the specified frequency. As observed from the simulation results, the individual odd harmonics are greater in dq reference frame as compared to $\alpha\beta$ reference frame, but, THD is more or less equal.

7 dSPACE and Model verification

7.1 Center for Research On Microgrids (CROM)

CROM is a world renowned research center at Aalborg University doing cutting-edge research in the field of both AC and DC microgrids, smart-grid and IoT (Internet of Things) energy systems. It aims for sustainable development providing latest energy solutions in the area of Maritime Microgrids, Space Microgrids, Energy Management Systems, etc. Academicians and researchers of CROM are highly innovative and renowned for publishing research papers in journals and conferences. It has close collaborations with many universities and industries like Atos, Huawei Technologies etc.

7.2 Hardware in the Loop

Hardware-in-the-loop (HIL) tests are commonly used in the University and companies to test the validation of the simulation results. Before building any instrument or plant, the prototype is built to check the possible outcomes. When the outcome is favorable, then only original designed is implemented in the real world. But, most of the time to build the prototype is also expensive and time consuming so the lab results or simulation outcomes are performed in HIL tests. Moreover, researchers and scientists also use HIL to know the various characteristics and compare with results obtained with MATLAB and other simulation software.

7.3 LAB SET-UP

In CROM, there are eight dSPACE set-up with independent Personal Computer (PC), a DC source and an AC grid emulator which is shown in figure 7.1

Figure 7.1: Outline of dSPACE set-up in CROM Laboratory [27]

Likewise, each set-up have dSPACE 1006 platform, 4 Danfoss inverters, 4 sets of LCL filter (to reduce harmonics), LEM signal conditioning boards, the interface board, relays and PC [27]. Figure 7.2 shows front view and back side view of installed set-up. And values of different parameters mentioned in set-up is shown in table 7.1.

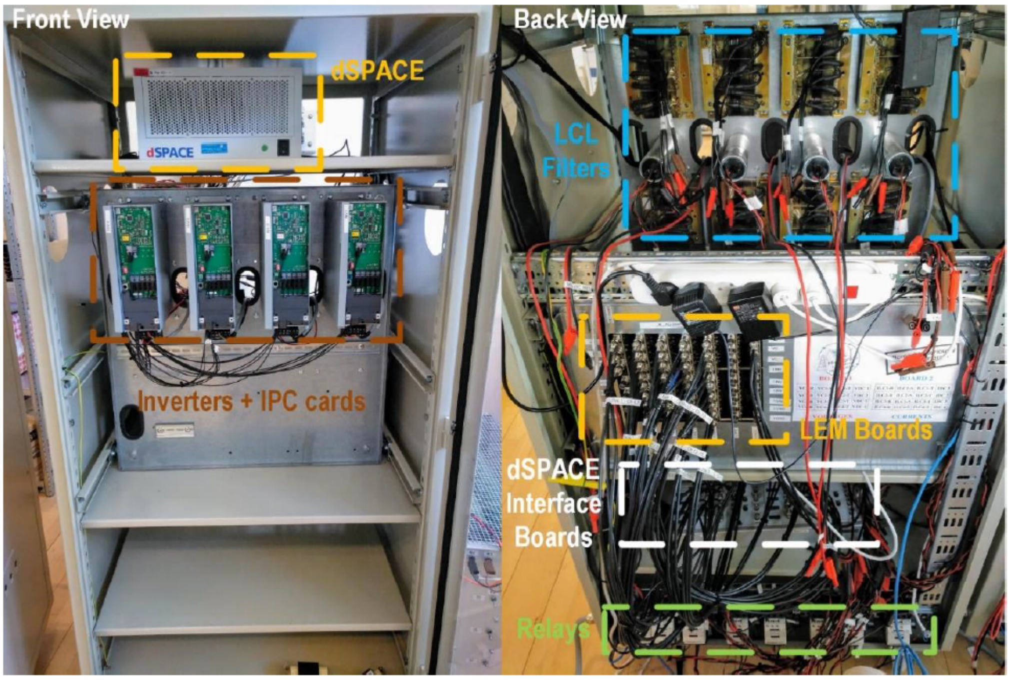

Figure 7.2: Outline of dSPACE set-up in CROM Laboratory [27]

Table 7.1: System parameter value of the set-up [27]

Parameter	Notation	Value
Input/Output Inductors	L_{in}, L_{on}	1.8mH
Capacitors	C_{Δ}	$3 \times 9\mu$F
DC Bus	V_{DC}	650V
AC Grid	V_g	3×400V
Transformer	P_{trans}	DYn11@12.5kVA
Switching Frequency	f_{swich}	10 kHz
Danfoss inverter FC302	P_{inv}	2.2kW

Moreover, line diagram containing AC line, DC line and control signal with all the elements of the set-up is shown in figure 7.3.

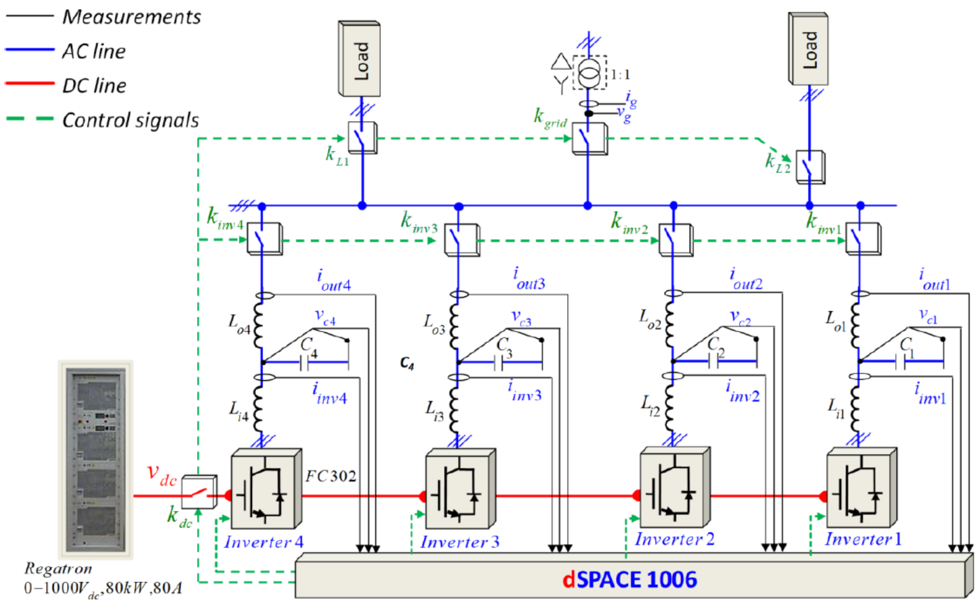

Figure 7.3: Line Diagram of all the elements in dSPACE set-up in CROM Laboratory [27]

7.3.1 Element of a Set-up

The set-up is basically a high efficiency motor control drive that provides better harmonic reduction [28]. The drive has a range of built-in features such as [28]-

- Fitted with protection such as short-circuit, over-voltage, over-current,etc.
- Automatic Energy Optimization
- Automatic Switching frequency Modulation
- Galvanic Isolation of control terminals
- Built-in PID controller
- Resonance damping

dSPACE-1006 has various cabinet mounted units which are explained in brief as follows-

1. **Inverters**: Each set-up consists of four inverters from Danfoss company (Danfoss VLT FC302). The inverter has IGBTs to convert DC voltage to AC voltage which is governed by PWM pulse signal.
2. **Interface and Protection Card (IPC)**: Each inverter is controlled by an interface and protection card (IPC). There are two versions of the IPC boards but have same functionality i.e. input/output signals and LED interface. During the start up, the IPC board is programmed to trip mode and is only reset after first 5 seconds and two mechanical clicks is heard during the start-up, 2 seconds after each other.
3. **Relays**: There are eight sets of relays fitted in the back of the cabinet which is shown in bottom of right side of figure 7.2. These relays are used to create the different test conditions in dSPACE.

7.4 Model Development

7.5 Control Desk Interface

Control desk is a dSPACE experiment software which performs all the necessary tasks and gives the user a single working interface to performs all the tasks from the start to the end. Some interface blocks need to be included in the Matlab simulation file as shown in figure 7.4.

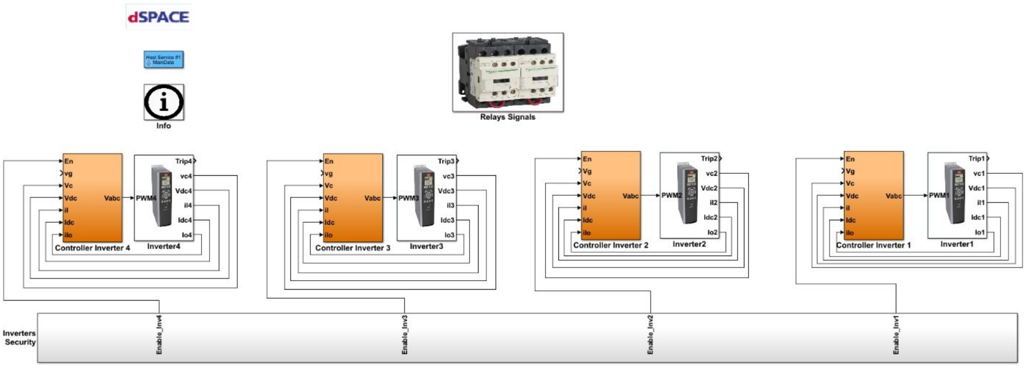

Figure 7.4: Overview of the test block

As seen in the figure 7.4, it contains the following blocks-

1. Inverter Controller block: Inverter Controller block is in orange color and control strategies are implemented in this block. The model tested has following content shown in figure 7.5.

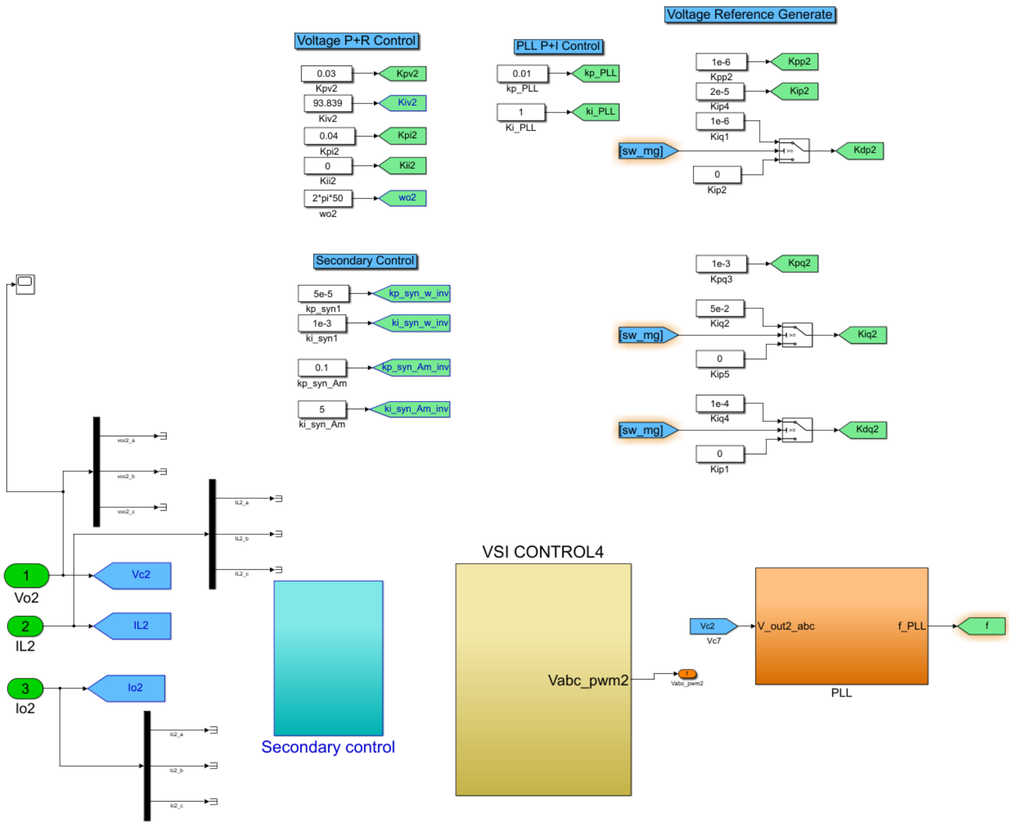

Figure 7.5: Overview of the Controller Inverter block

2. Inverter: The design of a inverter is made in this block. The content of a inverter is shown in figure 7.6.

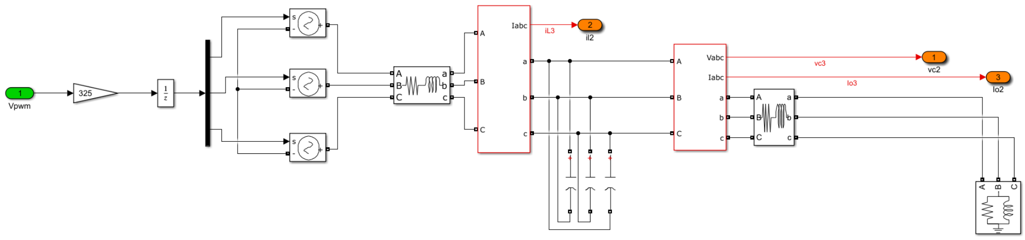

Figure 7.6: Overview of the Inverter block

3. Info block: Info block contains the layout used for the different dSPACE boards.
4. Host Service ♯1 MainData block: Host Service ♯1 MainData can be found at the top left of the figure 7.4 . It controls the rate at which data is sampled.
5. Relay Signal block: Relay signal block contains the signals for enabling the relays and the output bit so that their actual closure status can be checked and controlled [27]. Due to the limitation of the scope of the project, there is no need of Relay signal block and moreover, the test is checked and validated for a single inverter, the resultant test block is shown in figure 7.7.

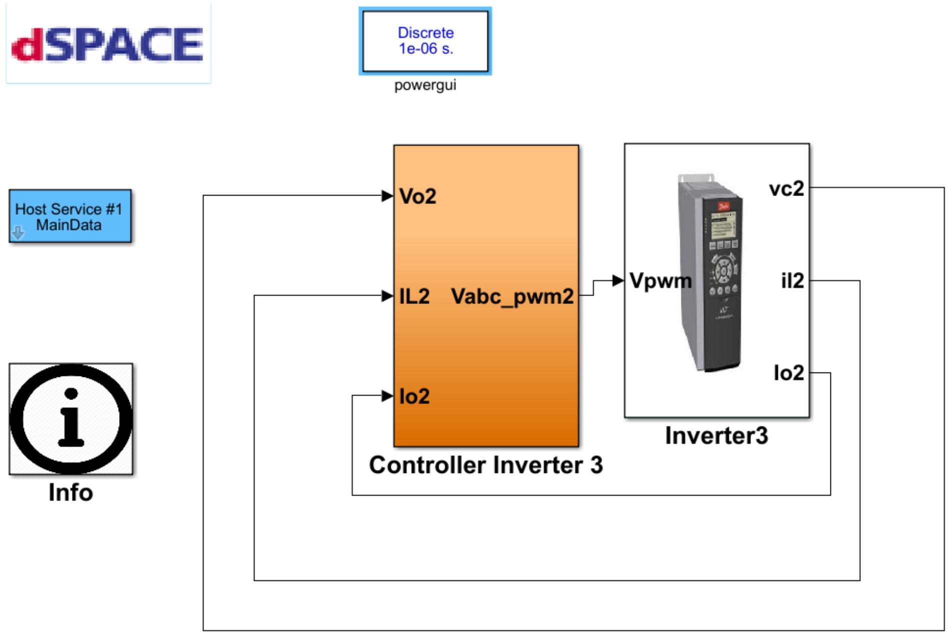

Figure 7.7: Overview of the test block used in the Model

7.6 Control Desk Software

dSPACE provides the easy user interface in conducting the experiment. After loading the software in .sd FORMAT successfully and on opening the interface, the dSPACE DS1006 platform and the connected board are listed as shown in figure 7.9.

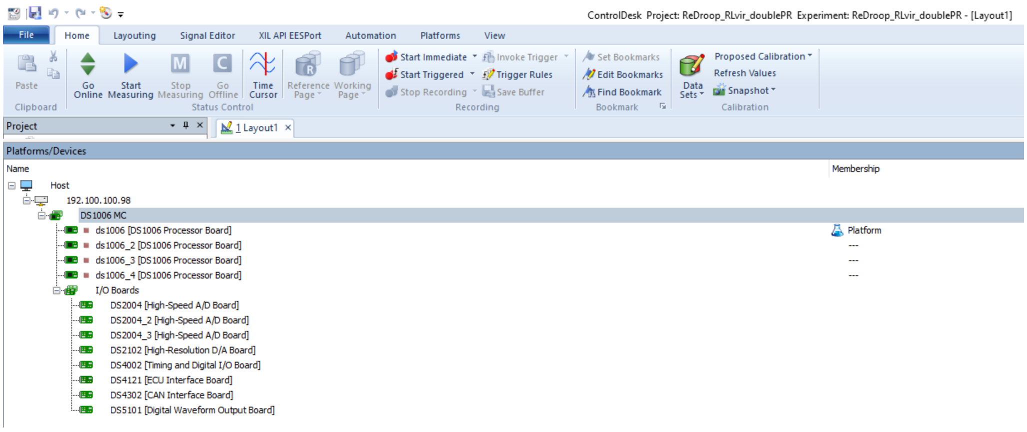

Figure 7.8: Opening interface of the Control Desk Software

To create the new project. First file is opened as shown in figure 7.9. Then new project and finally new experiment is clicked. In the same project, many new experiment has be made and saved.

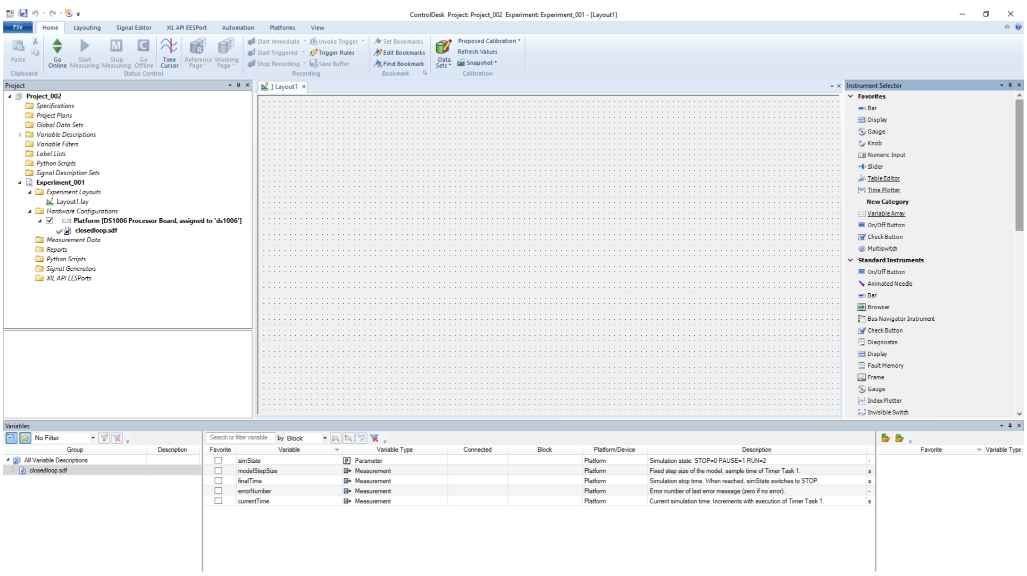

Figure 7.9: Opening interface of the Control Desk Software

7.6.1 Creating a new layout

Layouts provide graphical platform or interfaces between the model (.sdf fie) running on the dSPACE and the user. To accomplish this, different instruments are needed to transmit the signal. The different Instruments types usually used in the interfaces are listed below-

- Bar
- Display
- Time Plotter
- Gauge
- Numeric Input
- Slider

- Push Button
- On/Off Buttom
- Multiswitch
- Table Editor

7.6.2 Monitoring the variables

User needs to know how the parameters defined in control strategy affects the change in variables. Linking the variables in the dSPACE can be done in two ways. Variable values of a running real-time application can be connected to the previous instrument to monitor or change their values. To link a model variable to an instrument there are two different ways.

The first way is to right click on the required instrument and go to Variable and Add. After this, the selected Variable Dialog will open and will show the whole structure that is compiled in the Simulink model.
Other easy way is to find **All Variable Descriptions**, which is found in the bottom of the interface as shown in figure 7.9. For example, it is also shown in bottom of figure 7.10. After clicking **All Variable Descriptions**, then **closedloop.sdf** (which is file name saved in dSPACE) and finally **Labels**. Since in Simulink file, the voltage have been labelled, it is automatically detected in the interface. Then the same voltage labelled is dragged on time plotter.

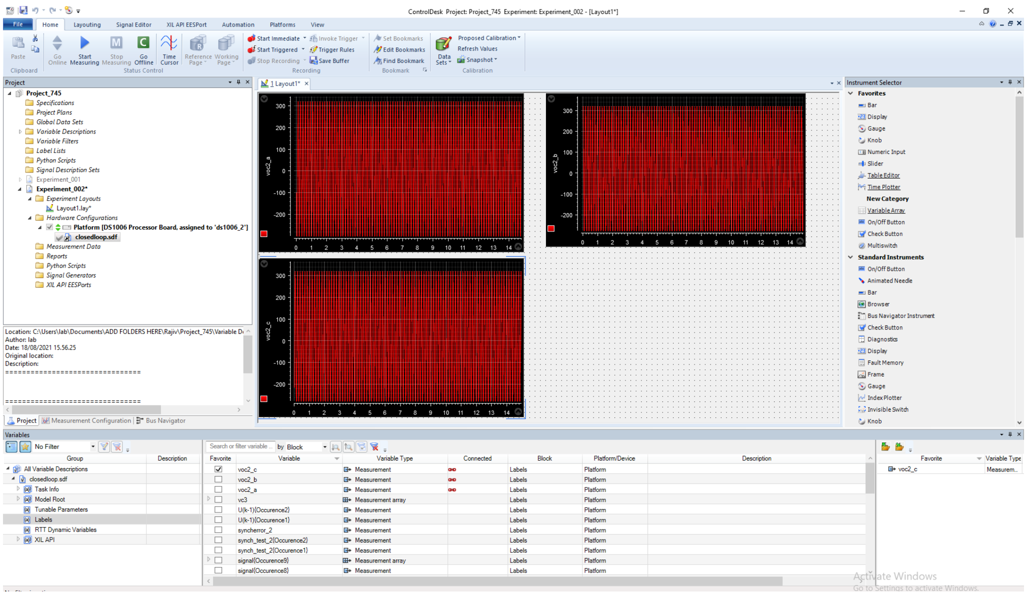

Figure 7.10: Interface of the Control Desk Software showing Voltage variable

7.6.3 Running an Experiment

There are different options to control the running functions of the experiment.

- Go Online: This functions will automatically run the file on dSPACE 1006. But, it will not show any data for any Instrument selector block.
- Start Measuring: With this command is implemented, data can be seen in Instrument selector block like time plotter or Slider, etc.

- Stop Measuring: This command stops the measuring process of any Instrument selector panel.

- Go offline: It will stop the platform monitoring. All the above mentioned control options can be found in top left of the figure 7.10.

7.7 Results and Discussion

The Simulink file is validated on the dSPACE-1006 platform. Figure 7.11 shows Grid voltage of three phase separately in dSPACE and grid voltage obtained in Simulink. While observing figure 7.11, it can be seen in both dSPACE and Simulink, we obtain the same peak value around 325V (Volts). Similarly, in figure 7.12, we see that both platform produces current around 5-6A (Ampere). Likewise, in figure 7.13, we can see frequency slowly settles from around 49.7 or 50.3 Hz to 50 Hz.

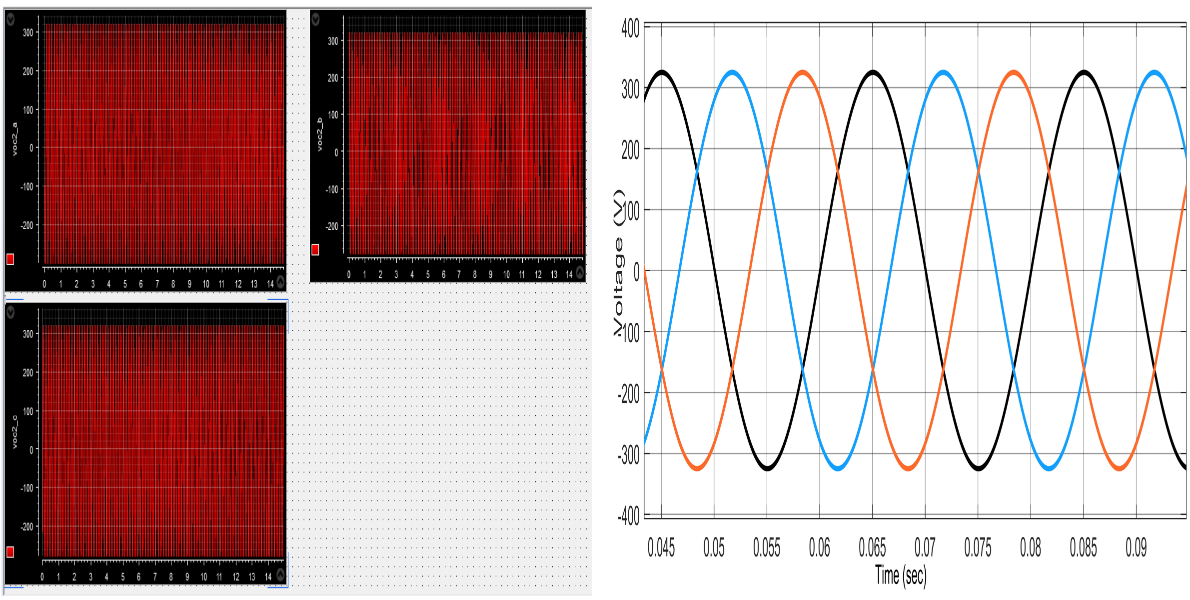

(a) Grid Voltage in dSPACE (b) Grid voltage in Simulink

Figure 7.11: Grid Voltage of three phase in dSPACE and Simulink

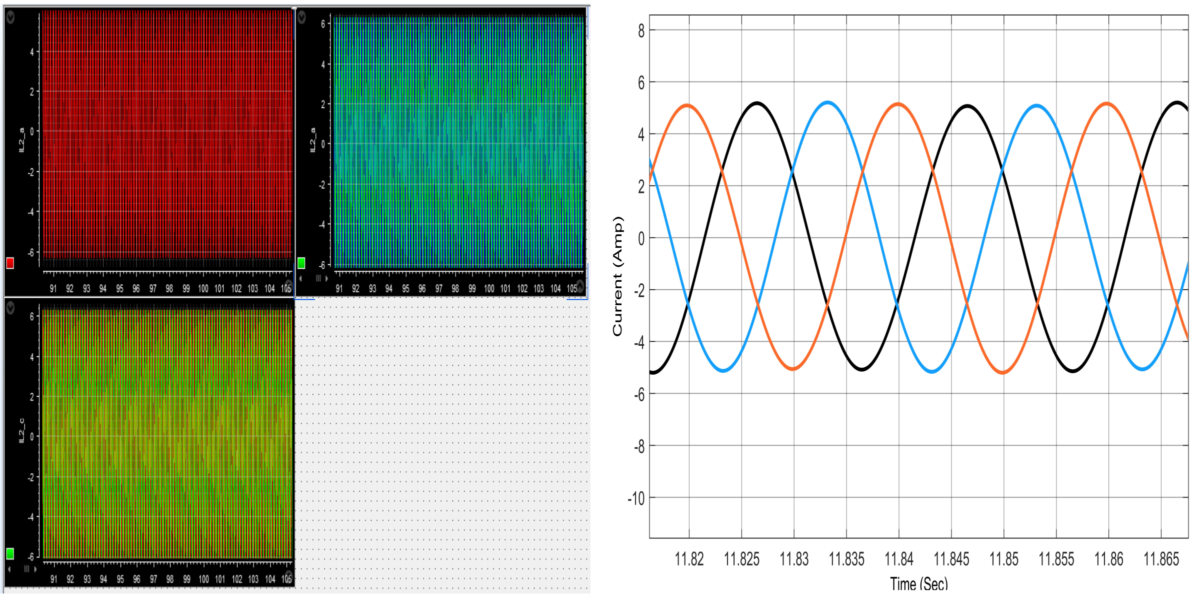

(a) Grid Voltage in dSPACE (b) Load Current in Simulink

Figure 7.12: Load Current of three phase in dSPACE and Simulink

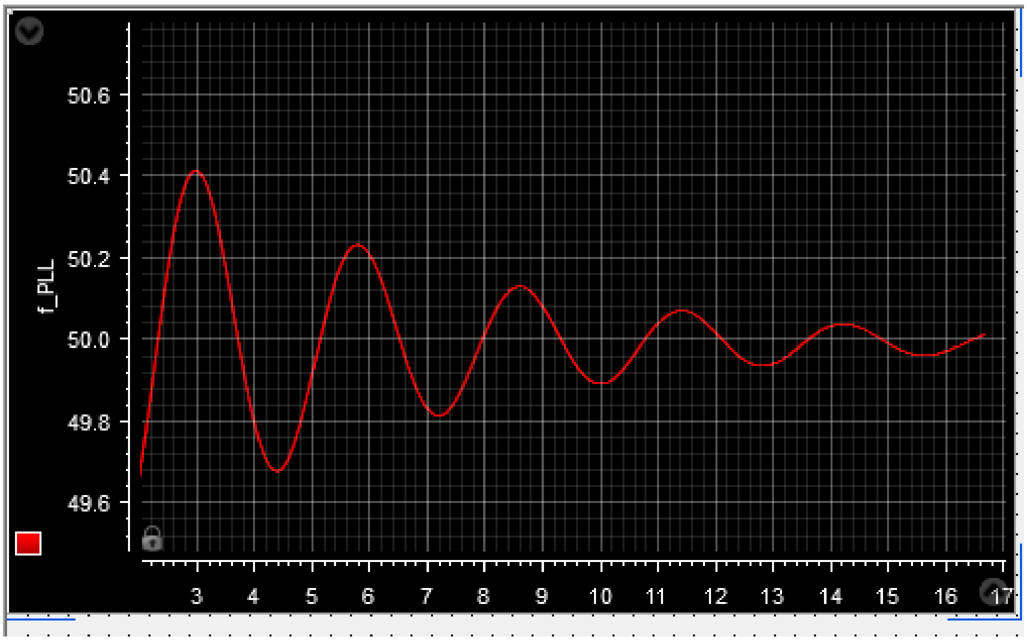

Figure 7.13: Frequency plot in dSPACE

7.8 Summary

Hardware-in-the-loop (HIL) tests for an islanded microgrid are tested based on dSPACE 1006 platform. The grid voltage is 325 V and the current is 5-6 A. The bus frequency stabilized at 50 Hz.

8 Conclusion and Future Work

8.1 Conclusion

Chapter-1

It deals with general introduction of Microgrid and its features in integrating distributed energy resources especially green energy. Problem formulation, objective and methodology are listed together with limitation of the thesis.

Chapter-2

This chapter introduces the state of the art of the control strategies for parallel inverters, hierarchical control for microgrids, and relevant topics like PLL and SOGI. The primary control Level focuses on the stability of voltage and frequency. The secondary control level eliminates frequency and voltage deviations caused by the power droop controllers at the primary layer. And finally Tertiary level deals with power flow and Energy Management systems.

Chapter-3

In this chapter, the zero control level namely the nested loop of voltage and current loops is formulated and the parameters are designed. The proportional term and resonant term for the PR controller in the voltage loop are designed by the bandwidth approach. The same approach is implemented for the current loop too. The designed controllers are validated by bode plot and step response.

Chapter-4:

Power droop method is used in primary control. Droop equations for inverters are derived and proved mathematically that active power output is mainly dominated by angular frequency, while reactive power output is mainly dominated by voltage magnitude when the line impedance is inductance dominated. The droop control is applied to achieve active and reactive power sharing without using communication channels.

Chapter-5

In this chapter, secondary control is used to restore frequency and voltage droops that are introduced by the power droop method. Centralized and distributed secondary control are presented. Finally, four different simulation cases are performed for centralized and distributed manners respectively and it was found that the distributed secondary control performed better than the centralized controller in most of the cases.

Chapter-6

In this chapter, the origin and harmful effects of harmonics are discussed. Harmonics compensation approaches and simulation results with proportional integral (PI) controllers in dq reference frame is compared with proportional resonance (PR) controllers in $\alpha\beta$ reference frame are presented. It can be seen that the total harmonic distortion is almost the same in both frames.

Chapter-7

Hardware-in-the-loop (HIL) simulation is done to validate the simulation results. Different components in the dSPACE 1006 platform like Danfoss Inverter, LCL filter, LEM signal conditioning boards, the interface board and relays are explained. HiL simulation results for an islanded microgrid are obtained which are consistent with simulation results obtained from Matlab/Simulink.

8.2 Future Work

Microgrids will play a very important role in integrating distributed energy resources especially renewable sources and energy storage systems. So, in the future, the following tasks could be considered:

- Due to the limitation of the project scope, the tertiary layer is not included with the developed primary and secondary control. The tertiary control could be included to provide power flow in a grid-tied inverter and achieve optimal operation.
- The latest trend in energy management systems with the inclusion of Electric Vehicles, P2X could be included at the tertiary layer with the developed primary and secondary controllers.
- Only one testing scenario is validated with HiL simulation in the thesis. More testing scenarios for the developed centralized and distributed secondary control strategies and harmonic suppression controllers could be validated with HiL simulation and experiments.
- Additionally, the Internet of Things (IoT) interaction may be included in future research interest.

Appendices

A Figures

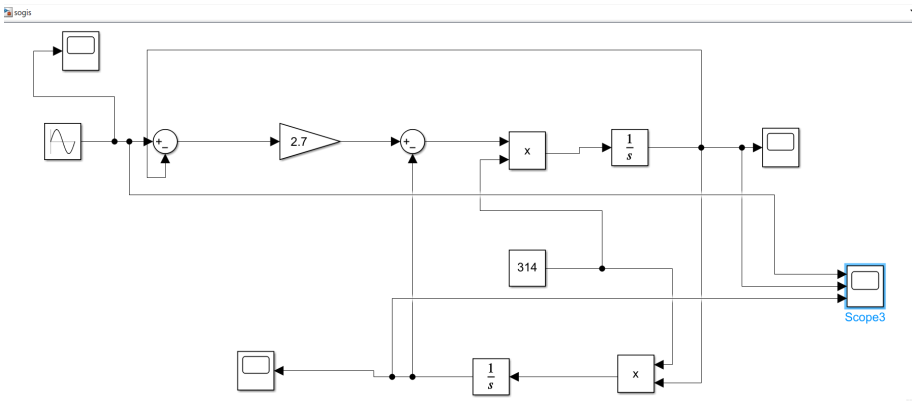

Figure A.1: General Representation of the Second Order Generalized Integrator in SIMULINK

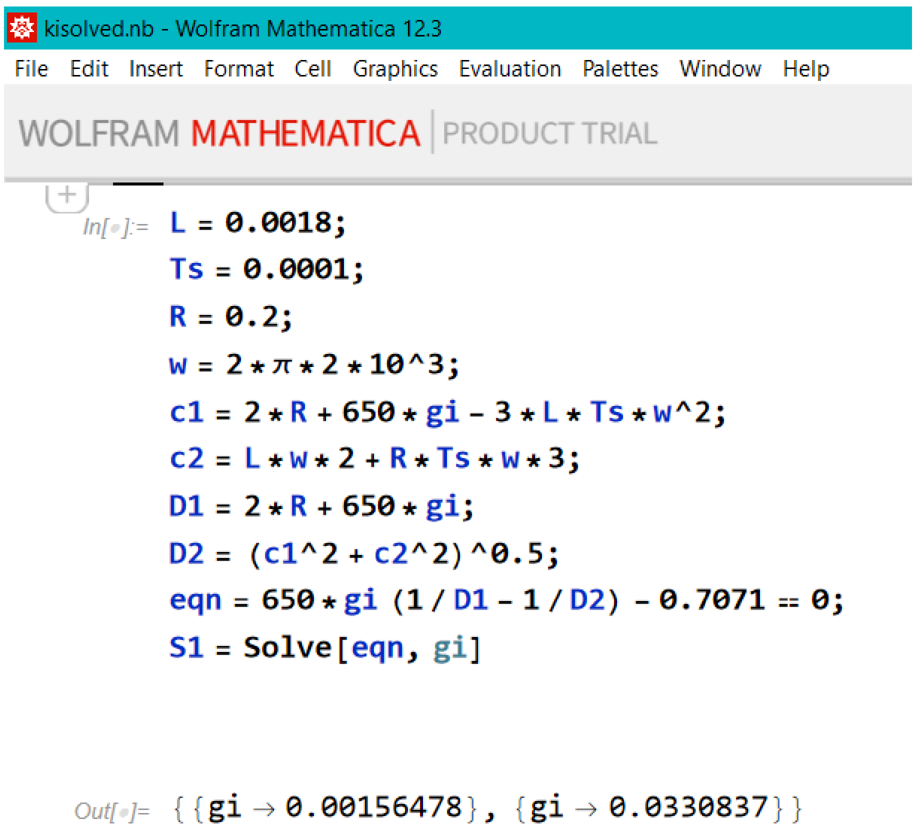

Figure A.2: Solution of k_{pI} by Wolfram Mathematica Software

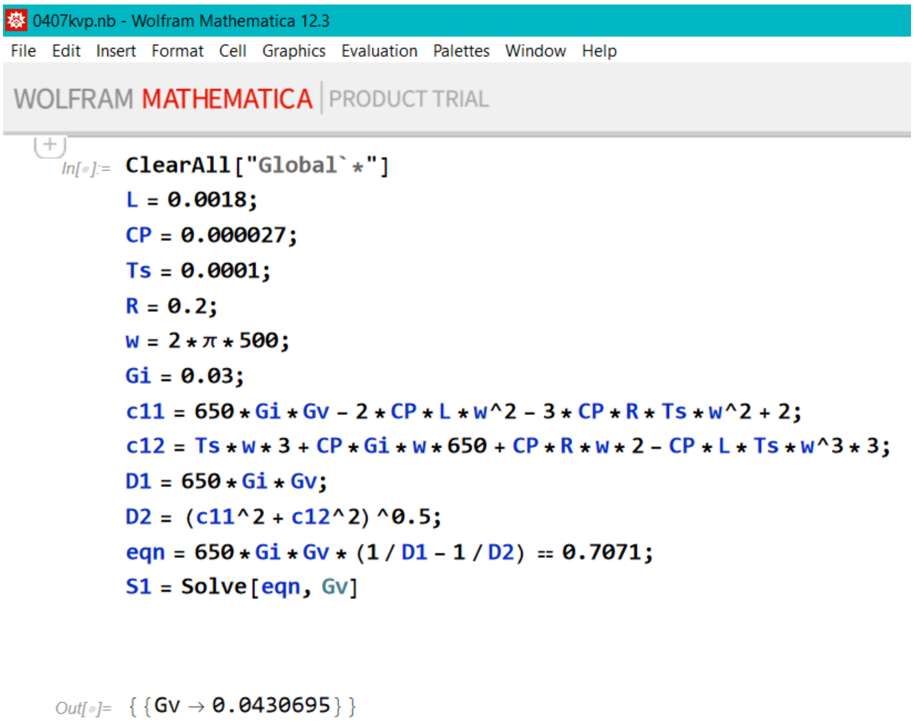

Figure A.3: Solution of k_{pV} by Wolfram Mathematica Software

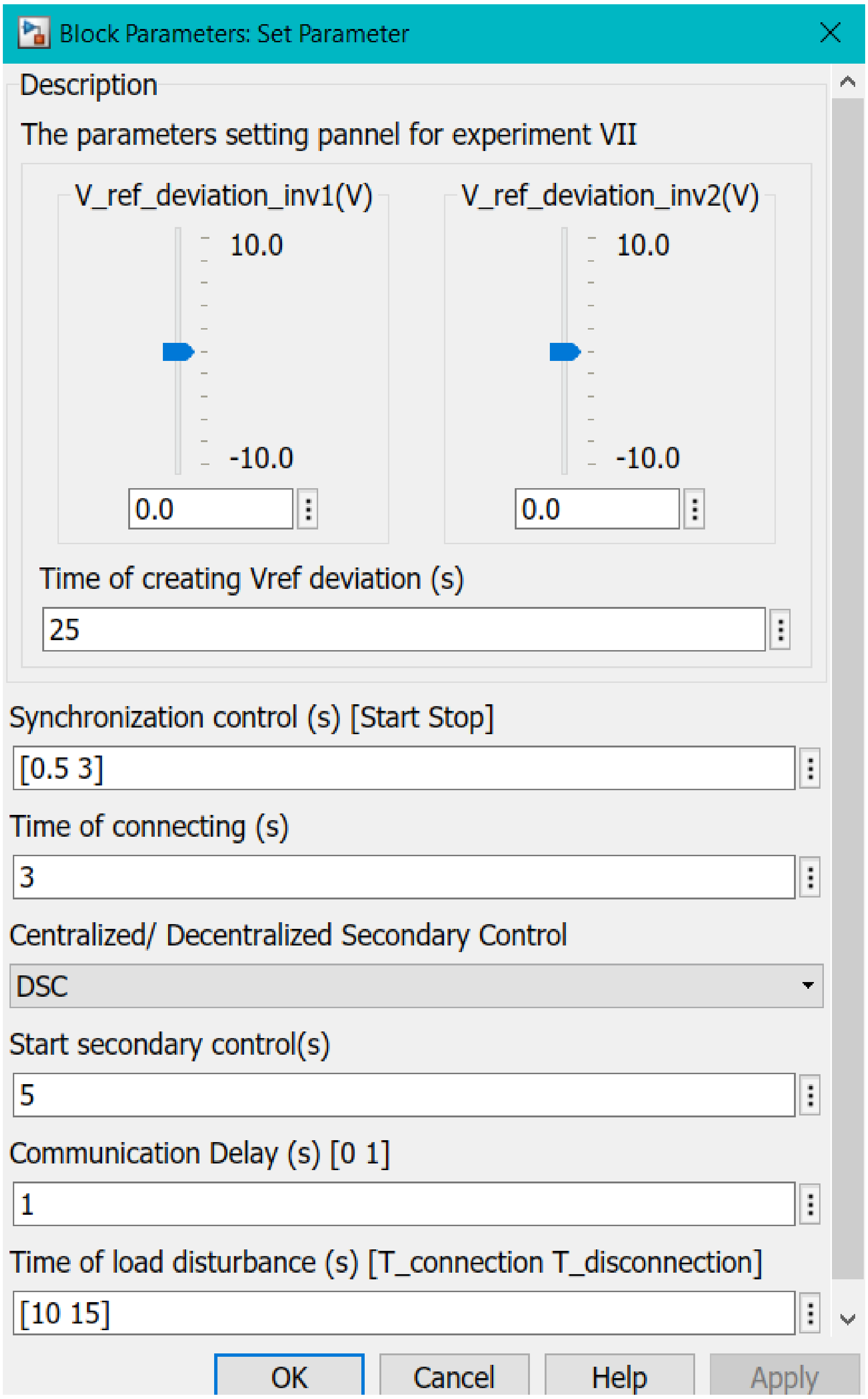

Figure A.4: Schematic diagram of the parameter that is changed during set-up

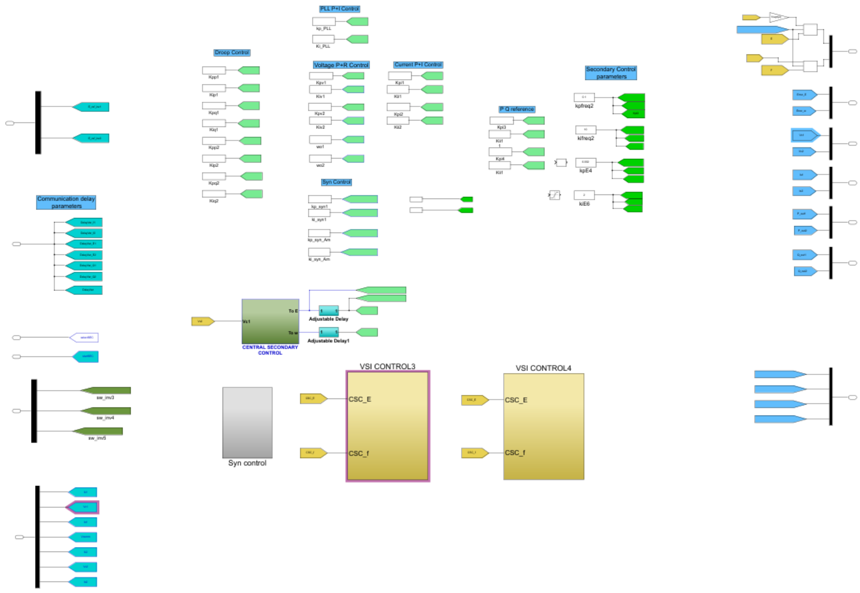

Figure A.5: Schematic diagram of the controller in secondary set-up

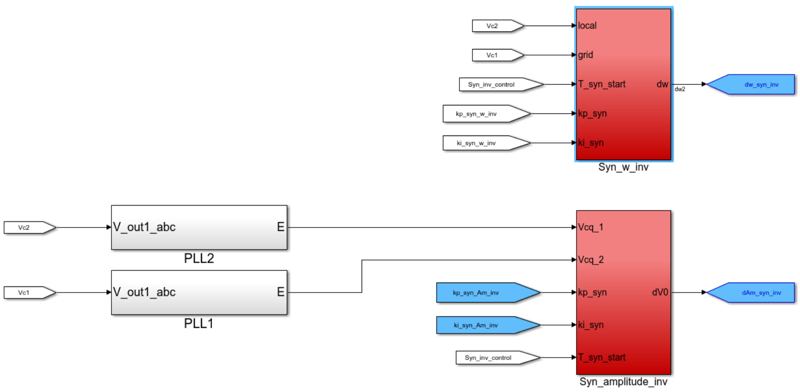

Figure A.6: Schematic diagram of the synchronization block for frequency and voltage amplitude

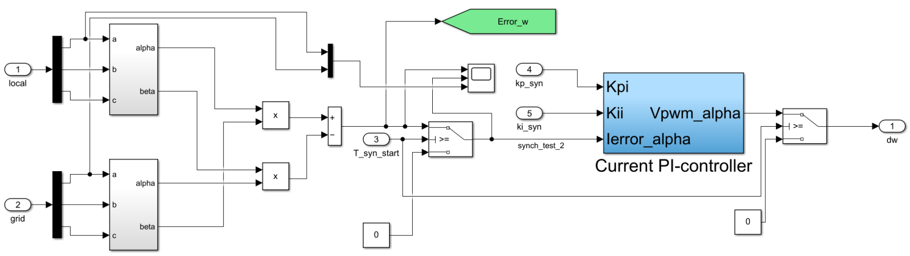

Figure A.7: Schematic diagram of the synchronization block for frequency

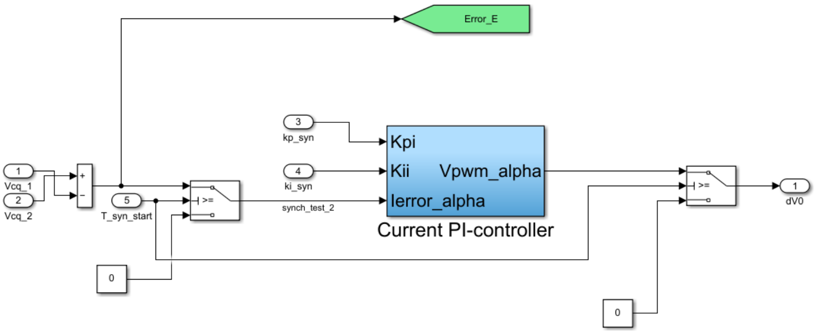

Figure A.8: Schematic diagram of the synchronization block for voltage amplitude

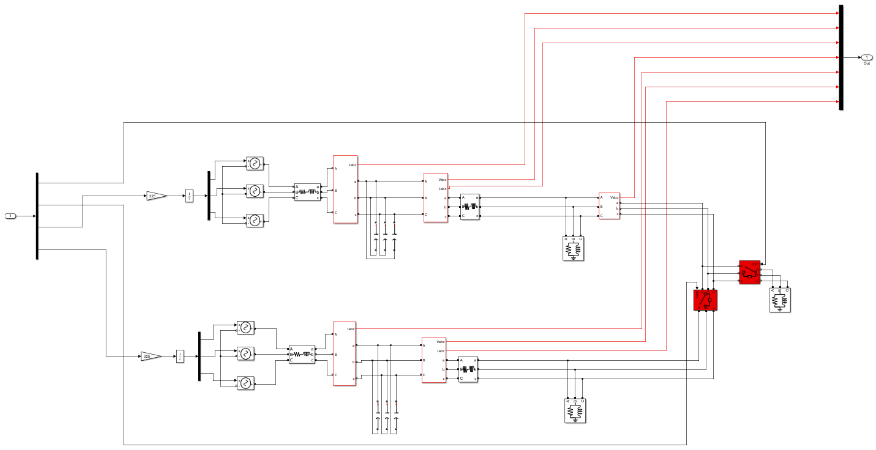

Figure A.9: Schematic diagram of the Grid containing two parallel Inverter

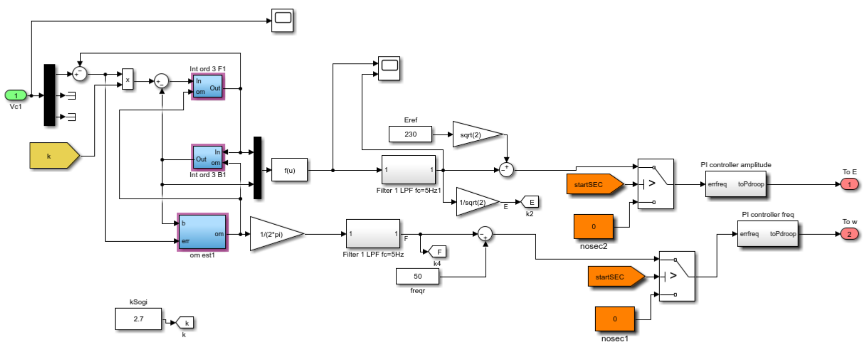

Figure A.10: Block diagram of Centralized Secondary Control

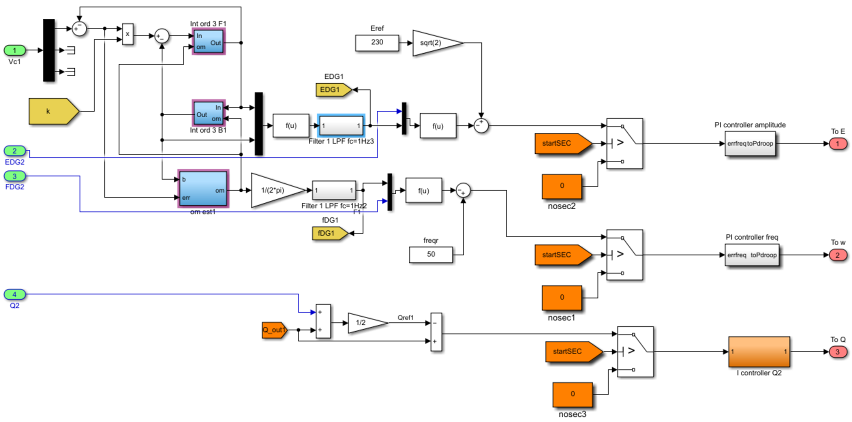

Figure A.11: Block diagram of Distributed Secondary Control

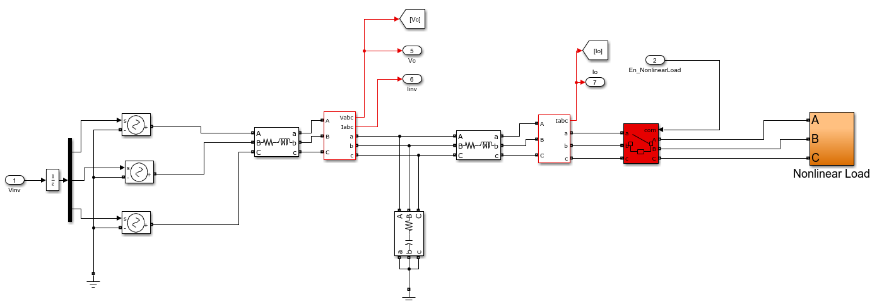

Figure A.12: Schematic diagram for measuring grid side parameters

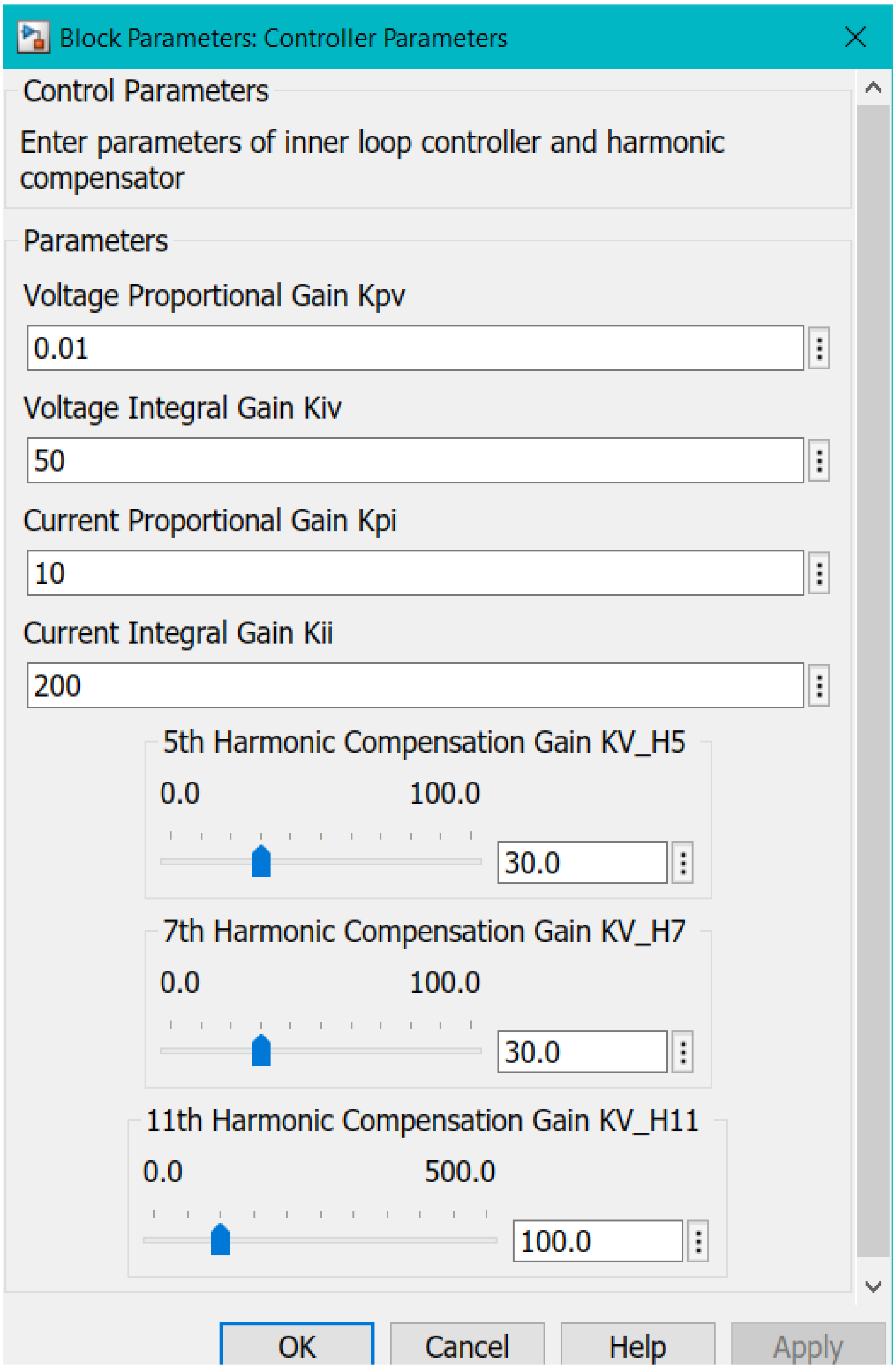

Figure A.13: Schematic diagram of controller parameter

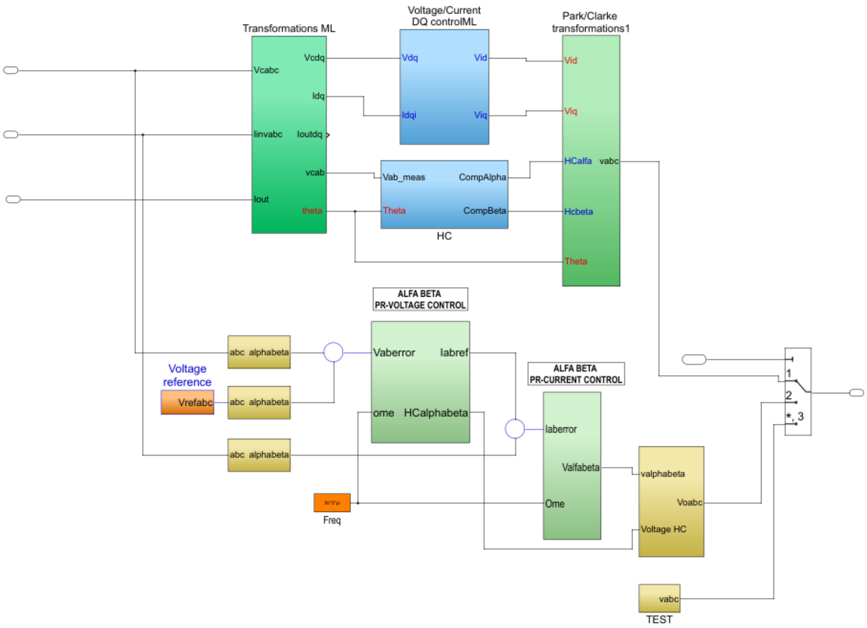

Figure A.14: Layout of controller block

B MATLAB CODE

B.1 SOGI

```
clc
clear all
close all
s=tf('s');
wo=2*pi*50;

for k=1:1:3;
Gv = k*s*wo/(s^2+k*wo*s+wo^2);
figure(1),bode(Gv)
%step(Gv)
hold on
end

for k=1:1:3;
Gv1 = k*wo^2/(s^2+k*wo*s+wo^2);
figure(2),bode(Gv1)
hold on
end
```

```
close all;
syms gi R Ts w L s Gv kiv
%%
L = 0.0018;
C = 0.000027;
Ts = 0.0001;
R = 0.2;
wo = 2*pi*50;
wc=0.001*2*pi*50;
%Gi = 0.0718;
Gi = 0.04;
%%
x1 = -13*Gi*1397*wo*wc;
x2 = 13*Gi*kiv*10000;
n1 = x1^2+x2^2;
c11 = -800*wc*wo-18161*Gi*wc*wo+800*C*L*wc*wo^3+1200*C*R*Ts*wc*wo^3
c12 = Gi*kiv*130000-Ts*wc*wo^2*1200-C*Gi*wc*wo^2*260000-C*R*wc*wo^2*800+C*L*Ts
    *wc*wo^4*1200
eqn = n1-(c11^2+c12^2)==0
S1 = solve(eqn,kiv)
y = round(S1,5)
```

Bibliography

[1] C. Sulzberger. "Pearl Street in Miniature: Models of the Electric Generating Station [History]". In: *IEEE Power and Energy Magazine* 11.2 (2013), pp. 76–85. DOI: 10.1109/MPE.2012.2233591.

[2] Rajiv Karn. *An Energy Management Solution for Renewable Energy Integrated Residential Homes*. https://projekter.aau.dk/projekter/. Jan. 2021.

[3] Jyothi Mahalingam. "MICROGRIDS". English. In: *Energy future (New Delhi)* 5.1 (Oct. 2016), p. 22. URL: https://search.proquest.com/docview/1839580505.

[4] Antonio Carlos Zambroni de Souza and Miguel Castilla. *Microgrids Design and Implementation*. Springer, 2019, pp. 172–173. ISBN: 3319986864.

[5] J. M. Guerrero et al. *Hierarchical Control of Droop-Controlled AC and DC Microgrids—A General Approach Toward Standardization*. ID: 1. 2011.

[6] J. M. Guerrero, L. Hang, and J. Uceda. *Control of Distributed Uninterruptible Power Supply Systems*. ID: 1. 2008.

[7] Danilo P. Mandic et al. *A Data Analytics Perspective of the Clarke and Related Transforms in Power Grid Analysis*. English. https://arxiv.org/pdf/1807.08720.pdf. July 2018.

[8] Mathworks. *Park Transform*. https://www.mathworks.com/help/physmod/sps/ref/parktransform.html.

[9] Hans Eklund. *Real Time Phase Locked Loops*.

[10] P. Rodríguez et al. *A Stationary Reference Frame Grid Synchronization System for Three-Phase Grid-Connected Power Converters Under Adverse Grid Conditions*. ID: 1. 2012.

[11] Jin-Wook Kang et al. "A Study on Stability Control of Grid Connected DC Distribution System Based on Second Order Generalized Integrator-Frequency Locked Loop (SOGI-FLL)". In: *Applied sciences* 8.8 (Aug. 2018), p. 1387. URL: https://search-proquest-com.zorac.aub.aau.dk/docview/2322347902.

[12] M. Ciobotaru, R. Teodorescu, and F. Blaabjerg. "A new single-phase PLL structure based on second order generalized integrator". In: *- 2006 37th IEEE Power Electronics Specialists Conference*. ID: 1. 2006, pp. 1–6. ISBN: 2377-6617.

[13] Md S. Reza. PhD thesis. 2014. URL: http://handle.unsw.edu.au/1959.4/54129.

[14] J. C. Vasquez et al. *Modeling, Analysis, and Design of Stationary-Reference-Frame Droop-Controlled Parallel Three-Phase Voltage Source Inverters*. ID: 1. 2013.

[15] O. Vodyakho and C. C. Mi. *Three-Level Inverter-Based Shunt Active Power Filter in Three-Phase Three-Wire and Four-Wire Systems*. ID: 1. 2009.

[16] Ahmed O. Althobaiti. "Proportional resonant control of three-phase grid-connected inverter during abnormal grid conditions". PhD thesis. 2018. URL: http://ethos.bl.uk/OrderDetails.do?uin=uk.bl.ethos.757166.

[17] Daniel Zammit et al. "Design of PR current control with selective harmonic compensators using Matlab". In: *Journal of Electrical Systems and Information Technology* 4.3 (2017). ID: 305924, pp. 347–358. URL: https://www.sciencedirect.com/science/article/pii/S2314717217300053.

[18] X. Meng, J. Liu, and Z. Liu. *A Generalized Droop Control for Grid-Supporting Inverter Based on Comparison Between Traditional Droop Control and Virtual Synchronous Generator Control*. ID: 1. 2019.

[19] *ENTSO-E AISBL Rate of Change of Frequency (ROCOF) withstand capability ENTSO-E guidance document for national implementation for network codes on grid connection*. -03-29 2017.
[20] J. Rocabert et al. *Control of Power Converters in AC Microgrids*. ID: 1. 2012.
[21] A. Milczarek, M. Malinowski, and J. M. Guerrero. *Reactive Power Management in Islanded Microgrid—Proportional Power Sharing in Hierarchical Droop Control*. ID: 1. 2015.
[22] J. M. Guerrero et al. *Hierarchical Control of Droop-Controlled AC and DC Microgrids—A General Approach Toward Standardization*. ID: 1. 2011.
[23] Q. Shafiee, J. M. Guerrero, and J. C. Vasquez. *Distributed Secondary Control for Islanded Microgrids—A Novel Approach*. ID: 1. 2014.
[24] E. Acha et al. *7 - Harmonic studies of power compensating plant*. ID: 275240. 2002. URL: https://www.sciencedirect.com/science/article/pii/B9780750651264500079.
[25] D. Shmilovitz. *On the definition of total harmonic distortion and its effect on measurement interpretation*. ID: 1. 2005.
[26] Sung-Il Jang and Kwang-Ho Kim. *An islanding detection method for distributed generations using voltage unbalance and total harmonic distortion of current*. ID: 1. 2004.
[27] *MICROGRIDS AND ENERGY INTERNET LABORATORY TUTORIAL V. 1.0*.
[28] *Design Guide VLT ® AutomationDrive FC 302 315-1200 kW*.

Aalborg
University

Fredrik Bajers Vej 7K
9220 Aalborg East
Tlf. 4525 1700

www.en.aau.dk/